Alma Mater Studiorum – Università di Bologna

DOTTORATO DI RICERCA IN
Automatica e Ricerca Operativa

NLGA based Active Control in Aerospace: fault tolerability, disturbance rejection, and parameter estimation
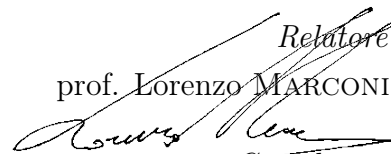
Presentata da: Nicola Mimmo
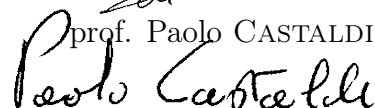
Coordinatore Dottorato
prof. Daniele VIGO

Relatore
prof. Lorenzo MARCONI

Correlatore
prof. Paolo CASTALDI

Esame finale anno 2015

"... mais de toutes les sciences la plus absurde, à mon avis, et celle qui est la plus capable d'étouffer toute espèce de génie, c'est la géométrie. Cette science ridicule a pour objet des surfaces, des lignes, et des points, qui n'existent pas dans la nature. On fait passer en esprit cent mille lignes courbes entre un cercle et une ligne droite qui le touche, quoique dans la réalité on n'y puisse pas passer un fétu. La géométrie, en vérité, n'est qu'une mauvaise plaisanterie."

Voltaire

ALMA MATER STUDIORUM – UNIVERSITA' DI BOLOGNA

Abstract

School of Engineering and Architecture

Department of Electrical, Electronic and Information Engineering

"Guglielmo Marconi"

Doctor of Philosophy

NLGA based Active Control in Aerospace: fault tolerability, disturbance rejection, and parameter estimation

by Nicola MIMMO

A new control scheme has been presented in this thesis. Based on the NonLinear Geometric Approach, the proposed Active Control System represents a new way to see the reconfigurable controllers for aerospace applications. The presence of the Diagnosis module (providing the estimation of generic signals which, based on the case, can be faults, disturbances or system parameters), mean feature of the depicted Active Control System, is a characteristic shared by three well known control systems: the Active Fault Tolerant Controls, the Indirect Adaptive Controls and the Active Disturbance Rejection Controls. The standard NonLinear Geometric Approach (NLGA) has been accurately investigated and than improved to extend its applicability to more complex models. The standard NLGA procedure has been modified to take account of feasible and estimable sets of unknown signals. Furthermore the application of the Singular Perturbations approximation has led to the solution of Detection and Isolation problems in scenarios too complex to be solved by the standard NLGA. Also the estimation process has been improved, where multiple redundant measuremtent are available, by the introduction of a new algorithm, here called "Least Squares - Sliding Mode". It guarantees optimality, in the sense of the least squares, and finite estimation time, in the sense of the sliding mode. The Active Control System concept has been formalized in two controller: a nonlinear backstepping controller and a nonlinear composite controller. Particularly interesting is the integration, in the controller design, of the estimations coming from the Diagnosis module. Stability proofs are provided for both the control schemes. Finally, different applications in aerospace have been provided to show the applicability and the effectiveness of the proposed NLGA-based Active Control System.

Acknowledgements

Contents

List of Figures

Abbreviations

ADRC	**A**ctive **D**isturbance **R**ejection **C**ontrol
AFTC	**A**ctive **F**ault **T**olerant **C**ontrol
BS	**B**ack**S**tepping
CAS	**C**alibrated **A**ir **S**peed
DD	**D**etection and **D**iagnosis
DI	**D**etection and **I**solation
FL	**F**eedback **L**inearization
LS	**L**east **S**quares
LES	**L**ocally **E**xponentially **S**table
NED	**N**orth-**E**ast-**D**own local inertial axes
NLGA	**N**on**L**inear **G**eometric **A**pproach
RBF-NN	**R**arial **B**asis **F**unctions **N**eural **N**etwork
RPM	**R**evolution **P**er **M**inutes
RM	**R**esidual **M**atrix
SM	**S**liding **M**ode
SP	**S**ingular **P**erturbations
TAS	**T**rue **A**ir **S**peed
UAV	**U**nmanned **A**erial **V**ehicle
o.c.a.	**o**bservability **c**odistribution **a**lgorithm

Symbols

$\mathbf{x}$	state vector
$\bar{\mathbf{x}}_1$	state vector of the first subsystem provided by the NLGA
$\bar{\mathbf{x}}_2$	state vector of the second subsystem provided by the NLGA
$\bar{\mathbf{x}}_3$	state vector of the third subsystem provided by the NLGA
$\mathbf{y}$	output vector
$\bar{\mathbf{y}}_1$	output vector of the first subsystem provided by the NLGA
$\bar{\mathbf{y}}_2$	output vector of the second subsystem provided by the NLGA
$\mathbf{u}$	input vector
$\mathbf{f}$	unknown signals vector
$\mathbf{f}_u$	input faults vector
$\mathbf{f}_{sys}$	disturbance and system faults vector
$\mathbf{f}_y$	output faults vector
$\mathbf{f}_s$	set of undesired signals to be diagnosed
$\mathbf{d}_s$	generalized disturbance to be decoupled
$\mathbf{h}\left(\mathbf{x}\right)$	output map
$\mathbf{n}\left(\mathbf{x}\right)$	vector field
$\mathbf{g}\left(\mathbf{x}\right)$	input vector field
$\mathbf{l}\left(\mathbf{x}\right)$	$\mathbf{f}_s$ vector field
$\mathbf{p}\left(\mathbf{x}\right)$	$\mathbf{d}_s$ vector field
$\hat{(\cdot)}$	estimation of $(\cdot)$
$\mathcal{X}$	compact set in the state space
$\mathcal{Y}$	compact set in the output space
$\mathcal{U}$	compact set in the input space

$\mathcal{F}_u$ compact set in the input faults space

$\mathcal{F}_y$ compact set in the output faults space

$\mathcal{F}_{sys}$ compact set in the disturbances and system faults space

N_r number of minimal detection and isolation sets

S_i^{min} i-th minimal detection and isolation set

$\mathcal{R}$ residuals set

$\boldsymbol{\Omega}$ residual subset

$\mathbf{r}$ analog residuals vector

$\mathbf{r}^d$ digital residuals vector

J_r residual evaluation function

J_{th} residual evaluation function threshold

ℓ_n state space dimension

ℓ_m output space dimension

ℓ_u input space dimension

ℓ_{sys} disturbances and system faults space dimension

ℓ_f dimension of $\mathbf{f}$

ν_s dimension of $\mathbf{f}_s$

Σ_*^P minimal conditioned invariant distribution containing P

P distribution spanned by the columns of $\mathbf{p}_s$

$(\Sigma_*^P)^\perp$ codistribution orthogonal to Σ_*^P

Ω^* maximal observability codistribution contained in $(\Sigma_*^P)^\perp$

$\boldsymbol{\xi}$ vector of estimation activation signals

ε singular perturbation parameter

m rigid body mass

$\mathbf{V}_{I,B}$ inertial speed expressed in body axes

$\boldsymbol{\Omega}_B$ rotational speed in body axes

$\mathbf{F}_B$ external forces expressed in body axes

$\mathbf{I}$ rigid body inertia matrix

$\mathbf{M}_B$ external torques expressed in body axes

$\mathbf{P}_I$ inertial rigid body position

$\mathbf{R}_{B \to I}$ rotation matrix from body to inertial axes

$\mathbf{S}(\cdot)$ skew-symmetric matrix

ρ air density

S reference area

V_a True AirSpeed

M Mach number

$\bar{c}$ aerodynamic mean chord

C_x x-body aerodynamic force coefficient

C_y y-body aerodynamic force coefficient

C_z z-body aerodynamic force coefficient

C_D x-wind aerodynamic force coefficient

C_Y y-wind aerodynamic force coefficient

C_L z-wind aerodynamic force coefficient

C_l x-body aerodynamic momentum coefficient

C_m y-body aerodynamic momentum coefficient

C_n z-body aerodynamic momentum coefficient

To my parents
for their unwavering love

Chapter 1

Introduction and Motivations

The unknown and unmeasurable variations of the process parameters or exogenous unknown signals can degrade the performances of the control systems. Feedback is basically used in conventional control systems to reject the effect of disturbances or model uncertainties upon the controlled variables and to bring them back to their desired values according to the requirements. To achieve this, the controlled variables are measured, then the measurements are compared with the desired values and the difference is fed into the controller which generates the appropriate control. Modern technological systems rely on sophisticated robust controls to meet increased performance requirements. For such systems, the required robustness can be achieved via advanced control systems, which can be broadly classified into active and passive.

A **Passive Control System** can tolerate a predefined set of exogenous unknown signals (such as disturbances, faults, . . .) or model mismatching (parameters uncertainties) while accomplishing its mission satisfactory without the need for control reconfiguration.

An **Active Control System**, on the other hand, relies on a Diagnosis process to estimate uncertain model parameters or exogenous unknown functions affecting the system's performance. Accordingly, the control law is reconfigured on-line.

In the presence of variations of the dynamic characteristics of a plant to be controlled, passive robust control design of the conventional feedback control system is a powerful tool for achieving a satisfactory level of performance for a family of plant models. This family is often defined by means of a nominal model and a size of the uncertainties. The range of uncertainty domain for which satisfactory performances can be achieved depends upon the problem. Sometimes, a large domain of uncertainty can be tolerated, while in other cases, the uncertainty tolerance range may be very small. If the desired performances cannot be achieved for the full range of possible parameter variations, active control has to be considered in addition to a passive robust control

design. Furthermore, the tuning of a passive robust design for the true nominal model using an active control technique will improve the achieved performance of the passive robust controller design. Therefore, robust control design will benefit from the use of active control in terms of performance improvements and extension of the range of operation.

This work groups under the same root several Active Control techniques whose main three representatives are:

Active Fault Tolerant Controls. An Active Fault Tolerant Control System (AFTCS) represents a strategy for increasing plant reliability and availability and for reducing the risk of safety hazard [1]. An AFTCS is designed to continue operations, with graceful degradation in performance, by accommodating faults in early stage of their development, such that minor fault in a subsystem do not develop in a failure at system level [2]. **A fault is defined as an unpermitted deviation of at least one characteristic property or parameter of the system from the acceptable behavior. Faults may take place in any system component (actuators, sensors, plant components, or any combination) [3].** The fault is a state that may lead to a malfunction or a failure in the system. The main task of AFTCS is on-line reconfiguration of the controller. For this to be possible, detailed information about fault-induced changes is required. In this context, a fault Detection and Diagnosis module plays a crucial role in AFTCS: it monitors system performance, detect the occurrence of faults, and to determine their magnitude, indeed.

Indirect Adaptive Controls. An Adaptive Controller changes itself so that its behavior will conform to new or changed circumstances. The words "adaptive systems" and "adaptive control" have been used as early as 1950 [4]. The design of autopilots for high-performance aircraft was one of the primary motivations for active research on adaptive control in the early 1950s. Aircraft operate over a wide range of speeds and altitudes, and their dynamics are nonlinear and conceptually time varying. As aircraft go through different flight conditions, the operating point changes and the output response $y(t)$ carries information about the state x as well as the parameters. In principle, a sophisticated feedback controller should be able to learn about parameter changes by processing $y(t)$ and use the appropriate gains to accommodate them. This argument led to a feedback control structure on which adaptive control is based, see [5]. An Adaptive Controller is formed by combining an on-line parameter estimator (Diagnosis module), which provides estimates of unknown parameters at each instant, with a control law that is motivated from the known parameter case. In Indirect Adaptive Control, the plant parameters are estimated on-line by the Diagnosis module and used to calculate the controller parameters. This approach has also been referred to as explicit adaptive control, because the design is based on an explicit plant model. The basic idea is that a suitable controller can be designed on-line if a model of the plant is estimated on-line, by an appropriate Diagnosis module, from the available

input-output measurements. The scheme is termed indirect because the adaptation of the controller parameters is done in two stages: on-line estimation of the plant parameters and on-line computation of the controller parameters based on the current estimated plant model.

Active Disturbance Rejection Controls. Active Disturbance Rejection Control (ADRC) is Han's way out of the robust control paradox [6]. The term was first used in [7] where his unique ideas were first systematically introduced into the English literature. The central idea of Active Disturbance Rejection is recalled in [8]: the control of a complex nonlinear, time-varying, and uncertain process is reduced to a simple problem by a direct and active estimation, by a Diagnosis module, and rejection (cancellation) of the generalized disturbance, interpreted as the vector field representing all the model uncertainties affecting the system dynamics. Anyway, information about physical disturbance acting on the systems can be very useful for performance evaluation, so, in this thesis, the model uncertainties to be estimated, by the Diagnosis module, and rejected are represented by exogenous unknown signals, such as non-manipulable inputs, rather than their effects on the system dynamics.

The above mentioned active control techniques share a common feature: the presence the Diagnosis module. Literature presents plenty of techniques for the Diagnosis process and, in general, these approaches can be categorized into signal-based and model based technique [9]. Signal-based methods detect the occurrence of undesired signals by testing specific properties of measurements. In a model-based method, the Diagnosis module is, in the most general abstraction, composed by two parts: the Detection and Isolation block and the Estimation unit. In turn, the Detection and Isolation module can be formally divided in two subsystems: the Detection system, which provides a set of residuals indicating the occurrence of a certain signal, and an Isolation logic, that elaborates these residuals to indicate the location of this signal into the system. Usually, the analog detection residuals are converted to digital by comparing the residual with a possibly adaptive threshold [10], [11], [12], [13]. Depending on the case, the Detection module can be indispensable, when information about the occurrence of a signal is needed despite the presence of other unknowns, or not necessarily present, when information about the occurrence of a signal is not required. The existence of a Detection system implies the presence of a set of residuals and consequently, of an Isolation logic, that can be, depending on the structure of the residuals, as complicated as required or so obvious to be neglected. As example, let's image the possibility to have a set of "dedicated" residuals (each residual in this set is dedicated to only and only one signal among the set of unknown signals to be estimated, in a one-to-one correspondence). In this case the isolation logic can be represented by an "identity" matrix, so, it exists but is straightforward. Usually the Estimation unit is switched on, after the occurrence of the signal has been detected and the location of the signal has been determined,

by an activation signal coming from the Detection and Isolation module. In the special case of dedicated residuals set the estimation can always be kept active if there is the need of a continuous estimation.

Two major approaches have been used in model-based detection residual generation: qualitative (heuristic) methods and quantitative (analytic) methods [11], [14]. To design an Active Control, precise knowledge about the plant dynamics need to be known after the occurrence of a undesired signals corrupting the nominal system behavior. Hence, more emphasis has been placed upon quantitative model-based diagnosis approaches.

Three main classes of analytical model-based residual generators exist: observer-based approaches, parity relations approaches and parameter estimation (or system identification) approaches. The principle of observer-based approaches is to estimate the system variables with an observer (Luenberger, Kalman, . . .) and to use the estimation errors/innovations as residuals [12], [15], [16], [17], [18], [19]. In the parity relations approaches, the residuals are computed as difference between the measured outputs and the estimated outputs and their associated derivatives. The method reshapes the primary residual signals using a transformation matrix to make the residual insensitive to unknown disturbances and to increase signal estimation performances. The parity relations approach has been developed in time domain [20] and in frequency domain [21]. The parameter estimation methods, for Detection and Isolation, are particularly suitable for systems where the undesired signals correspond to an undesired behavior of physical coefficients of the process. By continuously estimating the parameters of a process model, residuals are computed as the parameter estimation errors. To successfully isolate the undesired signal, the mapping from the model coefficients to the process parameters must exist and be known. Different algorithms for parameter estimation have been proposed: least square estimation, instrumental variable approach, output error methods [22], sliding mode estimation [23], neural network estimation [24], and extended Kalman filters [25].

Furthermore, several interesting approaches have been utilized to design and implement Detection and Isolation algorithms such as the Geometric Approach for both linear and non linear cases.

Starting from the theoretical seminal works [26] and [27], the Linear Geometric Approach has been investigated in [28] and [29], whereas several interesting applications can be found in [30] for periodic systems and in [31] and [32] for systems whose dynamics has a Markovian description. Linear systems with time delays have been investigate in [33], [34] and [35], and further particular applications can be found about Fornasini-Marchesini 2D Systems [36], discrete time systems [37] and systems with time varying perturbations [38].

On the road toward nonlinear systems, [39] presented remarkable aspects on bilinear systems.

The NonLinear Geometric Approach came as natural development of its linear counterpart. The first theoretical works is [40], further developed in [41] and [42], and investigated in [43] and [44]. Interesting applications of the NLGA can be found in [45] for hybrid systems, in [46] and [47] for parabolic and hyperbolic partial differential equations, in [48] for robotic applications, in [49] for industrial applications. A tutorial on the NLGA has been provided in [50]. Finally, lots of NLGA aerospace applications for fault detection and isolation have been published: [51] on a Vertical Take Off and Landing aircraft, [52] on a network of UAV, [53], [54], [55], [56], [57], [58] and [59] on aircraft and [60], [61] and [62] for satellites. The NLGA applicability, typically committed to detect and isolate faults, has be extended for the isolation and the successive estimation of external disturbances. Interesting works are [63] and [64] for aircraft applications and [65] in the case of quadrotors.

In this thesis, the NLGA constitutes the base for the design of Active Controls in aerospace.

Model-based Detection and Isolation techniques makes use of mathematical model of the system. However, a perfectly accurate mathematical model of a physical system is never available. Hence, there is always a mismatch between the actual process and its mathematical model. The effects of modeling uncertainties, disturbances and noise are therefore the most crucial point in the model-based Detection and Isolation concept and the solution of this problem is the key for its practical applicability [3]. To overcome this problems, a model-based Detection and Isolation scheme has to be insensitive to model uncertainties. Sometimes, a simple reduction of the sensitivity to model uncertainties does not solve the problem: the sensitivity reduction may be also associated to a reduction of the sensitivity to the signals to be detected and isolated [3], indeed. In this thesis, in order to accommodate the application of the Detection and Isolation concepts, disturbances and parameter uncertainties of the monitored plans, as well as faults are modeled in the form of unknown input signals. The application of the NLGA, provided certain conditions are satisfied, allows the generation of residuals that are perfectly (analytically) decoupled from the sources of uncertainty but not trivially dependent on the unknown signal to be detected and isolated.

1.1 Thesis contribution

This work presents an Active Control scheme, for aerospace applications, whose main features are the Diagnosis module and its design technique, *i.e.* the NonLinear Geometric Approach. The main contributions of this thesis are:

- **Control systems unification**: the Active Fault Tolerant Controls, the Indirect Adaptive Controls and the Active Disturbance Rejection Controls can be regarded as members of the same family of controllers, characterized by the presence of a Diagnosis module. This thesis proposes a more general concept of Active Control that, based on the definition of the unknown undesired signals acting on the plant, covers all these three methodologies, see Section 2;

- **Standard NLGA applicability improvement**: the application of the Singular Perturbations approximation allows, with a weaker decoupling property, the solution of the problem of Detection and Isolation where multiple non concurrent faults are affecting both the inputs and the outputs, see Section 2.1.1.3;

- **Standard NLGA procedure improvement**: the standard NLGA proposed by [40] and improved by [41] can be further extended by modifying the algorithm proposed in [41]. This work suggests two algorithm modifications to take account of feasible and estimable sets of unknown signals, see Section 2.1.1.4;

- **A new estimation algorithm**: the Detection and Isolation robustness is important as well as the estimation accuracy. In the context of multiple redundant measurements, this works proposes a knew estimation algorithm that represents a fusion between two well known techniques, *i.e.* the Least Squares (LS) and the Sliding Modes (SM), that guarantees optimality, in the sense of the least squares, and finite estimation time, in the sense of the sliding mode. See Section 2.1.4.3;

- **Design, with stability proofs, of two Active Control Systems for aerospace applications**: a complete design of a nonlinear backstepping controller and a nonlinear composite controller is shown in Section 2.2. For these two controllers a proper Diagnosis module is associated and the stability proof for the overall Active Control System is provided. The controllers structure, based on the elementary brick of the Feedback Linearisation, is particularly suitable to exploit the estimations coming from the Diagnosis module;

- **Aerospace applications**: the methodology developed in this this work has been applied to typical aerospace systems such as aircraft, spacecraft, fixed wind UAVs and quadrotors. The results in Section 3 are encouraging and show the applicability effectiveness of the

NLGA-based methodology, able to cover different applications in aerospace. The application of the improved NLGA to these aerospace systems has led to the design of new controllers and new Diagnosis schemes able to solve, for the first time, complex problems such as the detection and the isolation of multiple faults of all actuators and sensors.

1.2 Thesis Outline

This work is organized in two main Sections: Section 2 describes all the methodological aspects related to the proposed NLGA-based Active Control System, whereas Section 3 shows the application of the hereafter mentioned methodology to aerospace cases.

In particular, Section 2 is divided to detail, step by step, all the components of the NLGA-based Active Control System: Section 2.1.1 recalls the standard NLGA and presents some methodological advances, Section 2.1.2 depicts how to design robust Detection residual sets, Section 2.1.3 presents the residual matrix concept at the base of the Isolation technique, Section 2.1.4 details three kind of estimation algorithms and, finally, Section 2.2 shows, with stability proofs, how to integrate, in the controller design, the estimation coming from the Diagnosis module.

Section 3 is dedicated to the application of the NLGA-based Active Control System. After a brief introduction highlighting the model commonalities of all the proposed aerospace plants (see Section 3), five different scenarios of faults, disturbances and flight parameters are considered for aircraft in Section 3.1 whereas Sections from 3.2 to 3.4 cover the remaining plants that are a fixed wing UAV, a spacecraft and a quadrotor.

Final remarks and conclusions are presented in Section 4.

Chapter 2

NLGA based Active Control Scheme

T he Active Control schemes considered in this thesis are composed by two main parts: the Nominal Controller and the Estimation Module. These two modules work together to achieve the output tracking, that is the control goal, *i.e.* to make $\mathbf{y}(t)$ following the reference time function, $\mathbf{y}_{REF}(t)$, despite the presence of faults, uncertainties and disturbances. Generically speaking, the control loop can be affected by three kind of disturbances:

- unknown functions affecting the input, $\mathbf{f}_u$;

- unknown functions affecting the plant dynamics, $\mathbf{f}_{sys}$;

- unknown functions affecting the output, $\mathbf{f}_y$.

Figure 2.1 schematically depicts the control problem and the unknown functions scenario: the plant is forced by the controller actions $\mathbf{u}$, linearly corrupted by the unknown $\mathbf{f}_u$, while the dynamics of the plant is influenced by the unknown functions $\mathbf{f}_{sys}$. The state $\mathbf{x}$ is measured by $\mathbf{y}$, through $\mathbf{h}(\mathbf{x})$ which is affected by the unknown functions $\mathbf{f}_y$. Finally, the nominal controller receives the estimation $\hat{\mathbf{f}}_s$ of some of (at most all of) the unknown functions.

The scheme presented in Figure 2.1 is mathematically described by the following Multi Input – Multi Output (MIMO) system:

$$\begin{cases} \dot{\mathbf{x}} &= \mathbf{n}(\mathbf{x}) + \mathbf{g}(\mathbf{x}) \left[\mathbf{u}(t) + \mathbf{f}_u(\mathbf{x}, t) \right] + \mathbf{l}(\mathbf{x}) \mathbf{f}_{sys}(\mathbf{x}, t) \\ \mathbf{y} &= \mathbf{h}(\mathbf{x}) + \mathbf{f}_y(\mathbf{x}, t) \end{cases} \tag{2.1}$$

where $\mathbf{x} \in \mathcal{X} \subset \mathbb{R}^{\ell_n}$, $\mathbf{y} \in \mathcal{Y} \subset \mathbb{R}^{\ell_m}$, $\mathbf{u} \in \mathcal{U} \subset \mathbb{R}^{\ell_u}$, $\mathbf{f}_u \in \mathcal{F}_u \subset \mathcal{U}$, $\mathbf{f}_y \in \mathcal{F}_y \subset \mathcal{Y}$, $\mathbf{f}_{sys} \in \mathcal{F}_{sys} \subset \mathbb{R}^{\ell_{sys}}$ and $\mathbf{n}(\mathbf{x})$, the columns of $\mathbf{g}(\mathbf{x})$ and $\mathbf{l}(\mathbf{x})$ are smooth vector fields, and $\mathbf{h}(\mathbf{x})$ is a smooth map.
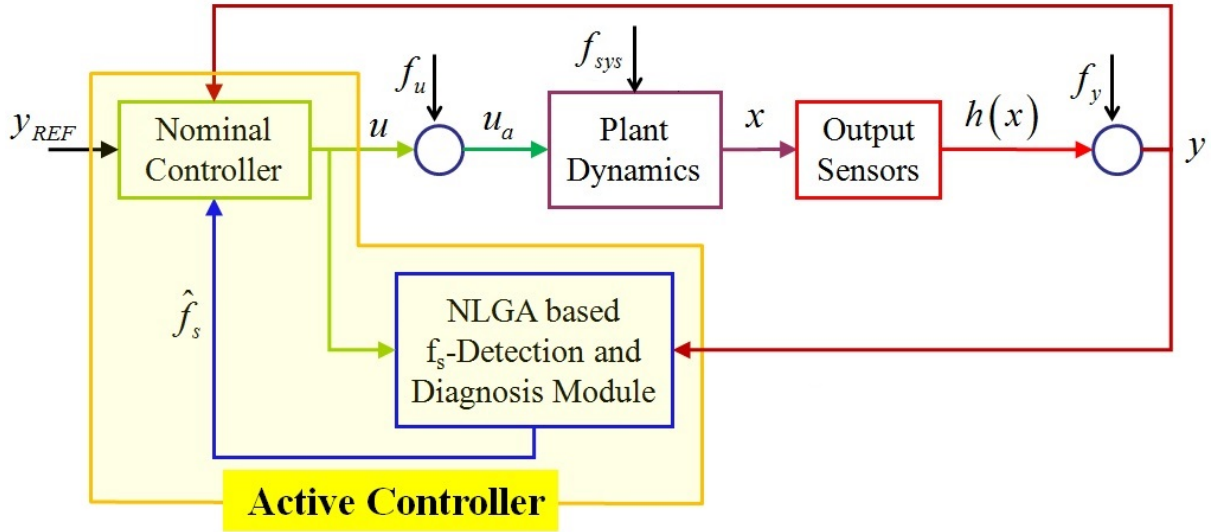
FIGURE 2.1: Active Control Scheme

Finally $\mathbf{f}_s \subseteq \mathbf{f} = \{\mathbf{f}_u \cup \mathbf{f}_{sys} \cup \mathbf{f}_y\}$, $\mathbf{f}_s \in \mathbb{R}^{\nu_s}$ with $\nu_s \leq \ell_f = \ell_u + \ell_{sys} + \ell_y$, represents the set of unknown functions estimated by $\hat{\mathbf{f}}_s$.

As stated in Section 1, Active Control Systems strictly rely on a Diagnosis process to estimate uncertain model parameters or exogenous unknown functions affecting the system's performance. Then, since the Diagnosis module assumes a great relevance for this kind of control schemes it's worth understand its mean features. The estimation module can be characterized by the presence of a detection logic which activate the estimation process only in the case where the fault is detected affecting the system. This simple, but important, aspect allows to avoid the continuous noisy feedback, which is typical of adaptive control schemes. Generally speaking, the estimations are obtained by means of the following three steps:

1. **Detection**: this initial stage tips off, and indicates by a binary signal, the presence of the unknown functions (*e.g.* is the system affected by a fault or not?);

2. **Isolation**: the second phase identifies, usually by a boolean logics, the location of unknown functions (where the unknown function is affecting the system);

3. **Estimation**: the final step provides the estimation of the detected and isolated unknown function.

The Active Control scheme presented in this work, can assume the features proper of the adaptive controls: as detailed in Section 2.1.1.1, the definition of $\mathbf{f}_s$, and its isolation properties can avoid the need of an isolation logic, indeed. In this scenario, the three phases of Detection – Isolation – Estimation are collapsed into one stage, continuously providing unknown functions estimation.

Before entering in the detail of the NLGA, it is necessary to introduce the concept of the generalized disturbance. As mentioned in this Section, this work deals with generic unknown functions which can be interpreted as:

- $\mathbf{f}_u(\mathbf{x}, t)$ faults affecting the actuators;

- $\mathbf{f}_y(\mathbf{x}, t)$ faults corrupting the sensors;

- $\mathbf{f}_{sys}(\mathbf{x}, t)$ faults, disturbances and unknown parameters directly influencing the plant dynamics.

Furthermore, the following classifications are important to get the generality of the proposed solution. The first division is based on the cardinality of $\mathbf{f}_s$:

- cardinality of $\mathbf{f}_s = 1$: $\mathbf{f}_s$ is a scalar, *i.e.* $\mathbf{f}_s = f$. In this scenario, $\mathbf{f}_s$ is called "**single**" unknown function;

- cardinality of $\mathbf{f}_s > 1$: $\mathbf{f}_s$ is a vector. This scenario covers the so called "**multiple**" unknown functions.

The second grouping is made, only for the multiple unknown functions scenarios, on the contemporaneity. The multiple unknown functions are said to be:

- **non-concurrent** if the system is affected by just one component of $\mathbf{f}_s$ per time;

- **concurrent** when the system is corrupted by more than one component of $\mathbf{f}_s$ at the same time, *i.e.* simultaneously.

The Active Control scheme proposed in this work is quite general and, based on the definition of the Detection and Diagnosis module, allows the representation of three different well known families of control schemes:

- **Active Fault Tolerant Controls**: these control systems is based on the Detection and Isolation module to provide a system's health monitoring function too. In this context, the control actively reacts by exploiting the fault estimation only after the faults (seen as external unknown functions) are detected and isolated. A common aerospace fault scenario is represented by multiple non-concurrent faults (both on actuators and sensors);

- **Indirect Adaptive Controls**: the indirect adaptive controls are control systems able to adapt themselves thanks to the estimation of unknown, possibly time varying, plant parameters. In this control schemes the estimation is always active (it isn't switched on by

any activation signal, and the detection-isolation-estimation functions are collapsed and indivisible). The set of the unknown varying parameters can be seen as scenario of multiple concurrent unknown functions.

- **Active Disturbance Rejection Controls**: this class of controls shares some features with both the Active Fault Tolerant Controls and the Indirect Adaptive Controls. Active Disturbance Rejection systems are based on the estimation of external disturbances (such as faults) that are always present on the system (such as plant parameters). Also this scenario is characterized by the presence of multiple concurrent unknown functions, but, the presence of a Detection and Isolation module is not ruled out: image, as example, an aircraft landing in turbulences and wind shear conditions. The goal is to feedback only the estimation of the wind shear components that overcome a threshold determined by the turbulences intensity. In this way the nominal controller is not fed by pure noisy estimations.

Thanks to the active structure, the Nominal Controller reacts to unknown functions affecting the system by properly exploiting the estimations coming from the Estimation Module. On the other hand, the Estimation Module should provide correct estimations as necessary, but not sufficient condition, to allow a good active reaction (the necessary conditions stay in the nominal controller). In this context, the NonLinear Geometic Approach (NLGA) constitutes a suitable tools for constructing robust estimations.

The next Section describes the basics of the NLGA and the improvements that can be introduced in the case of aerospace systems.

2.1   NLGA based Detection and Diagnosis Module

The Detection and Diagnosis Module, depicted in Figure (2.2), aims to provide the estimation of the selected part of the unknown functions, *i.e.* $\mathbf{f}_s$, by using all the available information. In particular, it can exploit the corrupted output $\mathbf{y}$, the uncorrupted control law $\mathbf{u}$ and the plant model. The Detection and Diagnosis module, designed be the NonLinear Geometric Approach, represents a solution of the following problem.

Problem 1. $\mathbf{f}_s$-**DD Problem**: Take the plant model 2.1 with the associated unknown functions sets $\mathbf{f}$ and $\mathbf{f}_s$. Design, if possible, a Detection and Diagnosis module with inputs $\mathbf{y}$ and $\mathbf{u}$, and output $\hat{\mathbf{f}}_s$ such that $\hat{\mathbf{f}}_s$ asymptotically estimates the function $\mathbf{f}_s$, *i.e.* $\lim_{t \to \infty} \hat{\mathbf{f}}_s = \mathbf{f}_s$. $\square$
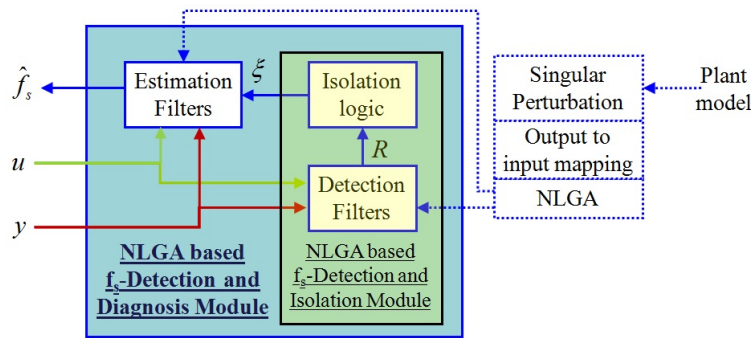
FIGURE 2.2:   NLGA based Detection and Diagnosis Module

Figure 2.2 contains two fluxes of information: the first one (dotted lines) represents the information associated to the knowledge of the mathematical model of the plant whereas the second (continuous lines) indicates the information related to physical signals.

The NonLinear Geometric Approach, based on the knowledge of the plant model (model based technique), provides new variables representing a subsystem of system (2.1) on which the estimation filters are designed. The estimation module contains a bank of ν_s estimation filters, each of them switched-on by its relative activation signal, *i.e.* ξ_i, component of the activation vector $\boldsymbol{\xi}$. Finally, the activation vector $\boldsymbol{\xi}$ is the output of the Detection and Identification Module, also based on the NLGA.

2.1.1 NLGA based Detection and Isolation Technique

The first part of this Section details the standard NonLinear Geometric Approach whereas the second and third parts respectively show how to extend the applicability of the standard NLGA to more interesting scenarios and how to exploit the aerospace model common features to solve real case problems.

2.1.1.1 The standard NLGA based Detection and Isolation Technique

This subsection recalls the standard NLGA, which was formally developed in [40] and generalized by [41], on which both the detection residuals and the estimators design methodology are based.

The NLGA procedure for the solution of Detection and Isolation problem starts by defining two quantities:

- the subsets $\mathbf{f}_s = \{f_1, ..., f_{\nu_s}\} \subseteq \mathbf{f}$;

- the complementary subset $\mathbf{d}_s = \mathbf{f} \setminus \mathbf{f}_s$

The subset $\mathbf{f}_s$ contains all the unknown functions that have to be estimated and, based on the definition of "faults" in Section 1, it can be seen as a set of *generalized faults*, whereas $\mathbf{d}_s$, here called *generalized disturbances*, collects all the remaining unknown functions from which the residual $\mathbf{r}_s$ has to be analytically decoupled, as described below.

This method relies on coordinate changes in the state and output spaces thus allowing to determine new descriptive variables, allowing to determine a sub-system affected only by $\mathbf{f}_s$. In other words, the method provides one observable subsystem which, if it exists, is only affected by $\mathbf{f}_s$, but unaffected by the other components of $\mathbf{f}$ to be decoupled, *i.e.* $\mathbf{d}_s$. For a comprehensive detailed application of the NLGA, referee to [50]. More precisely, the approach consider a nonlinear system model in the form:

$$\begin{cases} \dot{\mathbf{x}} &= \mathbf{g}_0(\mathbf{x}) + \sum_{i=1}^{\ell_u} \mathbf{g}_i(\mathbf{x})\, u_i + \mathbf{l}_s(\mathbf{x})\, \mathbf{f}_s + \mathbf{p}_s(\mathbf{x})\, \mathbf{d}_s \\ \mathbf{y} &= \mathbf{h}(\mathbf{x}) \end{cases} \tag{2.2}$$

in which $\mathbf{x} \in \mathcal{X} \subset \mathbb{R}^{\ell_n}$ is the state vector, $\mathbf{u}(t) \in \mathbb{R}^{\ell_u}$ is the control input vector, $\mathbf{f}_s(t) \in \mathbb{R}^{\ell_s}$ is the s-th unknown function set to be estimated, $\mathbf{d}_s(t) \in \mathbb{R}^{\ell_d = n - \ell_s}$ the generalized disturbance vector embedding the remaining unknown function sets to be decoupled, $\mathbf{y} \in \mathbb{R}^{\ell_m}$ the output vector, $\mathbf{n}(\mathbf{x})$, $\mathbf{g}_i(\mathbf{x})$ for $1 \leq i \leq \ell_u$, $\mathbf{l}_s(\mathbf{x}) = \{\mathbf{l}_1, ..., \mathbf{l}_{\nu_s}\}$ and the columns of $\mathbf{p}_s(\mathbf{x})$ are smooth vector fields, and $\mathbf{h}(\mathbf{x})$ is a smooth map. Equation (2.2) implicitly contains the assumption that $\mathbf{y} = \mathbf{h}(\mathbf{x})$, *i.e.* that $\mathbf{f}_y = \mathbf{0}$.

Therefore, if P represents the distribution spanned by the column of $\mathbf{p}_s(\mathbf{x})$, the design of the strategy for the isolation of the generalized faults set $\mathbf{f}_s$ with de–coupling from the generalized disturbance $\mathbf{d}_s$, by means of the considered NLGA [40], is organised as follows:

- computation of Σ_*^P, *i.e.* the minimal conditioned invariant distribution containing P (where P is the distribution spanned by the columns of $\mathbf{p}_s(\mathbf{x})$);

- computation of Ω^*, *i.e.* the maximal observability codistribution contained in $(\Sigma_*^P)^\perp$;

- if $\mathbf{l}_k(\mathbf{x}) \notin (\Omega^*)^\perp \; \forall \, k \in \{1,...,\nu_s\}$, $\mathbf{f_s}$–detectability condition, the generalized faults set is detectable and a suitable change of coordinate can be determined.

The minimal conditioned invariant distribution Σ_*^P can be computed by means of the following recursive algorithm:

$$\begin{cases} S_0 & = \; \bar{P} \\ S_{k+1} & = \; \bar{S}_k + \sum_{i=0}^{\ell_u} \left[\mathbf{g}_i, \bar{S}_k \cap \ker\{d\mathbf{h}\} \right] \end{cases} \tag{2.3}$$

where ℓ_u is the number of inputs, $\bar{S}$ represents the involutive closure of S, $[g, \Delta]$ is the distribution spanned by all vector fields $[g, \tau]$, with $\tau \in \Delta$, and $[g, \tau]$ the Lie bracket of g, τ.

It can be shown that if there exists a $k \geq 0$ such that $S_{k+1} = S_k$, the algorithm (2.3) stops and $\Sigma_*^P = S_k$ [40].

Once Σ_*^P has been determined, Ω^* can be obtained by exploiting the following algorithm:

$$\begin{cases} Q_0 & = \; (\Sigma_*^P)^\perp \cap \operatorname{span}\{d\mathbf{h}\} \\ Q_{k+1} & = \; (\Sigma_*^P)^\perp \cap \sum_{i=0}^{\ell_u} \left[L_{\mathbf{g}_i} Q_k + \operatorname{span}\{d\mathbf{h}\} \right] \end{cases} \tag{2.4}$$

where $L_{\mathbf{g}}\Gamma$ denotes the codistribution spanned by all covector fields $L_{\mathbf{g}}\omega$, with $\omega \in \Gamma$, and $L_{\mathbf{g}}\omega$ the derivative of ω along $\mathbf{g}$.

If there exists an integer k^* such that $Q_{k^*} = Q_{k^*+1}$, Q_{k^*} is indicated as o.c.a. $\left((\Sigma_*^P)^\perp\right)$, where the acronym o.c.a. stands for *observability codistribution algorithm*.

It can be shown that $Q_{k^*} = $ o.c.a. $\left((\Sigma_*^P)^\perp\right)$ represents the maximal observability codistribution contained in $P^\perp$, i.e. Ω^* [40]. Therefore, with reference to the model (2.2), when $\mathbf{l}_k(\mathbf{x}) \notin (\Omega^*)^\perp$ $\forall \, k \in \{1,...,\nu_s\}$, the generalized disturbance $\mathbf{d}_s$ can be decoupled and the generalized faults set $\mathbf{f}_s$ is detectable.

All the conditions above depicted are only "necessary" and nothing can be said about the possibility to create a residual if the following "sufficient" conditions are not verified.

As mentioned above, the application of the NLGA for solving the generalized faults set diagnosis problem, described in [40], is based on a coordinate change in the state space and in the output

space, $\Phi(\mathbf{x})$ and $\Psi(\mathbf{y})$, respectively. They consist in a surjection Ψ_1 and a function Φ_1 such that $\Omega^* \cap \text{span}\{d\mathbf{h}\} = \text{span}\{d(\Psi_1 \circ \mathbf{h})\}$ and $\Omega^* = \text{span}\{d\Phi_1\}$, where:

$$
\begin{cases}
\Phi(\mathbf{x}) &= \begin{pmatrix} \bar{\mathbf{x}}_1 \\ \bar{\mathbf{x}}_2 \\ \bar{\mathbf{x}}_3 \end{pmatrix} = \begin{pmatrix} \Phi_1(\mathbf{x}) \\ \mathbf{H}_2\mathbf{h}(\mathbf{x}) \\ \Phi_3(\mathbf{x}) \end{pmatrix} \\[2em]
\Psi(\mathbf{y}) &= \begin{pmatrix} \bar{\mathbf{y}}_1 \\ \bar{\mathbf{y}}_2 \end{pmatrix} = \begin{pmatrix} \Psi_1(\mathbf{y}) \\ \mathbf{H}_2\mathbf{y} \end{pmatrix}
\end{cases}
\tag{2.5}
$$

are (local) diffeomorphisms, whilst $\mathbf{H}_2$ is a selection matrix, *i.e.* its rows are a subset of the rows of the identity matrix. If the coordinate changes in (2.5) can be found, the "sufficient" conditions are verified and, by using the new (local) state and output coordinates $(\bar{\mathbf{x}}, \bar{\mathbf{y}})$, the system (2.2) is transformed as follows:

$$
\begin{cases}
\dot{\bar{\mathbf{x}}}_1 &= \mathbf{n}_1(\bar{\mathbf{x}}_1, \bar{\mathbf{x}}_2) + \mathbf{g}_1(\bar{\mathbf{x}}_1, \bar{\mathbf{x}}_2)\,\mathbf{u} + \mathbf{l}_{s_1}(\bar{\mathbf{x}})\,\mathbf{f}_s \\
\dot{\bar{\mathbf{x}}}_2 &= \mathbf{n}_2(\bar{\mathbf{x}}) + \mathbf{g}_2(\bar{\mathbf{x}})\,\mathbf{u} + \mathbf{l}_{s_2}(\bar{\mathbf{x}})\,\mathbf{f}_s + \mathbf{p}_{s_2}(\bar{\mathbf{x}})\,\mathbf{d}_s \\
\dot{\bar{\mathbf{x}}}_3 &= \mathbf{n}_3(\bar{\mathbf{x}}) + \mathbf{g}_3(\bar{\mathbf{x}})\,\mathbf{u} + \mathbf{l}_{s_3}(\bar{\mathbf{x}})\,\mathbf{f}_s + \mathbf{p}_{s_3}(\bar{\mathbf{x}})\,\mathbf{d}_s \\
\bar{\mathbf{y}}_1 &= \mathbf{h}_1(\bar{\mathbf{x}}_1) \\
\bar{\mathbf{y}}_2 &= \bar{\mathbf{x}}_2
\end{cases}
\tag{2.6}
$$

with $\mathbf{l}_{s_1}(\bar{\mathbf{x}})$ not identically zero. As described in [40], the subsystem $\bar{\mathbf{x}}_1$ in Equation (2.6) is locally weakly observable and $\bar{\mathbf{x}}_3$ is not directly available for measurements. In particular, the third subsystem, *i.e.* the $\bar{\mathbf{x}}_3$-subsystem, is not present if the whole state $\mathbf{x}$ is measurable.

This transformation can be applied to the system (2.2) if and only if the $\mathbf{f}_s$–detectability condition is satisfied. The system (2.2), in the new reference frame, can be decomposed into three subsystems (2.6) where the first one (the so–called $\bar{\mathbf{x}}_1$–subsystem) is always de–coupled from the disturbance vector $\mathbf{d}_s$ and affected by the generalized faults set $\mathbf{f}_s$ as follows:

$$
\begin{cases}
\dot{\bar{\mathbf{x}}}_1 &= \mathbf{n}_1(\bar{\mathbf{x}}_1, \bar{\mathbf{y}}_2) + \mathbf{g}_1(\bar{\mathbf{x}}_1, \bar{\mathbf{y}}_2)\,\mathbf{u} + \mathbf{l}_{s_1}(\bar{\mathbf{x}}_1, \bar{\mathbf{y}}_2, \bar{\mathbf{x}}_3)\,\mathbf{f}_s \\
\bar{\mathbf{y}}_1 &= \mathbf{h}_1(\bar{\mathbf{x}}_1)
\end{cases}
\tag{2.7}
$$

where, as the state $\bar{\mathbf{x}}_2$ in (2.6) is assumed to be measured, the variable $\bar{\mathbf{x}}_2$ in (2.7) is considered as independent input and denoted with $\bar{\mathbf{y}}_2$. Even if the state $\bar{\mathbf{x}}_3$ isn't available for direct measurements, the detection of $\mathbf{f}_s$ is always guaranteed by observing that, since $\mathbf{l}_{s_1}(\bar{\mathbf{x}})$ is not identically zero, the presence of $\mathbf{f}_s$ can be always find out by designing a filter for the detection of $\mathbf{l}_{s_1}\mathbf{f}_s$.

2.1.1.2 NLGA Applicability Improvement: Output to Input Mapping Technique

The methodology applicability can be extended by removing the hypothesis of the standard NLGA, *i.e.* $\mathbf{f}_y = \mathbf{0}$ and assuming that the state $\mathbf{x}$ is directly available for measurement. In this scenario, the plant dynamics is expressed by:

$$\begin{cases} \dot{\mathbf{x}} &=& \mathbf{n}(\mathbf{x}) + \mathbf{g}(\mathbf{x})\,(\mathbf{u} + \mathbf{f}_u) + \mathbf{l}(\mathbf{x})\,\mathbf{f}_{sys} \\ \mathbf{y} &=& \mathbf{x} + \mathbf{f}_y \end{cases} \tag{2.8}$$

Let's rewrite the dynamics of (2.8) in terms of the output variables by introducing a simple coordinate change $T : \mathbb{R}^{\ell_n} \to \mathbb{R}^{\ell_n}$, $\mathbf{z} = \mathbf{y} = \mathbf{x} + \mathbf{f}_y$:

$$\begin{cases} \dot{\mathbf{z}} &=& \mathbf{n}(\mathbf{z} - \mathbf{f}_y) + \mathbf{g}(\mathbf{z} - \mathbf{f}_y)\,(\mathbf{u} + \mathbf{f}_u) + \mathbf{l}(\mathbf{z} - \mathbf{f}_y)\,\mathbf{f}_{sys} + \dot{\mathbf{f}}_y \\ \mathbf{y} &=& \mathbf{z} \end{cases} \tag{2.9}$$

Even if the (2.9) has been obtained in a straightforward way, the resulting model is not affine with respect to the faults and, as consequence, the NLGA can not be applicable. To overcome this problem, [49] proposes a different coordinate change, from the state to the output variables, which allows to write an unknown functions affine model, thus allowing the application of the standard NLGA procedure.

The scenario of Equation (2.9), in terms of number of potentially concurrent unknown functions versus the number of available information (*i.e.* the number of states and outputs), is really complex and generically not solvable with the standard NLGA. On the other hand, for aerospace systems, taking into account $\mathbf{f}_u$ and $\mathbf{f}_y$ which represent faults and assuming that also $\mathbf{f}_{sys}$ represents only faults, it's not wrong the assumption that the faults, even if multiple, are non-concurrent (aerospace systems are such that the probability of multiple concurrent faults is very low compared to the probability of multiple non-concurrent faults). The scenario, represented by multiple non-concurrent faults, can not describe disturbances because they are concurrent functions always affecting the system, despite the presence of faults.

The procedure proposed in [49] exploits the hypothesis of multiple but non-concurrent faults to associate to the i-th component of $\mathbf{f}_y$, *i.e.* the physical output fault f_{y_i}, a number ν_i of equivalent mathematical faults that are state dependent functions, generally without physical interpretation and with a different time behavior respect to the physical fault f_{y_i}. Following the procedure stated in [49] for modeling the sensor faults, it's possible to introduce $\nu_i \geq 1$ always concurrent mathematical faults, $f^*_{y_{i,k}}(k = 1, ..., \nu_i)$, in place of the physical fault f_{y_i} $\forall i \in \{1, ..., \ell_n\}$. Whenever a physical sensor fault occurs, *i.e.* $f_{y_i} \neq 0$, all associated mathematical faults $f^*_{y_{i,k}}(i = 1, ..., \nu_i)$ will become nonzero.

According to this modeling, in order to detect and isolate the single physical fault on the i-th sensor, it will be sufficient to recognize the occurrence of any (one or more) of its associated mathematical faults. To isolate a given set of faults from the remaining ones, as formalized in [42], for the generic i-th sensor fault, [49] proposes the following modeling procedure:

1. Take the i-th element of $\mathbf{x}$, *i.e.* x_i, and look in the system model for all different (and, in general, nonlinear) expressions $\phi_{i,k}(\mathbf{x}, \mathbf{u})$, involving x_i and such that the model is affine in $\phi_{i,k}(\mathbf{x}, \mathbf{u})$;

2. For each expression $\phi_{i,k}(\mathbf{x}, \mathbf{u})$ found at the step 1, define the fault input $f^*_{y_{i,k}} = \phi_{i,k}(\mathbf{x}, \mathbf{u}) - \phi_{i,k}(\mathbf{x}, \mathbf{u})|_{x_i=y_i}$, i.e., the error induced in the computation of $\phi_{i,k}(\mathbf{x}, \mathbf{u})$ by the use of the measured value y_i in place of the real value x_i, and compute the corresponding fault vector field $\mathbf{l}^*_{i,k}(\mathbf{x})$. Let us denote the number of faults introduced in this way by $\nu_i - 1$. Note that $f^*_{y_{i,k}}$ is, by definition, only affected by a fault of the i-th state sensor (which is consistent with the assumption of non-concurrency), and is zero whenever $f_{y,i} = 0$, *i.e.*, when $x_i = y_i$. As a result of this modeling step, any occurrence of the expression $\phi_{i,k}(\mathbf{x}, \mathbf{u})$ in the system model can be replaced by $\phi_{i,k}(\mathbf{x}, \mathbf{u})|_{x_i=y_i} + f^*_{y_{i,k}}$, and the model is certainly affine in the fault input $f^*_{y_{i,k}}$. Note that the right-hand side of Equation (2.8) will now be only dependent on the variable y_i and not on x_i;

3. Define the further fault input $f^*_{y_{i,\nu_i}} = \dot{x}_i - \dot{y}_i$. The introduction of this additional fault input in the model allows writing also the left-hand side of the i-th system equation in terms of the new variable y_i (with dynamics $\dot{y}_i = \dot{x}_i - f^*_{y_{i,\nu_i}}$). The fault vector field associated to $f^*_{y_{i,\nu_i}}$ is, thus, $\mathbf{l}^*_{i,\nu_i} = -I_i$ (I_i is the i-th column of the identity matrix);

4. If, for two indices j, k, we can write for $\mathbf{l}^*_{i,j} = \alpha(\mathbf{x})\mathbf{l}^*_{i,k}$ some real function $\alpha(\mathbf{x})$, then set $f^*_{i,k} = f^*_{i,k} + \alpha(\mathbf{x})f^*_{i,j}$ and eliminate $f^*_{i,j}$ (vector field $\mathbf{l}^*_{i,k}$ clearly remains the same). With a slight abuse of notation, the symbol ν_i is still used to indicate the final number of mathematical fault inputs corresponding to the i-th state sensor fault.

At this point, when the outputs are taken as new state variables for the system dynamics, the general structure of Equation (2.2) is recovered. The final model, including the effect of all (non-concurrent) faults of actuators and state sensors, is:

$$\begin{cases} \dot{\mathbf{z}} &= \mathbf{g}_0(\mathbf{z}) + \sum_{i=1}^{\ell_u} \mathbf{g}_i(\mathbf{z})(u_i + f_{u_i}) + \sum_{i=1}^{\ell_n} \sum_{j=1}^{\nu_i} \mathbf{l}^*_{i,j}(\mathbf{z}) f^*_{y_{i,j}} + \sum_{i=1}^{\ell_{sys}} \mathbf{l}_i(\mathbf{z}) f_{sys_i} \\ \mathbf{y} &= \mathbf{z} \end{cases} \qquad (2.10)$$

The set of the equivalent mathematical faults associated to the physical output fault f_{y_i} is indicated with $\mathbf{f}^*_{y_i} = \left\{ f^*_{y_{i,j}} \right\}$ with $j \in \{1, ..., \nu_i\}$ whereas the set of all the the equivalent mathematical faults associated to all the output physical faults $\mathbf{f}_y$ is $\mathbf{f}^*_y = \left\{ \mathbf{f}^*_{y_i} \right\}$ with $i \in \{1, ..., \ell_n\}$.

The multiple non-concurrent fault scenario is represented by $\mathbf{f} = \{\mathbf{f}_u \cup \mathbf{f}_{sys} \cup \mathbf{f}_y^*\}$ and contains $\ell_u + \ell_{sys} + \sum_{i=1}^{\ell_n} \nu_i$ elements. The definition of the s-th elements, $\mathbf{f}_s$, is made by following this scheme:

- for the i-th input fault f_{u_i}, $\mathbf{f}_s = f_{u_i}$ and $\mathbf{l}_s = \mathbf{g}_i$;

- for the i-th system fault f_{sys_i}, $\mathbf{f}_s = f_{sys_i}$ and $\mathbf{l}_s = \mathbf{l}_i$;

- for the i-th output fault f_{y_i}, $\mathbf{f}_s = \mathbf{f}_{y_i}^*$ and $\mathbf{l}_s = \left[\mathbf{l}_{y_{i_1}}^*, ..., \mathbf{l}_{y_{i_{\nu_i}}}^* \right]$.

where, the number of element of $\mathbf{l}_s$ is defined as μ_s (that is equal to 1 for input and system faults and ν_i for the output faults).

Introducing the additional assumption of non-concurrency of faults, results into much weaker conditions for $\mathbf{f}_s$-DI than those given in [40]. In particular, the necessary and sufficient condition for non-concurrent $\mathbf{f}_s$-DI (under full state availability and absence of disturbances) is, see [42]:

$$\forall s, \, \forall j \neq s, \, \exists k \in \{1, ..., \mu_s\} : span\{\mathbf{l}_{s_k}\} \nsubseteq \bar{P}_j \quad OR \quad \exists h \in \{1, ..., \mu_j\} : span\{\mathbf{l}_{j_h}\} \nsubseteq \bar{P}_s \quad (2.11)$$

where $\bar{P}_j = span\{\mathbf{l}_{j_1}, ..., \mathbf{l}_{j_{\mu_j}}\}$ and $\bar{P}_j$ denotes the involutive closure of P_j, *i.e.*, the closure of under the Lie bracket operator. Finally, the elements of $\mathbf{l}_s$, the vector field associated to $\mathbf{f}_s$, are indicated by $\mathbf{l}_{s_1}, ..., \mathbf{l}_{s_{\mu_s}}$. Note that, the two conditions in the left- and right-hand sides of the "OR" operator in Equation (2.11) may not hold at the same time. Thus, it may happen that a residual generator exists, that is affected by $\mathbf{f}_s$ and not by $\mathbf{f}_j$, but that any residual affected by $\mathbf{f}_j$ is necessarily also affected by $\mathbf{f}_s$.

2.1.1.3 NLGA Applicability Improvement: the Singular Perturbation Approximation

Aerospace systems such as aircraft, UAV, quadrotors, satellites, ... show interesting common plant features: their dynamics is describes with a six degrees of freedom model, indeed. Three of these six degrees of freedom are relative to the rotational dynamics whereas the second group of three degrees of freedom are representative of the translational dynamics. All of these aerospace systems also show an inherent separation between rotational and translational dynamics where, usually, the rotational dynamics is pretty faster than the translational one.

Systems characterized by dynamics evolving on separated time scales are well represented, by using the Singular Perturbation (SP) theory, as:

$$
\begin{aligned}
\dot{\mathbf{x}}_1 &= \mathbf{n}_1(\mathbf{x}_1, \mathbf{x}_2, \mathbf{u}, \mathbf{f}_u, \mathbf{f}_{sys}, \varepsilon) \\
\varepsilon\dot{\mathbf{x}}_2 &= \mathbf{n}_2(\mathbf{x}_1, \mathbf{x}_2, \mathbf{u}, \mathbf{f}_u, \mathbf{f}_{sys}, \varepsilon) \\
\mathbf{y}_1 &= \mathbf{x}_1 + \mathbf{f}_{y_1} \\
\mathbf{y}_2 &= \mathbf{x}_2 + \mathbf{f}_{y_2}
\end{aligned}
\tag{2.12}
$$

where ε is the (small) perturbation parameter. As assumed in the previous Section, all the unknown functions affecting the system are considered as non-concurrent faults.

In order to make clear the final benefit introduced by the Singular Perturbation approximation, the Output to Input mapping procedure is firstly attempted without any approximation:

$$
\begin{aligned}
\dot{\mathbf{z}}_1 &= \tilde{\mathbf{n}}_1(\mathbf{z}_1, \mathbf{z}_2, \mathbf{f}_{y_1}^*, \mathbf{f}_{y_2}^*, \mathbf{u}, \mathbf{f}_u, \mathbf{f}_{sys}, \varepsilon) \\
\varepsilon\dot{\mathbf{z}}_2 &= \tilde{\mathbf{n}}_2(\mathbf{z}_1, \mathbf{z}_2, \mathbf{f}_{y_1}^*, \mathbf{f}_{y_2}^*, \mathbf{u}, \mathbf{f}_u, \mathbf{f}_{sys}, \varepsilon) \\
\mathbf{y}_1 &= \mathbf{z}_1 \\
\mathbf{y}_2 &= \mathbf{z}_2
\end{aligned}
\tag{2.13}
$$

Equation (2.13) shows that both the equivalent output faults $\mathbf{f}_{y_1}^*$ and $\mathbf{f}_{y_2}^*$ are influencing both the dynamics of $\mathbf{z}_1$ and $\mathbf{z}_2$.

Hypothesis 1. The Tikhonov's theorem in [66] is valid even in presence of faults, *i.e.* it's possible to approximate the actual dynamics of the system (2.12) by it's reduced and boundary layer models.

Assuming that the Hypothesis 1 is verified then it's possible to approximate the actual dynamics of the aircraft (2.12) by its reduced and boundary layer models ($\varepsilon = 0$):

$$
\begin{aligned}
\dot{\tilde{\mathbf{x}}}_1 &= \mathbf{n}_1(\tilde{\mathbf{x}}_1, \mathbf{x}_{2_{\mathcal{M}}}, \mathbf{u}, \mathbf{f}_u, \mathbf{f}_{sys}, 0) \\
\boldsymbol{\eta}_2' &= \boldsymbol{\phi}_2(\tilde{\mathbf{x}}_1, \boldsymbol{\eta}_2, \mathbf{u}, \mathbf{f}_u, \mathbf{f}_{sys}, 0) \\
\mathbf{y}_1 &= \tilde{\mathbf{x}}_1 + \mathbf{f}_{y_1} \\
\mathbf{y}_2 &= \mathbf{x}_{2_{\mathcal{M}}} + \boldsymbol{\eta}_2 + \mathbf{f}_{y_2}
\end{aligned}
\tag{2.14}
$$

where $\mathbf{x}_{2_{\mathcal{M}}} = \mathbf{H}\left(\tilde{\mathbf{x}}_1, \mathbf{u}, \mathbf{f}_u, \mathbf{f}_{sys}\right)$ is an isolated root $\mathbf{x}_2$ such that $0 = \mathbf{n}_2(\tilde{\mathbf{x}}_1, \mathbf{x}_2, \mathbf{u}, \mathbf{f}_u, \mathbf{f}_{sys}, 0)$ and $\boldsymbol{\eta}_2 = \mathbf{x}_2 - \mathbf{x}_{2_{\mathcal{M}}}$. The term $\boldsymbol{\eta}_2'$ represents the derivative respect to the "fast" time scale τ, *i.e.* $\boldsymbol{\eta}_2' = \frac{\boldsymbol{\eta}_2}{d\tau} = \frac{\boldsymbol{\eta}_2}{d(t/\varepsilon)}$.

Following the same fault mapping procedure exploited in Section 2.1.1.2, it's possible to rewrite the approximated dynamics in terms of output variables:

$$
\begin{aligned}
\dot{\tilde{\mathbf{z}}}_1 &= \tilde{\mathbf{n}}_1(\tilde{\mathbf{z}}_1, \mathbf{f}_{y_1}^*, \mathbf{u}, \mathbf{f}_u, \mathbf{f}_{sys}, 0) \\
\mathbf{z}_2' &= \tilde{\mathbf{n}}_2(\tilde{\mathbf{z}}_1, \mathbf{z}_2, \mathbf{f}_{y_1}^*, \mathbf{f}_{y_2}^*, \mathbf{u}, \mathbf{f}_u, \mathbf{f}_{sys}, 0) \\
\mathbf{y}_1 &= \mathbf{z}_1 \\
\mathbf{y}_2 &= \mathbf{z}_2
\end{aligned}
\tag{2.15}
$$

Comparing the systems (2.13) and (2.15) it's easy to see how, thanks to the application of the SP, the equivalent mathematical output faults, $\mathbf{f}_{\mathbf{y}_2}^*$ are mapped only in the fast dynamics $\mathbf{z}_2$ thus helping to meet the conditions required by the relaxed NLGA for non-concurrent fault isolation, see Section 2.1.1.2.

Remark 1. Thanks to the Output to Input mapping procedure the systems (2.13) and (2.15) are affine with respect to the unknown functions to be estimated.

The Detection and Isolation based on the singular perturbation approximation is valid only if the Hypothesis 1 is verified, see [47]. In turn, this hypothesis relies on the stability of the approximated system that is strictly related to the implemented control law. In conclusion, in order to make the singular perturbation detection and isolation technique valid, the controller have to guarantee the stability of the system at any time: in absence of faults, during the detection, isolation and estimation transient and during the fault accommodation phase. Section 2.2.2 proposes a stability analysis for an Active Fault Tolerant Control based on Singular Perturbations.

2.1.1.4 Formulations and Solutions of Detection and Isolation Problems

Problem 1 on the Detection and Diagnosis of the generalized faults set $\mathbf{f}_s$ can be solved if all the active components of $\mathbf{f}_s$ can be estimated. This requirement is translated in the Detection and Isolation of the active components of $\mathbf{f}_s$. So, one question arises: what is the maximum level of information about the Detection and the Isolation of (sets of) generalized faults affecting the system (2.2)?

The answer to this question has been provided in [41] and is based on the Set Detection and Isolation procedure, in turn exploiting the NLGA detailed in 2.1.1.1. The solution has been found by the introduction of the so-called "minimal" $\mathbf{f}_{s_i}$–Detection ans Isolation sets (S_i^{min}), *i.e.* subsets of generalized faults, *i.e.* $\mathbf{f}_{s_i} \subset \mathbf{f}_s$, such that:

- $\mathbf{f}_{s_i}$ is a Detection and Isolation set ($\mathbf{f}_s$–DI–set);

- $\mathbf{f}_{s_i}$ does not strictly include any other $\mathbf{f}_s$–DI–set.

where an $\mathbf{f}_s$–DI–sets is defined as a subset $\mathbf{f}_{s_i} \subset \mathbf{f}_s$ such that is possible to find a residual r_i^d affected by each of the components in $\mathbf{f}_{s_i}$ and not affected by any other components in generalized disturbance $\mathbf{d}_{s_i} = \mathbf{d}_s \cup (\mathbf{f}_s \setminus \mathbf{f}_{s_i})$.

For the computation of the list S_{list} of all minimal $\mathbf{f}_s$-DI-sets $S_1^{min}, ..., S_{N_r}^{min}$ for system (2.2), a recursive algorithm, having the structure of a tree exploration, can be devised. The root of the tree corresponds to the trivial $\mathbf{f}_s$-DI-set $\mathbf{f}_s$. The children of each node are all subsets obtained by removing one element from the parent set. The exploration proceeds in depth as far as the current set/node includes at least one generalized fault that can be isolated from its associated generalized disturbance set. When this does not hold anymore, the algorithm steps back to the parent node and explores the other children. When no child allows the prosecution of the search, then the current node necessarily corresponds to a minimal $\mathbf{f}_s$-DI-set.

This thesis introduce a slight modification to the above mentioned algorithm by introducing a new concept that lead to an "recursive" Detection and Isolation based on Estimation. The concept is shown by the following didactic example where $x = (x_1, x_2, x_3)$:

$$
\begin{aligned}
\dot{x}_1 &= n_1(x) + g_1(x)u + l_{1_1}(x)f_1 \\
\dot{x}_2 &= n_2(x) + g_2(x)u + l_{2_1}(x)f_1 + l_{2_2}(x)f_2 + l_{2_3}(x)f_3 \\
\dot{x}_3 &= n_3(x) + g_3(x)u + l_{3_1}(x)f_1 + l_{3_2}(x)f_2 + l_{3_3}(x)f_3 \\
y &= x
\end{aligned}
\tag{2.16}
$$

The first minimal $\mathbf{f}$-DI-set, S_1^{min}, can be intuitively found by observing system (2.16). The first equation can be directly exploited to design a residual for the detection and the isolation of f_1, So, it is straightforward to define $S_1^{min} = \{f_1\}$. On the other hand, the possibility to create a residual sensitive only to f_2 (or f_3) have to be checked by applying the NLGA procedure, as example, by defining $\mathbf{f}_s = \{f_2\}$ and $\mathbf{d}_s = \{f_1, f_3\}$. Even if the necessary conditions are satisfied, this residual may not be found because the sufficiency conditions, listed in Section 2.1.1.1, may not be verified thus leading to the impossibility of finding the needed coordinate change. So, even if the procedure in [41] can find two new minimal sets $S_2^{min} = \{f_2\}$ and $S_3^{min} = \{f_3\}$, if the sufficient conditions are not verified, the second **feasible** minimal set is $S_2^{min} = \{f_2, f_3\}$. The author introduces the concept of Detection and Isolation based on Estimation by observing that, if f_1 can be detected, isolated and also estimated, after the estimation convergence transient, f_1 can be considered a known quantity. With this assumption the sufficiency may be verified by eliminating the quantity f_1 from the generalized disturbance $\mathbf{d}_s$. As example, for the isolation of f_2, the NLGA procedure is now applied on $\mathbf{f}_s = \{f_2\}$ and $\mathbf{d}_s = \{f_3\}$. At the end, the coordinate change can be easier to be found. This new Detection and Isolation concept has been inserted in the algorithm of [41] for the determination of the minimal **feasible** $\mathbf{f}_{s_i}$–DI–sets Detection and Isolation sets, and highlighted in **bold**.

$$\text{Minimal } \textbf{Feasible } \mathbf{f}_s\text{-DI-sets Algorithm}$$

$$L = L_0 = \{\mathbf{l}_1, ..., \mathbf{l}_s\}$$
$$S_{list} = \{0\}$$
$$k = 0$$
$$\textbf{Flag} = \mathbf{X} \quad \% D\&I \, based \, on \, Estimation \, (0 = OFF, \, 1 = ON)$$
$$[S_{list}, N_r] = explore \, (L, S_{list}, k)$$

with

$$function \, [S_{list}, k] = explore \, (L, S_{list}, k)$$
$$k_{loc} = k$$
$$P = span\{\mathbf{d}_s, L_0 \setminus L\}$$
$$if \, \exists \, \mathbf{l}_\sigma \in L : \, span\{\mathbf{l}_\sigma\} \not\subseteq \left[o.c.a. \left((\Sigma_*^P)^\perp \right) \right]^\perp$$
$$\quad for \, \mathbf{l}_i \in L$$
$$\quad [S_{list}, k] = explore \, (L \setminus \mathbf{l}_i, S_{list}, k)$$
$$\quad \textbf{feas}_{\textbf{test}} = \textbf{feasibiltiy} \left(\textbf{o.c.a.} \left((\mathbf{\Sigma}_*^\mathbf{P})^\perp \right) \right)$$
$$\quad if \, (k == k_{loc}).\textbf{AND}. (\textbf{feas}_{\textbf{test}} == \mathbf{1})$$
$$\quad\quad k = k + 1$$
$$\quad\quad S_k^{min} = \{f_j : \mathbf{l}_j \in L\}$$
$$\quad\quad S_{list} = \left\{ S_{list}, S_k^{min} \right\}$$
$$\quad\quad \textbf{if} \, (\mathbf{S_k^{min} \, is \, estimable}).\textbf{AND}.(\textbf{Flag} == \mathbf{1})$$
$$\quad\quad\quad \mathbf{L_0} = \mathbf{L_0} \setminus \mathbf{S_k^{min}}$$
$$\quad\quad\quad \mathbf{L} = \mathbf{L} \setminus \mathbf{S_k^{min}}$$
$$\quad\quad \textbf{end}$$
$$\quad end$$
$$end$$

$$\textbf{function} \, [\textbf{feas}_{\textbf{test}}] = \textbf{feasibiltiy} \, (\mathbf{\Omega}^*)$$
$$\textbf{if} \, \textbf{sufficiency conditions in Section 2.1.1.1 are verified for } \mathbf{\Omega}^*$$
$$\quad \textbf{feas}_{\textbf{test}} = \mathbf{1}$$
$$\textbf{else}$$
$$\quad \textbf{feas}_{\textbf{test}} = \mathbf{0}$$
$$\textbf{end}$$

The set of residuals $\mathcal{R} = \{r_1^d, ..., r_{N_r}^d\}$, with r_i^d designed to detect and isolate the $\mathbf{f}_{s_i}^{min}$–DI–set, provides all the available information about the detection and isolation of (sets of) generalized faults in $\mathbf{f}_s$ for the system (2.2). Finally, the "Minimal **Feasible** $\mathbf{f}_s$-DI-sets Algorithm" can be exploited to solve classical $\mathbf{f}_s$-DI problems.

Problem 2. $\mathbf{f}_s$-**Detection.** Given the system (2.2) with the associated $\mathbf{f}_s$ and $\mathbf{d}_s$. Find, if possible, a dynamic system whose output $r^d \in \{0, 1\}$ is affected by each of the generalized faults in $\mathbf{f}_s$, is not affected by any of the components of $\mathbf{d}_s$ and asymptotically converges to zero whenever all generalized faults in $\mathbf{f}_s$ are zero, no matter what $\mathbf{u}$ is. □

Solution. Apply the "Minimal Feasible $\mathbf{f}_s$-DI-sets Algorithm": if $\cup_{k_1}^{N_r} S_k^{min} = \mathbf{f}_s$ the generalized faults set $\mathbf{f}_s$ is detectable. Furthermore the residual, r^d can be designed as $r^d = \vee_{i=1}^{N_r} r_i^d$ where $r_i^d \in \{0, 1\}$ is designed to detect and isolate S_i^{min} and $\vee$ represents the logical OR operator.

Problem 3. $\mathbf{f}_s$-**Generalized Isolation.** Given the system (2.2) with the associated $\mathbf{f}_s$ and $\mathbf{d}_s$. Find, if possible, ν_s dynamic systems, where ν_s is the cardinality of $\mathbf{f}_s$, whose output $r_i^d \in \{0, 1\}$ is affected by each of the generalized faults in $\mathbf{f}_s$ but one, namely f_i, is not affected by any of the components of $\mathbf{d}_s \cup f_i$ and asymptotically converges to zero whenever all unknown functions in $\mathbf{f}_s \setminus f_i$ are zero, no matter what $\mathbf{u}$ is. □

Solution. Apply the "Minimal Feasible $\mathbf{f}_s$-DI-sets Algorithm": if $\forall i \in \{1, ..., n\}$ $S_i = \{\mathbf{f}_s \setminus f_i\}$ can be expressed as $S_i = \cup_{k=1}^{N_r} \alpha_k S_k^{min}$ with $\alpha_k \in \{0, 1\}$, then a set of n residual $r_{gen_i}^d$ can be designed ("generalized" residual set). Furthermore each $r_{gen_i}^d$ is obtained as $r_{gen_i}^d = \vee_{k=1}^{N_r} \alpha_k r_k^d$ where $r_k^d \in \{0, 1\}$ is designed to detect and isolate S_k^{min} and $\vee$ represents the logical OR operator.

Problem 4. $\mathbf{f}_s$-**Dedicated Isolation (or concurrent $\mathbf{f}_s$-Isolation).** Given the system (2.2) with the associated $\mathbf{f}_s$ and $\mathbf{d}_s$. Find, if possible, ν_s dynamic systems whose output $r_i^d \in \{0, 1\}$ is affected only by f_i, the i-th component of $\mathbf{f}_s$, is affected neither by any other component of $\mathbf{f}_s$ nor by the components of $\mathbf{d}_s$, and asymptotically converges to zero whenever the function f_i is zero, no matter what $\mathbf{u}$ is. □

Solution. Apply the "Minimal Feasible $\mathbf{f}_s$-DI-sets Algorithm": if $\forall i \in \{1, ..., n\}$ $S_i^{min} = \{f_i\}$, then a set of n residual $r_{ded_i}^d$ can be designed ("dedicated" residual set). Furthermore each $r_{ded_i}^d$ is obtained as $r_{ded_i}^d = r_i^d$ where $r_i^d \in \{0, 1\}$ is designed to detect and isolate S_i^{min}.

Problem 5. **Non-concurrent $\mathbf{f}_s$ Isolation.** Given the system (2.2) with the associated $\mathbf{f}_s$ and $\mathbf{d}_s$. Find, if possible, a residuals generator that is able to detect and isolate any single function f_i, $i = 1, ..., \nu_s$, from the other functions f_k, $k \neq i$, and the disturbances $\mathbf{d}_s$.

Solution. Apply the "Minimal Feasible $\mathbf{f}_s$-DI-sets Algorithm" and if for each couple of unknown functions f_i and f_k, there always exists a minimal $\mathbf{f}_s$-DI-set, S_i^{min}, that includes f_i but not f_k, then a set of $\sigma \leq n$ residuals r_{nc}^d can be designed, where the single $r_{nc_i}^d$ is relative to the minimal set S_i^{min}. This solution is classified, see [52], as "strong" isolation whereas, the counterpart is called "weak" isolation because the solution if found by selecting also non minimal $\mathbf{f}_s$-DI-sets. The latter isolation solution is said to be *weak* because in a subset–supersets structure, proper of the use of non minimal $\mathbf{f}_s$-DI-sets, an incorrect detection may occurs when some of the residuals relative to one unknown function do not exceed the respective thresholds while the others do.

2.1.2 Detection Residuals

The detection residuals constitute the information base on which the isolation logic creates the activation signals. As required in Problem 2 the detection residuals must be:

- non trivially dependent on $\mathbf{f}_s$;

- trivially dependent on $\mathbf{d}_s$;

- convergent to zero whenever $\mathbf{f}_s = \mathbf{0}$, no matter the behavior of $\mathbf{u}$.

The first two properties are guaranteed if the detection residuals are obtained by following the design procedure explained in Section 2.1.1. In particular, thanks to the NLGA procedure of Section 2.1.1.1, relaxed in Section 2.1.1.2 and approximated in Section 2.1.1.3, it's possible to find a subsystem, namely the $\bar{\mathbf{x}}_1$-subsystem, that matches the two above mentioned requirements:

$$\begin{cases} \dot{\bar{\mathbf{x}}}_\mathbf{1} &= \mathbf{n}_1(\bar{\mathbf{x}}_1, \bar{\mathbf{y}}_2) + \mathbf{g}_1(\bar{\mathbf{x}}_1, \bar{\mathbf{y}}_2)\,\mathbf{u} + \mathbf{l}_{s_1}(\bar{\mathbf{x}}_1, \bar{\mathbf{y}}_2, \bar{\mathbf{x}}_3)\,\mathbf{f}_s \\ \bar{\mathbf{y}}_1 &= \mathbf{h}_1(\bar{\mathbf{x}}_1) \end{cases} \tag{2.17}$$

The detection residuals are obtained by implementing state observers for the nonlinear, non autonomous time varying systems expressed by:

$$\begin{cases} \dot{\bar{\mathbf{x}}}_\mathbf{1} &= \mathbf{n}_1(\bar{\mathbf{x}}_1, \bar{\mathbf{y}}_2) + \mathbf{g}_1(\bar{\mathbf{x}}_1, \bar{\mathbf{y}}_2)\,\mathbf{u} \\ \bar{\mathbf{y}}_1 &= \mathbf{h}_1(\bar{\mathbf{x}}_1) \end{cases} \tag{2.18}$$

The $\bar{\mathbf{x}}_1$-subsystem is generically nonlinear, non autonomous due to the presence of $\mathbf{u}$ and also time varying due to the presence of $\bar{\mathbf{y}}_2$. State observers for this class of nonlinear systems are hard to design and significant efforts have led to remarkable solutions exploiting coordinates changes based on observability concepts, see [67], [68] and [69]. On the other hand, simpler, but only locally applicable, observers can be obtained by copying the structure of Equation (2.18) and adding a feedback term, $\mathbf{K}\left(\hat{\bar{\mathbf{x}}}_1, \mathbf{r}\right)$, properly designed to guarantee the observer stability:

$$\begin{cases} \dot{\hat{\bar{\mathbf{x}}}}_1 &= \mathbf{n}_1(\hat{\bar{\mathbf{x}}}_1, \bar{\mathbf{y}}_2) + \mathbf{g}_1(\hat{\bar{\mathbf{x}}}_1, \bar{\mathbf{y}}_2)\,\mathbf{u} + \mathbf{K}\left(\hat{\bar{\mathbf{x}}}_1, \mathbf{r}\right) \\ \hat{\bar{\mathbf{y}}}_1 &= \mathbf{h}_1\left(\hat{\bar{\mathbf{x}}}_1\right) \\ \mathbf{r} &= \bar{\mathbf{y}}_1 - \hat{\bar{\mathbf{y}}}_1 \end{cases} \tag{2.19}$$

where $\mathbf{r}$ represents the residual. The feedback term $\mathbf{K}\left(\hat{\bar{\mathbf{x}}}_1, \mathbf{r}\right)$ can be designed with the Thau's method or the Raghavan's method exploiting the first stability method of Lyapunov, see [70] and [71]. A special case, very attractive from the practical implementation point of view, is represented by a directly measurable $\bar{\mathbf{x}}_1$, *i.e.* $\bar{\mathbf{y}}_1 = \bar{\mathbf{x}}_1$. In this case, it's possible to design a

filter, that differs from an observer on the use of the $\bar{\mathbf{y}}_1$ in the differential equation:

$$
\begin{cases}
\dot{\hat{\bar{\mathbf{x}}}}_1 & = \mathbf{n}_1(\bar{\mathbf{y}}_1, \bar{\mathbf{y}}_2) + \mathbf{g}_1(\bar{\mathbf{y}}_1, \bar{\mathbf{y}}_2)\,\mathbf{u} + \mathbf{Kr} \\
\hat{\bar{\mathbf{y}}}_1 & = \hat{\bar{\mathbf{x}}}_1 \\
\mathbf{r} & = \bar{\mathbf{y}}_1 - \hat{\bar{\mathbf{y}}}_1
\end{cases}
\tag{2.20}
$$

For the filter in Equation (2.20) the feedback matrix $\mathbf{K}$ can be designed with standard linear tools by observing that the residual dynamics is:

$$
\dot{\mathbf{r}} = \mathbf{l}_{s_1}(\bar{\mathbf{x}}_1, \bar{\mathbf{y}}_2, \bar{\mathbf{x}}_3)\,\mathbf{f}_s - \mathbf{Kr}
\tag{2.21}
$$

where the stability of the residual origin, $\mathbf{r} = \mathbf{0}$, in absence of $\mathbf{f}_s$ is guaranteed by $\mathbf{K} > 0$.

Anyway, regardless the design technique, the detection observers based on the NLGA have some interesting commonalities:

- are **analytically decoupled** from whatever has been considered as a generalized disturbance, *i.e.* $\mathbf{d}_s$. This aspect, of huge theoretical importance, guarantee no disturbance robustness issues;

- have **reduced orders**. The subsystem's state $\bar{\mathbf{x}}_1 \in \mathcal{X}_1 \subseteq \mathcal{X} \subset \mathbb{R}^{\ell_n}$, indeed. The reduction of the model order may be associated to a reduction of the number of the involved model parameters, thus leading to an alleviation of the parameter uncertainty robustness issues;

- have **reduced implementability issues**: if the cardinality of $\mathbf{f}_s = 1$ it's possible to select and use just one scalar component of $\bar{\mathbf{x}}_1$.

The last step consists in the conversion from analog to digital values of the residual vector $\mathbf{r}$, *i.e.* $\mathbf{r} \to \mathbf{r}^d$. To this purpose several evaluation functions are available in literaute, see [52] and [72], and some of them are recalled here:

- Instantaneous value of the residual norm

$$
J_r(t) = ||\mathbf{r}(t)||
\tag{2.22}
$$

- The average value of the residual vector norm over a time interval $[t - T, t]$

$$
J_r(t) = \frac{1}{T} \int_{t-T}^{t} ||\mathbf{r}(\tau)|| d\tau
\tag{2.23}
$$

- The truncated root-mean-square which measures the average energy over a time interval $[t - T, t]$

$$
J_r(t) = \frac{1}{T} \int_{t-T}^{t} ||\mathbf{r}(\tau)||^2 d\tau
\tag{2.24}
$$

The threshold value for each of the above residual evaluation functions can be selected as:

$$J_{th} = \sup_{\mathbf{f}_s=\mathbf{0},\, \mathbf{d}_s \in \mathcal{D}} J_r \tag{2.25}$$

where $\mathcal{D}$ the set of allowable disturbances. Based on the thresholds and the evaluation functions, the occurrence $\mathbf{f}_s$ can be detected and isolated by using the following decision logic:

$$r^d = \begin{cases} 0 & if \quad J_r(t) \leq J_{th} \\ 1 & if \quad J_r(t) > J_{th} \end{cases} \tag{2.26}$$

2.1.3 Isolation Logic

The isolation logic constitutes a module, inside the Detection and Isolation system, whose inputs and outputs respectively are the digital residuals set, $\mathcal{R}$, and the activation (vectorial) signal, $\boldsymbol{\xi}$.

Before introducing the structure of the Isolation Logic module it's important to answer to the following question: when is the Isolation Logic necessary?

Let's imagine that Problem 4, the $\mathbf{f}_s$-Dedicated Isolation problem, can be solved. Than, there exist a residual set $\mathcal{R}$ such that all the residual subsets $\boldsymbol{\Omega}_i$ have not common elements. In this scenario, each digital residual r_i^d is responsible of the activation of the associated estimator and the isolation logic is not needed (the isolation logic is straightforward). Otherwise, in any other situation where the detection is possible, an isolation logic is required.

After the application of the "Minimal Feasible $\mathbf{f}_s$-DI-sets Algorithm", the construction of analog residuals and their conversion to digital values, all the information about the detectabiltiy and the isolability of (set of) generalized faults in $\mathbf{f}_s$ is contained in the set of residuals $\mathcal{R} = \{r_1^d, ..., r_{N_r}^d\}$. Such information can be completely summarized by a *residual matrix*, *i.e.* a binary matrix RM whose entry $RM(i,j)$ is "1" if the unknown function f_i is in the minimal $\mathbf{f}_s$-DI-set S_j^{min}, or, equivalently, if f_i affect the corresponding residual r_j.

Remark 2. The definition of the residual matrix RM only relies on the knowledge of the system vector fields, which are sufficient to compute all minimal $\mathbf{f}_s$-DI-set, and is therefore independent of the particular residual basis $\mathcal{R}$. This means that the whole analysis can be performed without the need of actually designing the specific residual generators.

Consider now the special case of non-concurrent generalized faults in $\mathbf{f}_s$ and imagine that a solution to the Problem 5, the non-concurrent $\mathbf{f}_s$ Isolation Problem, exists. In this case, the computation of the whole set of residuals $\mathcal{R} = \{r_1^d, ..., r_{N_r}^d\}$, of cardinality N_r, is not required, in general, to solve the problem. In fact, it can be shown that a number σ, with $\lceil \log_2 \nu_s \rceil \le \sigma \le \nu_s$, where ν_s is the cardinality of $\mathbf{f}_s$, of suitably chosen residuals is always sufficient to weakly solve the Problem 5, see [49].

2.1.4 Estimation Filters

The last component of the $\mathbf{f}_s$-DD module is represented by a bank of Estimation Filters, each on them dedicated to one, detected and isolated, component of $\mathbf{f}_s$, *i.e.* f_i. The inputs of this bank of filters are: three physical channels, *i.e.* the inputs $\mathbf{u}$, the outputs $\mathbf{y}$ and the activation signal $\boldsymbol{\xi}$, and one non-physical channel providing the structure of the estimation filter (NLGA).

It's convenient to exploit the structure of an $\bar{\mathbf{x}}_1$-subsystem, identified by the NLGA procedure, also to develop the estimation filters and, in particular:

- In case of non-concurrent generalized faults, the estimator can be designed on the $\bar{\mathbf{x}}_1$-subsystem obtained by only decoupling the generalized disturbance $\mathbf{d}_s$;

- In case of concurrent generalized faults, the estimator should be designed on the $\bar{\mathbf{x}}_1$-subsystem decoupled from $\mathbf{d}_{s_i}$, *i.e.* exactly the same exploited for the Detection and the Isolation of the generalized fault f_i.

Estimation filters can be designed by adopting several techniques and a rich literature is available. The need of estimation of diverse kind of generalized faults (parameters variation, faults, exogenous disturbances, . . .) has led to the use of different type of estimation algorithms. This work utilizes the following three methods:

- **Least Squares with forgetting factor**: it is a very light algorithm, particularly suitable for the estimation of unknown constants;

- **Radial Basis Functions Neural Network**: this method has an higher computational burden but is very useful for the estimation of state–functions;

- **Sliding Mode**: the last technique is characterized by a low computational burden and is indicated for the estimation of generic time–functions.

Each of the following three methods relies on the successive hypothesis:

- the $\bar{\mathbf{x}}_1$–subsystem is independent from the $\bar{\mathbf{x}}_3$ state components;

- $\bar{\mathbf{y}}_1 = \bar{\mathbf{x}}_1$;

- the following relation holds [54]:

$$\dot{\bar{\mathbf{y}}}_1(t) = \mathbf{M}_1(t) \cdot f_i + \mathbf{M}_2(t) \tag{2.27}$$

where $\mathbf{M}_1(t)$ and $\mathbf{M}_2(t)$ can be computed for each time instant, since they are functions just of input and output measurements, in particular:

$$
\begin{aligned}
\mathbf{M}_1(t) &= \mathbf{l}_{s_1}\left(\bar{\mathbf{y}}_1, \bar{\mathbf{y}}_2\right) \\
\mathbf{M}_2(t) &= \mathbf{n}_1\left(\bar{\mathbf{y}}_1, \bar{\mathbf{y}}_2\right) + \mathbf{g}_1\left(\bar{\mathbf{y}}_1, \bar{\mathbf{y}}_2\right)\mathbf{u}
\end{aligned}
\tag{2.28}
$$

The relation (2.27) describes the general form of the system under diagnosis.

2.1.4.1 Least Squares with forgetting factor

With reference to (2.7), the Least Squares with forgetting factor estimator can be designed if the condition in [40] are satisfied and the generalized fault f_i is a step function of the time, hence if f_i can be seen as a constant parameter to be estimated.

Hypothesis 2. The signal $\mathbf{M}_1(t)$ has the following two properties:

1. $\mathbf{M}_1(t) \in \mathcal{L}_\infty$, *i.e.* there exist a positive finite real $M \in \mathbb{R}$ such that

$$
M = \sup_{t \geq 0} ||\mathbf{M}_1(t)||
\tag{2.29}
$$

2. $\mathbf{M}_1(t)$ is Persistently Exciting in $\mathbb{R}$ with a level of excitation $\alpha_0 > 0$, *i.e.* $\forall t > 0$ there exists constants $\alpha_1 > 0$ and $T_0 > 0$ such that:

$$
\alpha_0 \leq \frac{1}{T_0}\int_t^{t+T_0}\breve{\mathbf{M}}_1^T(\tau)\breve{\mathbf{M}}_1(\tau)d\tau \leq \alpha_1
\tag{2.30}
$$

Under these conditions, the design of the adaptive filter is achieved, with reference to the system model (2.27), in order to provide an estimation $\hat{f}_i(t)$, which asymptotically converges to the magnitude of the unknown f_i.

The proposed adaptive filter is based on the least–squares algorithm with forgetting factor [5], and it is described by the following adaptation law:

$$
\begin{aligned}
\dot{P} &= \beta\,P - \tfrac{1}{m}P\,\breve{\mathbf{M}}_1^T\,\breve{\mathbf{M}}_1\,P & \mathbf{P}\,(0) &= P_0 > 0 \\
\dot{\hat{f}}_i &= P\,\breve{\mathbf{M}}_1^T\,\boldsymbol{\epsilon} & \hat{f}_i\,(0) &= 0
\end{aligned}
\tag{2.31}
$$

with the following equations representing the output estimation, and the corresponding normalised estimation error:

$$
\begin{aligned}
\hat{\bar{\mathbf{y}}}_1 &= \breve{\mathbf{M}}_2 + \breve{\mathbf{M}}_1\,\hat{f}_i + \lambda\,\breve{\bar{\mathbf{y}}}_1 \\
\boldsymbol{\epsilon} &= \tfrac{1}{\lambda m}\left(\bar{\mathbf{y}}_1 - \hat{\bar{\mathbf{y}}}_1\right)
\end{aligned}
\tag{2.32}
$$

where all the involved variables of the adaptive filter are scalar. In particular, $\lambda > 0$ is a parameter related to the bandwidth of the filter, $\beta \geq 0$ is the forgetting factor and $m =$

$1 + \breve{\mathbf{M}}_1^T \breve{\mathbf{M}}_1$ is the normalisation factor of the least–squares algorithm. Moreover, the proposed adaptive filter adopts the signals $\breve{\mathbf{M}}_1$, $\breve{\mathbf{M}}_2$, $\breve{\mathbf{y}}_{\mathbf{1s}}$ which are obtained by means of a low–pass filtering of the signals $\mathbf{M}_1$, $\mathbf{M}_2$, $\bar{\mathbf{y}}_{1s}$ as follows:

$$\begin{cases} \dot{\breve{\mathbf{M}}}_{\mathbf{1}} & = -\lambda \breve{\mathbf{M}}_1 + \mathbf{M}_1, \qquad \breve{\mathbf{M}}_1(0) = 0 \\ \dot{\breve{\mathbf{M}}}_{\mathbf{2}} & = -\lambda \breve{\mathbf{M}}_2 + \mathbf{M}_2, \qquad \breve{\mathbf{M}}_2(0) = 0 \\ \dot{\breve{\mathbf{y}}}_{\mathbf{1}} & = -\lambda \breve{\mathbf{y}}_{\mathbf{1}} + \bar{\mathbf{y}}_{\mathbf{1}}, \qquad \breve{\mathbf{y}}_1(0) = 0 \end{cases} \qquad (2.33)$$

Thus, the considered adaptive filter is described by the systems (2.31), (2.32), and (2.33).

It can be proved that the asymptotic relation between the normalised output estimation error $\boldsymbol{\epsilon}(t)$ and the estimation error $f_i - \hat{f}_i(t)$ is the following:

$$\lim_{t \to \infty} \boldsymbol{\epsilon}(t) = \lim_{t \to \infty} \frac{\breve{\mathbf{M}}_1(t)}{m} \left(f_i - \hat{f}_i(t) \right) \qquad (2.34)$$

Moreover, it can be proved that the adaptive filter described by the relations (2.31), (2.32), and (2.33) provides an estimation $\hat{f}_i(t)$ that asymptotically converges to the magnitude of the step fault f_i. The proofs are similar to those of [54] and have been omitted here.

Particular interest has been posed on the study of this algorithm for the case of scalar $\bar{\mathbf{y}}_1$, namely $\bar{y}_1$, because of its reduced computational burden. In the following the stability of this algorithm is analytically proved.

Let's start reviewing the filter equation:

$$\dot{\bar{y}}_1(\tau) = M_1(\tau) f_i + M_2(\tau) \qquad (2.35)$$

Add and subtract the quantity $\lambda \bar{y}_1(\tau)$, with $\lambda > 0$, and obtain:

$$\dot{\bar{y}}_1(\tau) + \lambda \bar{y}_1(\tau) = \lambda \bar{y}_1(\tau) + M_1(\tau) f_i + M_2(\tau) \qquad (2.36)$$

Apply now the Laplace operator $x(s) = \mathcal{L}\left[x(\tau)\right]$:

$$s\bar{y}_1(s) + \lambda \bar{y}_1(s) = \lambda \bar{y}_1(s) + M_1(s) f_i + M_2(s) \qquad (2.37)$$

where the function f_i is constant. Define now the *filtered* state $x_1(s)$ as:

$$\begin{aligned} x_1(s) & = \frac{1}{s+\lambda} \frac{1}{\lambda} \left[\lambda^2 \bar{y}_1(s) + \lambda M_1(s) f_i + \lambda M_2(s) \right] = \\ & = \frac{1}{\lambda} \left[\lambda \frac{\lambda}{s+\lambda} \bar{y}_1(s) + \frac{\lambda}{s+\lambda} M_1(s) f_i + \frac{\lambda}{s+\lambda} M_2(s) \right] \end{aligned} \qquad (2.38)$$

Observing the right side of this equation, it is easy to recognize the three terms listed in (2.33). Finally, by applying the inverse Laplace transform, the model becomes:

$$x_1(\tau) = \frac{1}{\lambda}\left[\lambda\breve{\ddot{y}}_1(\tau) + \breve{M}_1(\tau)f_i + \breve{M}_2(\tau)\right] \qquad (2.39)$$

It is possible to generate an *estimated* version of $x_1(\tau)$, *i.e.* $\hat{x}_1(\tau)$:

$$\hat{x}_1(\tau) = \frac{1}{\lambda}\left[\lambda\breve{\ddot{y}}_1(\tau) + \breve{M}_1(\tau)\hat{f}_i + \breve{M}_2(\tau)\right] \qquad (2.40)$$

The normalized estimation error is defined as

$$\epsilon = \frac{1}{1+\breve{M}_1^2}[x_1 - \hat{x}_1] = \frac{\breve{M}_1}{1+\breve{M}_1^2}\frac{1}{\lambda}\left[f_i - \hat{f}_i\right] = -\frac{\breve{M}_1}{1+\breve{M}_1^2}\frac{1}{\lambda}e_{f_i} \qquad (2.41)$$

where $e_{f_i} = \hat{f}_i - f_i$ represents the generalized fault estimation error. By assuming f_i as a constant, the time derivative of the estimation error is $\dot{e}_{f_i} = \dot{\hat{f}}_i - \dot{f}_i = \dot{\hat{f}}_i$. Recall now the second equation of (2.31):

$$\dot{\hat{f}}_i = P\breve{M}_1\epsilon \qquad \hat{f}_i(t_0) = 0 \qquad (2.42)$$

where t_0 is the time instant the estimator is switched-on by the activation signal. Substitute (2.41) in (2.42) to obtain:

$$\dot{e}_{f_i} = \dot{\hat{f}}_i = -P\frac{\breve{M}_1^2}{1+\breve{M}_1^2}\frac{1}{\lambda}e_{f_i}$$
$$e_{f_i}(t_0) = -f_i \qquad (2.43)$$

Let's introduce a new variable, $z = P^{-1}$, and rewrite the P dynamic equation (the first of (2.31)) in terms of z:

$$\dot{z} = -\beta z + \frac{1}{\lambda}\frac{\breve{M}_1^2}{1+\breve{M}_1^2} \qquad z(t_0) > 0 \qquad (2.44)$$

It can be easily proved that a positive real constant, z_{MAX}, exists such that $0 < z(\tau) < z_{MAX}$ $\forall\tau \geq t_0$: the proof is straightforward because the system is linear and the input is unlimited bounded.

Remark 3. From the Hypothesis 2 and from the boundedness of $z(\tau)$ is straightforward to see that the continuous signal $\frac{1}{z(\tau)\lambda}\frac{\breve{M}_1^2(\tau)}{1+\breve{M}_1^2(\tau)} : \mathbb{R} \to \mathbb{R}$ is Persistently Exciting (PE) in $\mathbb{R}$ with a level of excitation $\alpha_0 > 0$, *i.e.* there exists a constant $T_0 > 0$ such that:

$$\alpha_0 T_0 \leq \int_\tau^{\tau+T_0}\frac{1}{z(\xi)\lambda}\frac{\breve{M}_1^2(\xi)}{1+\breve{M}_1^2(\xi)}d\xi \qquad (2.45)$$

The differential equation (2.43) can be formally solved leading to the following expression:

$$e_{f_i}(\tau) = e_{f_i}(t_0)e^{-\frac{1}{\lambda}\int_{t_0}^\tau \frac{1}{z(\xi)}\frac{\breve{M}_1^2(\xi)}{1+\breve{M}_1^2(\xi)}d\xi} \qquad (2.46)$$

which, thanks to the PE property stated in Remark 3, give the following inequality:

$$e_{f_i}(\tau) \; = \; e_{f_i}(t_0) \, e^{-\frac{1}{\lambda}\int_{t_0}^{\tau}\frac{1}{z(\xi)}\frac{\breve{M}_1^2(\xi)}{1+\breve{M}_1^2(\xi)}d\xi} \le e_{f_i}(t_0) \, e^{-\alpha_0(\tau-t_0)} \qquad \forall \tau \ge t_0 \qquad (2.47)$$

which implies the exponential stability of the estimation error origin.

2.1.4.2   Radial Basis Functions

There are cases where the isolated generalized fault f_i can be conveniently represented by a function of states $\mathbf{x}$ and inputs $\mathbf{u}$, such as when f_i actually is a input-state–function or when a generic time behavior can be easily represented in term of simpler (at most constant) input and state–function. To this aim the Radial Basis Function Neural Network seems to be particularly suitable, and since it does not require any a priori information on the f_i internal model, it posses universal approximation capabilities [73].

The continuous function, f_i, is approximated by the RBF-NN:

$$f_i = \mathbf{W}^*\boldsymbol{\varphi}(\boldsymbol{v}) + e \qquad (2.48)$$

where $\boldsymbol{v} \in \mathcal{D} \subseteq \mathcal{Z}$ represents a vector in the space $\mathcal{Z} := \{\mathbf{z} = (\mathbf{x}, \mathbf{u})\}$, $\mathbf{W}^*$ is an unknown but constant optimal weight matrix, $\boldsymbol{\varphi} = [\varphi_1, ..., \varphi_N]^T$ is the radial basis function vector of N components and e is an approximation error of the function f_i due to the number and type of the selected RBFs.

In this paper, the RBFs are assumed to be modeled as Gaussian functions as follows:

$$\varphi_k(\boldsymbol{v}) = \exp\left(-\frac{||\boldsymbol{v}-\boldsymbol{v}_k||^2}{\sigma_k^2}\right) \qquad (2.49)$$

where $\boldsymbol{v}_{k_s}$ and σ_{k_s} respectively are the center and the width of the k–th radial basis function.

The vector $\mathbf{W}^*$ is chosen as the value of $\mathbf{W}$ that minimizes the distance between f_i and $\mathbf{W}\boldsymbol{\varphi}$ over all $\boldsymbol{v}$ in some compact learning domain $\mathcal{D}$, subject to the restriction that $\mathbf{W}^*$ belongs to a compact, convex region $\mathcal{M}_{\mathbf{W}} \subset \mathbb{R}^q$; *i.e.*:

$$\mathbf{W}^* := \arg\min_{\mathbf{W}} |f_i(\boldsymbol{v}) - \mathbf{W}\boldsymbol{\varphi}(\boldsymbol{v})| \qquad (2.50)$$

As stated in [74], given the continuous function f_i, for any $\varepsilon > 0$ there are: a positive integer N, N real positive constants $\sigma_k \in \mathbb{R}$ and N vectors $\boldsymbol{v}_k \in \mathcal{D}$, which are independent of f_i for $k = 1, ..., N$, and $1 \times N$ constant matrix $\mathbf{W}^*$, defined as in (2.50), such that:

$$|f_i(\boldsymbol{v}) - \mathbf{W}^*\boldsymbol{\varphi}(\boldsymbol{v})| < \varepsilon \qquad (2.51)$$

holds for all $\boldsymbol{v} \in \mathcal{D}$. In the development of the adaptive law, the parameter estimate vector $\hat{\mathbf{W}}$ is also restricted within $\mathcal{M}_{\mathbf{W}}$, using a projection algorithm. By doing so, we avoid any numerical problems that may otherwise arise due to very large parameter values. More importantly, the projection algorithm prevents parameter drift, a phenomenon that may occur with standard adaptive laws in the presence of modeling uncertainty [75], [76] and [77]. One of the problems associated with the projection algorithm is the selection of an appropriate region $\mathcal{M}_{\mathbf{W}}$ in the parameter space $\mathbb{R}^q$. In general, $\mathcal{M}_{\mathbf{W}}$ should be selected such that it contains the "optimal" parameter vector $\mathbf{W}^*$, which is the reason $\mathbf{W}^*$ is restricted within the region $\mathcal{M}_{\mathbf{W}}$ in (2.50). This restriction may, of course, undermine the approximation power of $\hat{f}_i$ by increasing the modeling error e; however, by choosing the "size" of $\mathcal{M}_{\mathbf{W}}$, sufficiently large, the increase will be negligible. Intuitively, the idea is to restrain the parameter estimation vector $\mathbf{W}$ from drifting to instability, and at the same time, make sure the parameters estimates $\hat{\mathbf{W}}(t)$ are not restrained to a level where they are prevented from evolving toward "optimal" subregions of the parameter space. Starting from (2.27), an estimation filter based on the NLGA and RBF-NN can be modeled in the following form:

$$
\begin{aligned}
\dot{\bar{\mathbf{y}}}_1(t) &= \mathbf{M}_1(t) f_i + \mathbf{M}_2(t) = \\
&= \mathbf{M}_1(t) \mathbf{W} \boldsymbol{\varphi}(\boldsymbol{v}) + \mathbf{M}_2(t)
\end{aligned}
\tag{2.52}
$$

The vector $\mathbf{W}$ is estimated by the following adaptation law:

$$
\begin{aligned}
\dot{\hat{\bar{\mathbf{y}}}}_1(t) &= \mathbf{M}_1(t) \cdot \hat{f}_i + \mathbf{M}_2(t) + \mathbf{K}\left(\bar{\mathbf{y}}_1 - \hat{\bar{\mathbf{y}}}_1\right) \\
\dot{\hat{\mathbf{W}}} &= \eta \, \mathbf{D} \, \mathbf{r} \, \boldsymbol{\varphi}^T(\boldsymbol{v}) \\
\hat{f}_i &= \hat{\mathbf{W}} \boldsymbol{\varphi}(\boldsymbol{v})
\end{aligned}
\tag{2.53}
$$

where $\eta > 0$ is the learning ratio, $\mathbf{r} = \bar{\mathbf{y}}_1 - \hat{\bar{\mathbf{y}}}_1$, and the matrix $\mathbf{D}$ is designed to guarantee the stability of the filter when investigated with the first Lyapunov method, see [78].

2.1.4.3 A new algorithm: Least Squares - Sliding Mode

This section presents a new Sliding Mode estimator, based on [79] and [80], which exploits the $\bar{\mathbf{x}}_1$-subsystems designed in the previous section thanks to the NLGA procedure.

This work also implements estimators based on the sliding mode concept because this technique possess the fascinating theoretical property of convergence in finite time. In other words, after the finite time transient due to the initialization, the unknown function f_i is theoretically estimated without time delays. This is a fundamental aspect to correctly face variable faults/disturbances.

Anyway, to the best of author's knowledge, all the estimators based on the sliding mode and available in literature assume that the number of outputs are equal or less than the number of the unknown functions to be estimated. The scenario depicted in (2.27) presents an outputs

$\bar{\mathbf{y}}_1 \in \mathcal{R}^{\ell_{n_1}}$ with $\ell_{n_1} \geq 1$ whereas f_i is just a scalar function. One can be tempted to use just one component of $\bar{\mathbf{y}}_1$, but, in this way, the effort of the NLGA to isolate f_i in the largest $\bar{\mathbf{x}}_1$ is totally lost. So the desire of use of all $\bar{\mathbf{y}}_1$ components has led to a modification of the classical Sliding Mode estimators by introducing the concept of Least Squares. This new algorithm has been called *Least Squares - Sliding Mode Estimator*.

With respect to the generic system (2.27) the following mathematical steps explain the way the new algorithm has been obtained. Starting with (2.27), here recalled:

$$\dot{\bar{\mathbf{y}}}_1(t) \quad = \quad \mathbf{M}_1(t)f_i + \mathbf{M}_2(t) \tag{2.54}$$

let's isolate $\mathbf{M}_1(t)f_i$:

$$\mathbf{M}_1(t)f_i \quad = \quad \dot{\bar{\mathbf{y}}}_1(t) - \mathbf{M}_2(t) \tag{2.55}$$

and multiply the left and right sides of this equation for $\mathbf{M}_1^T(t)$:

$$\mathbf{M}_1^T(t)\mathbf{M}_1(t)f_s \quad = \quad \mathbf{M}_1^T(t)\left[\dot{\bar{\mathbf{y}}}_1(t) - \mathbf{M}_2(t)\right] \tag{2.56}$$

If the Hypothesis 2 is verified, $\mathbf{M}_1(t)$ is persistently exciting and $\mathbf{M}_1^T(t)\mathbf{M}_1(t) > 0 \; \forall t > 0$. So, the inverse $\left[\mathbf{M}_1^T(t)\mathbf{M}_1(t)\right]^{-1}$ is well defined and the following hold:

$$f_i(t) \quad = \quad \left[\mathbf{M}_1^T(t)\mathbf{M}_1(t)\right]^{-1}\left\{\mathbf{M}_1^T(t)\left[\dot{\bar{\mathbf{y}}}_1(t) - \mathbf{M}_2(t)\right]\right\} \tag{2.57}$$

The estimation of f_i is then determined by substituting the unknown value $\bar{\mathbf{y}}_1$ with its estimation obtained with an high order sliding mode algorithm.

$$\hat{f}_i(t) \quad = \quad \left[\mathbf{M}_1^T(t)\mathbf{M}_1(t)\right]^{-1}\left\{\mathbf{M}_1^T(t)\left[\dot{\hat{\bar{\mathbf{y}}}}_1(t) - \mathbf{M}_2(t)\right]\right\} \tag{2.58}$$

For the i-th component of $\bar{\mathbf{y}}_1$, namely $\bar{y}_{1_i}$, the first time derivative, $\dot{\bar{y}}_{1_i}$, is estimated by:

$$\begin{aligned} \dot{z}_0 &= v_0 \\ \dot{z}_1 &= -\lambda_1 sign\left(z_1 - v_0\right) \\ v_0 &= -\lambda_0 \left|z_0 - \bar{y}_{1_i}\right|^{\frac{1}{2}} sign\left(z_0 - \bar{y}_{1_i}\right) + z_1 \\ \dot{\hat{\bar{y}}}_{1_i} &= z_1 \end{aligned} \tag{2.59}$$

where λ_0 and λ_1 are design parameters.

The algorithm merges two concepts: the least squares, exploited to minimize the estimation error, and the sliding mode, exploited to rapidly and in finite time converge to f_i by reaching the sliding surfaces represented by the errors between the actual and the estimated output first time derivative. After the finite time transient, $\hat{\bar{\mathbf{y}}}_1$ theoretically converges to $\dot{\bar{\mathbf{y}}}_1$ (see [80]) and

the algorithm exactly matches a pure Least Squares method with all its benefits and drawbacks, see [81] and [82].

The main problem of the estimator feedback application is the so-called separation problem. The separation principle means that a controller and an observer (estimator) can be separately designed, so that the combined observer-controller output feedback preserves the main features of the controller designed on the hypothesis of fully available state. The separation principle is trivially fulfilled for the proposed estimator. Indeed, the differentiator $\hat{\dot{\mathbf{y}}}_1$ being exact, the only requirements for its implementation are the boundedness of some higher-order derivative of its input and the impossibility of the finite-time escape during the differentiator transient. Hence, the differentiator may be used in almost any feedback. Furthermore it's worth nothing that the differentiator transient may be made arbitrarily short by a proper parameter design, and that the differentiator does not feature peaking effect (see Proposition 4 and the proof of Theorem 5 in [80]).

2.1.5 NLGA based Detection and Diagnosis module: Summary

Section 2.1 contains the main theoretical aspects of this thesis and this summary highlights the most important concepts, benefits and results arising from the use of the NLGA.

The first benefit of the NLGA use is the methodical construction of and $\mathbf{f}_s$-DD module that greatly simplifies the Diagnosis module design process. The NLGA offers the possibility to systematically understand if a generalized fault (or a set of generalized faults) can be detected and eventually isolated. Without these two checks any attempt of estimation is meaningless. Furthermore, the standard NLGA of [40] and extended by [41], has been beyond improved by introducing a feasibility check and by exploiting the singular perturbation technique. Thanks to these advances, the NLGA can solve more and more Detection and Diagnosis problems in aerospace.

The NLGA procedure ends with the determination of two coordinate changes, one in the state-space and the other one in the output-space, that describe the dynamics of a new subsystem, indicated by $\bar{\mathbf{x}}_1$. This subsystem has some interesting properties:

- is analytically decoupled from whatever has been considered as a disturbance, *i.e.* $\mathbf{d}_s$;

- has a reduced order respect to the full state;

- if the cardinality of $\mathbf{f}_s$ is equal to 1, it's possible to select and use just one scalar component of $\bar{\mathbf{x}}_1$.

The first feature is really important because classifies this method as a "robust" detection and isolation scheme, see [3]. More precisely, the decoupling provided by the application of the NLGA leads to an "ideal perfect robustness", *i.e.* the residual is analytically not influenced by the disturbance, no matter what the disturbance is.

The second and the third characteristics imply a reduction of observer oder and a possible decrement of the number of involved parameters. It is an important aspect that makes the results of the NLGA based method attractive for real case applications.

Furthermore, from the estimation point of view, consider various filters each designed to provide the estimation of one different component of $\mathbf{f}_s$. All these estimators are independent and any possible implementation error that affect only one filter doesn't corrupt the remaining estimations. To understand the importance of this feature, try to compare the behavior of this bank of dedicated filters versus a full-order observer that provides an estimation of the same $\mathbf{f}_s$. The latter provides a non-correct estimation, on all components of $\mathbf{f}_s$, when in presence of an error in one constitutive equation.

2.2   Nominal Controller

The last module, the nominal controller, completes the structure of the Active Control scheme proposed in this thesis. The purpose of an active control is the active modification of the nominal control laws when in off-design working conditions. As stated in Section 2 an active controller relies on a good estimation module but, at the same time, also the nominal controller has to properly use the information coming from the estimation module to achieve satisfying control performance. Model based nominal controllers seem to be very suitable in exploiting the estimations that, thanks to the controller structure, can be implemented by a straightforward substitution, indeed.

Aerospace systems share common model features because the nature of the physical plants is the same: they are flying objects subject to external forces and momentums. It's always possible to identify both rotational and translational dynamic and kinematic equations. Furthermore, usual rotational dynamics is faster than the translational one. This is a well known-concept that led to the nested controller structure for aerospace systems, such as nested PID and backstepping. On the other hand the inherent dynamics separation of aerospace plants suggest the design of a controller based on the singular perturbations method. So, these thesis shows how to design controllers exploiting two model based methodologies, *i.e.*:

- Backstepping;

- Singular perturbations.

Finally, each step inside backstepping and composite controller based on singular perturbations have been designed with a common technique that is the Feedback Linearization. In this way, both the controllers and the diagnosis module are designed with the same differential geometry tools.

2.2.1 Backstepping Controller

Many aerospace systems can be described in a *strict feedback form*, where the hypothesis of a fully measurable state has been added:

$$
\begin{aligned}
\dot{\mathbf{x}}_1 &= \mathbf{n}_1\left(\mathbf{x}_1\right) + \mathbf{g}_1\left(\mathbf{x}_1\right)\mathbf{x}_2 + \mathbf{l}_1\left(\mathbf{x}_1\right)\mathbf{f}_{sys} \\
\dot{\mathbf{x}}_2 &= \mathbf{n}_2\left(\mathbf{x}_1, \mathbf{x}_2\right) + \mathbf{g}_2\left(\mathbf{x}_1, \mathbf{x}_2\right)\mathbf{x}_3 + \mathbf{l}_2\left(\mathbf{x}_1, \mathbf{x}_2\right)\mathbf{f}_{sys} \\
&\quad ... \\
\dot{\mathbf{x}}_n &= \mathbf{n}_n\left(\mathbf{x}\right) + \mathbf{g}_n\left(\mathbf{x}\right)\left(\mathbf{u} + \mathbf{f}_u\right) + \mathbf{l}_n\left(\mathbf{x}\right)\mathbf{f}_{sys} \\
\mathbf{y}_1 &= \mathbf{x}_1 + \mathbf{f}_{\mathbf{y}_1} \\
&\quad ... \\
\mathbf{y}_n &= \mathbf{x}_n + \mathbf{f}_{\mathbf{y}_n}
\end{aligned}
\tag{2.60}
$$

where $\mathbf{x} = (\mathbf{x}_1, ..., \mathbf{x}_n) \in \mathcal{R}^{\ell_n}$ represents the state of the system, $\mathbf{u}$ and $\mathbf{f}_u$ respectively are the input and the input fault, $\mathbf{f}_{sys}$ is the unknown function effecting the system dynamics and, finally, $\mathbf{y}_i$ and $\mathbf{f}_{\mathbf{y}_i}$ with $1 \leq i \leq n$ represent the available measurements and sensors faults.

2.2.1.1 Active Backstepping Controller Design Concept

The idea of backstepping is to start with a system which is stabilizable with a known feedback law for a known Lyapunov function, and then to add to its input an integrator. For the augmented system a new stabilizing feedback law is explicitly designed and shown to be stabilizing for a new Lyapunov, and so on ...

Given the system in the strict feedback form (2.60), define a sufficiently smooth reference $\mathbf{x}_{1_R}$ and the state error $\mathbf{e}_1 = \mathbf{x}_1 - \mathbf{x}_{1_R}$. Rewrite the first subsystem in terms of errors:

$$
\dot{\mathbf{e}}_1 = \mathbf{n}_1\left(\mathbf{e}_1 + \mathbf{x}_{1_R}\right) + \mathbf{g}_1\left(\mathbf{e}_1 + \mathbf{x}_{1_R}\right)\mathbf{x}_2 + \mathbf{l}_1\left(\mathbf{e}_1 + \mathbf{x}_{1_R}\right)\mathbf{f}_{sys} - \dot{\mathbf{x}}_{1_R} \tag{2.61}
$$

Step 1. The first step of the design of a backstepping controller stays in the use of $\mathbf{x}_2$ to stabilize the origin of system (2.61) with an output-feedback law $\boldsymbol{\alpha}_1\left(\mathbf{e}_1, \mathbf{x}_{1_R}, \dot{\mathbf{x}}_{1_R}, \mathbf{f}_{sys}\right)$ so that

$$
\frac{\partial V_1}{\partial \mathbf{e}_1}\left(\mathbf{n}_1 + \mathbf{g}_1\,\boldsymbol{\alpha}_1 + \mathbf{l}_1\,\mathbf{f}_{sys} - \dot{\mathbf{x}}_{1_R}\right) < 0 \tag{2.62}
$$

where $V_1\left(\mathbf{e}_1\right)$ is a known Lyapunov function. Note that, $\mathbf{x}_2 = \boldsymbol{\alpha}_1\left(\mathbf{e}_1, \mathbf{x}_{1_R}, \dot{\mathbf{x}}_{1_R}, \mathbf{f}_{sys}\right)$ is achieved only with an error $\mathbf{e}_2 = \mathbf{x}_2 - \boldsymbol{\alpha}_1$, then, the first two equations are:

$$
\begin{aligned}
\dot{\mathbf{e}}_1 &= \mathbf{n}_1\left(\mathbf{e}_1 + \mathbf{x}_{1_R}\right) + \mathbf{g}_1\left(\mathbf{e}_1 + \mathbf{x}_{1_R}\right)\left(\mathbf{e}_2 + \boldsymbol{\alpha}_1\right) + \mathbf{l}_1\left(\mathbf{e}_1 + \mathbf{x}_{1_R}\right)\mathbf{f}_{sys} - \dot{\mathbf{x}}_{1_R} \\
\dot{\mathbf{e}}_2 &= \mathbf{n}_2\left(\mathbf{e}_1 + \mathbf{x}_{1_R}, \mathbf{e}_2 + \boldsymbol{\alpha}_1\right) + \mathbf{g}_2\left(\mathbf{e}_1 + \mathbf{x}_{1_R}, \mathbf{e}_2 + \boldsymbol{\alpha}_1\right)\mathbf{x}_3 + \\
&\quad + \mathbf{l}_2\left(\mathbf{e}_1 + \mathbf{x}_{1_R}, \mathbf{e}_2 + \boldsymbol{\alpha}_1\right)\mathbf{f}_{sys} - \dot{\boldsymbol{\alpha}}_1
\end{aligned}
\tag{2.63}
$$

Step 2. In the second step, $\mathbf{x}_3$ is used to stabilize the origin of $(\mathbf{e}_1, \mathbf{e}_2)$ with a feedback law

$$\boldsymbol{\alpha}_2\left(\mathbf{e}_1, \mathbf{x}_{1_R}, \dot{\mathbf{x}}_{1_R}, \mathbf{e}_2, \boldsymbol{\alpha}_1, \dot{\boldsymbol{\alpha}}_1, \mathbf{f}_{sys}\right) \tag{2.64}$$

To design $\boldsymbol{\alpha}_2$ a second Lyapunov function is constructed:

$$V_2\left(\mathbf{e}_1, \mathbf{e}_2\right) = V_1\left(\mathbf{e}_1\right) + \frac{1}{2}\mathbf{e}_2^T\mathbf{e}_2 \tag{2.65}$$

When $\mathbf{x}_3 = \boldsymbol{\alpha}_2$ the first time derivative $\dot{V}_2$ is:

$$\begin{aligned}
\dot{V}_2 \quad = \quad & \tfrac{\partial V_1}{\partial \mathbf{e}_1}\left(\mathbf{n}_1 + \mathbf{g}_1\,\boldsymbol{\alpha}_1 + \mathbf{l}_1\,\mathbf{f}_{sys} - \dot{\mathbf{x}}_{1_R}\right) + \\
& +\mathbf{e}_2^T\left[\left(\tfrac{\partial V_1}{\partial \mathbf{e}_1}\,\mathbf{g}_1\right)^T + \mathbf{n}_2 + \mathbf{g}_2\,\boldsymbol{\alpha}_2 + \mathbf{l}_2\,\mathbf{f}_{sys} - \dot{\boldsymbol{\alpha}}_1\right]
\end{aligned} \tag{2.66}$$

Recall that the first term was made negative in the first step, so the expression (2.66) can be made negative by choosing, for example:

$$\boldsymbol{\alpha}_2 \,:\, \mathbf{g}_2\,\boldsymbol{\alpha}_2 = -\mathbf{K}_2\mathbf{e}_2 - \left[\left(\frac{\partial V_1}{\partial \mathbf{e}_1}\,\mathbf{g}_1\right)^T + \mathbf{n}_2 + \mathbf{l}_2\,\mathbf{f}_{sys} - \dot{\boldsymbol{\alpha}}_1\right] \tag{2.67}$$

where $\mathbf{K}_2 > 0$. However, also $\boldsymbol{\alpha}_2$ is reached with an error $\mathbf{e}_3 = \mathbf{x}_3 - \boldsymbol{\alpha}_2$, and the actual (2.66) is:

$$\dot{V}_2 \quad = \quad \tfrac{\partial V_1}{\partial \mathbf{e}_1}\left(\mathbf{n}_1 + \mathbf{g}_1\,\boldsymbol{\alpha}_1 + \mathbf{l}_1\,\mathbf{f}_{sys} - \dot{\mathbf{x}}_{1_R}\right) - \mathbf{e}_2^T\mathbf{K}_2\mathbf{e}_2 + \mathbf{e}_2^T\,\mathbf{g}_2\,\mathbf{e}_3 \tag{2.68}$$

Repeat Step 1 and Step 2 for each subsystem until the last one and obtain:

$$\begin{aligned}
\dot{\mathbf{e}}_1 \quad &= \quad \mathbf{n}_1 + \mathbf{g}_1\left(\mathbf{e}_2 + \boldsymbol{\alpha}_1\right) + \mathbf{l}_1\,\mathbf{f}_{sys} - \dot{\mathbf{x}}_{1_R} \\
\dot{\mathbf{e}}_2 \quad &= \quad \mathbf{n}_2 + \mathbf{g}_2\left(\mathbf{e}_3 + \boldsymbol{\alpha}_2\right) + \mathbf{l}_2\,\mathbf{f}_{sys} - \dot{\boldsymbol{\alpha}}_1 \\
& \qquad \ldots \\
\dot{\mathbf{e}}_n \quad &= \quad \mathbf{n}_n + \mathbf{g}_n\left(\mathbf{u} + \mathbf{f}_u\right) + \mathbf{l}_n\,\mathbf{f}_{sys} - \dot{\boldsymbol{\alpha}}_{n-1}
\end{aligned} \tag{2.69}$$

For the last subsystem the associated Lyapunov function is:

$$\begin{aligned}
\dot{V}_n \quad = \quad & \tfrac{\partial V_1}{\partial \mathbf{e}_1}\left(\mathbf{n}_1 + \mathbf{g}_1\,\boldsymbol{\alpha}_1 + \mathbf{l}_1\,\mathbf{f}_{sys} - \dot{\mathbf{x}}_{1_R}\right) - \sum_{i=1}^{n-1}\mathbf{e}_i^T\mathbf{K}_i\mathbf{e}_i + \\
& +\mathbf{e}_n^T\left[\left(\mathbf{e}_{n-1}^T\,\mathbf{g}_{n-1}\right)^T + \mathbf{n}_n + \mathbf{g}_n\left(\mathbf{u} + \mathbf{f}_u\right) + \mathbf{l}_n\,\mathbf{f}_{sys} - \dot{\boldsymbol{\alpha}}_{n-1}\right]
\end{aligned} \tag{2.70}$$

and the physical control law, $\mathbf{u}$, designed to stabilize at the origin the last subsystem, is:

$$\mathbf{u} \,:\, \mathbf{g}_n\,\mathbf{u} = -\mathbf{K}_n\mathbf{e}_n - \left[\left(\mathbf{e}_{n-1}^T\,\mathbf{g}_{n-1}\right)^T + \mathbf{n}_n + \mathbf{g}_n\,\mathbf{f}_u + \mathbf{l}_n\,\mathbf{f}_{sys} - \dot{\boldsymbol{\alpha}}_{n-1}\right] \tag{2.71}$$

thus obtaining:

$$\dot{V}_n \quad = \quad \tfrac{\partial V_1}{\partial \mathbf{e}_1}\left(\mathbf{n}_1 + \mathbf{g}_1\,\boldsymbol{\alpha}_1 + \mathbf{l}_1\,\mathbf{f}_{sys} - \dot{\mathbf{x}}_{1_R}\right) - \sum_{i=1}^{n}\mathbf{e}_i^T\mathbf{K}_i\mathbf{e}_i < 0 \tag{2.72}$$

The controller scheme can be implemented by designing each $\boldsymbol{\alpha}_i$, for $1 \leq i \leq n$ ($\boldsymbol{\alpha}_n = \mathbf{u}$), with the Feedback Linearization technique.

This kind of controller relies on the full state availability and on the possibility to stabilize each state of each subsystem: this implies, for example, that there is no zero dynamics or, at most, the zero dynamics is stable. Anyway, even if the controller can be correctly designed, it's interesting to see how the estimation of $\mathbf{f}_s$ is exploited to make the controller "active". For each virtual control $\boldsymbol{\alpha}_i$ with $1 \leq i \leq n-1$ and the physical control $\mathbf{u}$ the unknown quantities $\mathbf{f}_{sys}$, $\mathbf{f}_y$ and $\mathbf{f}_u$ are substituted by their estimation coming from the Diagnosis Module:

$$
\begin{aligned}
\boldsymbol{\alpha}_1 : \quad \mathbf{g}_1\,\boldsymbol{\alpha}_1 =& \ -\mathbf{K}_1\hat{\mathbf{e}}_1 - \left[\mathbf{n}_1 + \mathbf{l}_1\,\hat{\mathbf{f}}_{sys} - \dot{\mathbf{x}}_{1_R}\right] \\[2mm]
\boldsymbol{\alpha}_i : \quad \mathbf{g}_i\,\boldsymbol{\alpha}_i =& \ -\mathbf{K}_i\hat{\mathbf{e}}_i - \left[\left(\hat{\mathbf{e}}_{i-1}^T\,\mathbf{g}_{i-1}\right)^T + \mathbf{n}_i + \mathbf{l}_i\,\hat{\mathbf{f}}_{sys} - \dot{\boldsymbol{\alpha}}_{i-1}\right] \quad 2 \leq i \leq n-1 \qquad (2.73) \\[2mm]
\mathbf{u} : \quad \mathbf{g}_n\,\mathbf{u} =& \ -\mathbf{K}_n\hat{\mathbf{e}}_n - \left[\left(\hat{\mathbf{e}}_{n-1}^T\,\mathbf{g}_{n-1}\right)^T + \mathbf{n}_n + \mathbf{g}_n\,\hat{\mathbf{f}}_u + \mathbf{l}_n\,\hat{\mathbf{f}}_{sys} - \dot{\boldsymbol{\alpha}}_{n-1}\right]
\end{aligned}
$$

where

$$
\hat{\mathbf{e}}_i \ = \ \mathbf{e}_i - \hat{\mathbf{f}}_{\mathbf{y}_i} \quad 1 \leq i \leq n \qquad (2.74)
$$

2.2.1.2 Stability analysis of the Active BackStepping Control

The nominal stability of this controller can be generally easily proved when:

- the Diagnosis Module fulfill the requirement of the separation principle (no singular perturbation approximation);

- there are not output faults, *i.e.* $\mathbf{f}_y = \mathbf{0}$;

- the controller can be implemented (no unstable zero dynamics).

Let's define the estimation errors as $\mathbf{e}_{\mathbf{f}_u} = \mathbf{f}_u - \hat{\mathbf{f}}_u$ and $\mathbf{e}_{\mathbf{f}_{sys}} = \mathbf{f}_{sys} - \hat{\mathbf{f}}_{sys}$ and rewrite the system (2.69) controlled by (2.73), in presence of estimation errors:

$$
\begin{aligned}
\dot{\mathbf{e}}_1 \ =& \ -\mathbf{K}_1\mathbf{e}_1 + \mathbf{g}_1\,\mathbf{e}_2 + \mathbf{l}_1\,\mathbf{e}_{\mathbf{f}_{sys}} \\
\dot{\mathbf{e}}_2 \ =& \ -\mathbf{K}_2\mathbf{e}_2 + \mathbf{g}_2\,\mathbf{e}_3 - \left(\mathbf{e}_1^T\,\mathbf{g}_1\right)^T + \mathbf{l}_2\,\mathbf{e}_{\mathbf{f}_{sys}} \\
& \qquad \dots \\
\dot{\mathbf{e}}_{n-1} \ =& \ -\mathbf{K}_{n-1}\mathbf{e}_{n-1} + \mathbf{g}_{n-1}\,\mathbf{e}_n - \left(\mathbf{e}_{n-2}^T\,\mathbf{g}_{n-2}\right)^T + \mathbf{l}_{n-1}\,\mathbf{e}_{\mathbf{f}_{sys}} \\
\dot{\mathbf{e}}_n \ =& \ -\mathbf{K}_n\mathbf{e}_n - \left(\mathbf{e}_{n-1}^T\,\mathbf{g}_{n-1}\right)^T + \mathbf{g}_n\,\mathbf{e}_{\mathbf{f}_u} + \mathbf{l}_n\,\mathbf{e}_{\mathbf{f}_{sys}}
\end{aligned} \qquad (2.75)
$$

Stability during the Detection and Isolation process

Take the system (2.75) and rewrite it in the following compact form:

$$
\begin{aligned}
\dot{\mathbf{e}} &= \mathbf{F}\left(\mathbf{e}, \mathbf{x}_{1_R}\right) + \mathbf{G}\,\mathbf{e}_{\mathbf{f}_u} + \mathbf{L}\,\mathbf{e}_{\mathbf{f}_{sys}} \\
&= \mathbf{F}\left(\mathbf{e}, \mathbf{x}_{1_R}\right) + \mathbf{G}^*\mathbf{e_f}
\end{aligned}
\tag{2.76}
$$

where $\mathbf{e} = (\mathbf{e}_1, ..., \mathbf{e}_n)$, $\mathbf{G}^* = [\mathbf{G}\ \mathbf{L}]$ and $\mathbf{e_f} = \left[\mathbf{e}_{\mathbf{f}_u}, \mathbf{e}_{\mathbf{f}_{sys}}\right]^T$.

Hypothesis 3. The function $\mathbf{G}^*$ is piecewise continuous and satisfy a Lipschitz condition and, furthermore, the fault estimation error $\mathbf{e_f}$ is bounded during the detection and isolation transient.

$$
\begin{aligned}
||\mathbf{G}^*\left(\mathbf{e}'\right) - \mathbf{G}^*\left(\mathbf{e}''\right)|| &< L_1 ||\mathbf{e}' - \mathbf{e}''|| \\
||\mathbf{e_f}|| &< L_2
\end{aligned}
\tag{2.77}
$$

for all $\mathbf{e}'$, $\mathbf{e}''$ in some neighborhood U of the origin, $\mathbf{e} = \mathbf{0}$.

Theorem 2.1. *Taken the model* (2.75), *if the Hypothesis 3 is verified, then* $\forall\ d > 0\ \exists\ \delta_1 > 0$ *and* $\delta_2 > 0$ *(both possibly dependent on d) such that if:*

$$
\begin{aligned}
||\mathbf{e}^o|| &< \delta_1 \\
||\mathbf{G}^*\left(\mathbf{e}\right)\mathbf{e_f}|| &< \delta_2 \quad \forall\,||\mathbf{e}|| < d
\end{aligned}
\tag{2.78}
$$

the solution, $\mathbf{e}(t)$, *of the differential equation* (2.113), *satisfying* $\mathbf{e}(0) = \mathbf{e}^o$, *is such that*

$$
||\mathbf{e}(t)|| < d
\tag{2.79}
$$

for all $t > 0$. $\diamond$

Proof The proof is based on the fundamental result of the so called *theorem of global stability* in [83]. Thanks to the controller design procedure, the origin is an equilibrium point for the unperturbed system

$$
\dot{\mathbf{e}} = \mathbf{F}\left(\mathbf{e}, \mathbf{x}_{1_R}\right)
\tag{2.80}
$$

Furthermore, the origin of (2.117) is also locally exponentially stable, see Section 2.2.2.3, Remark 6. Then, a Lyapunov function, $V\left(\mathbf{e}\right) : B_d \rightarrow \mathbb{R}$, $V \in C^1$, exists and, for some some $\mathcal{K}$-class functions $\underline{\alpha}(\cdot), \alpha(\cdot), \bar{\alpha}(\cdot)$ defined in $[0, d)$, it is such that:

$$
\begin{aligned}
\underline{\alpha}(||\mathbf{e}||) &\leq V\left(\mathbf{e}\right) \leq \bar{\alpha}(||\mathbf{e}||) \\
\frac{\partial V}{\partial \mathbf{e}}\mathbf{F}\left(\mathbf{e}, \mathbf{x}_{1_R}\right) &\leq -\alpha(||\mathbf{e}||) \\
&\forall\,||\mathbf{e}|| < d
\end{aligned}
\tag{2.81}
$$

Since the $\frac{\partial V}{\partial \mathbf{e}}$ is C^0, there exists a real number $M > 0$ such that:

$$||\frac{\partial V}{\partial \mathbf{e}}|| \leq M \tag{2.82}$$

for all $\mathbf{e} \in U$. Suppose that $d > 0$ is such that $B_d \subset U$ and let $c > 0$ be such that $c \leq \underline{\alpha}(d)$. Choose δ_2 such that:

$$- \alpha \left(\bar{\alpha}^{-1}(c) \right) + M\delta_2 < 0 \tag{2.83}$$

Let's define

$$\Omega_c = \{\mathbf{e} \in \mathbb{R}^n : V(\mathbf{e}) \leq c\} \tag{2.84}$$

By construction, $\mathbf{e} \in \Omega_c$ implies

$$||\mathbf{e}|| \leq d \tag{2.85}$$

In fact,

$$\underline{\alpha}(||\mathbf{e}||) \leq V(\mathbf{e}) \leq c \tag{2.86}$$

implies

$$||\mathbf{e}|| \leq \underline{\alpha}^{-1}(c) \leq \underline{\alpha}^{-1}(\underline{\alpha}(d)) = d \tag{2.87}$$

Also, at each point $\mathbf{e}$ of the boundary of Ω_c,

$$\alpha(||\mathbf{e}||) \geq \alpha(\bar{\alpha}^{-1}(V(||\mathbf{e}||))) = \alpha(\bar{\alpha}^{-1}(c)) \tag{2.88}$$

As a consequence, at each point $\mathbf{e}$ of the boundary of Ω_c,

$$\frac{\partial V}{\partial \mathbf{e}} \left[\mathbf{F}\left(\mathbf{e}, \mathbf{x}_{1_R}\right) + \mathbf{G}^* \mathbf{e_f} \right] \leq -\alpha(||\mathbf{e}||) + ||\frac{\partial V}{\partial \mathbf{e}}||\delta_2 \leq -\alpha(\bar{\alpha}^{-1}(c)) + M\delta_2 < 0 \tag{2.89}$$

From this, it can be concluded that, for any initial condition in the interior of Ω_c, the solution $\mathbf{e}$ of (2.113) is defined for all $t \geq 0$ and is such that $\mathbf{e}(t) \in \Omega_c$ for all $t \geq 0$. To complete the proof it is suffices to choose $\delta_1 < \bar{\alpha}^{-1}(c)$, for this guarantees that $\mathbf{e}^o$ is in the interior of Ω_c. In fact:

$$\bar{\alpha}^{-1}\left(V(\mathbf{e}^o)\right) \leq ||\mathbf{e}^o|| \leq \delta_1 < \bar{\alpha}^{-1}(c) \tag{2.90}$$

implies $V(\mathbf{e}^o) < c$. $\square$

2.2.1.3 Stability of the Active Control

Once the estimation module has been switched on and the separation principle is hold the estimation error start decrease. So, the system (2.76) can be seen as perturbed by a vanishing signal, the estimation error, indeed. Take, for instance, the Least Squares - Sliding Mode algorithm and remember that, this algorithm theoretically assures that the estimation goes to the actual

value of $\mathbf{f}_s$ in finite time. In this context the system (2.76) is driven by the exogenous vanishing signal $\mathbf{e_f}$. To prove the stability of the active control the concepts of the "cascade of connected systems" are exploited, for details see [83]. Before the statement of the stability theorem let's introduce the following notation:

$$
\begin{aligned}
\dot{\mathbf{e}} &= \mathbf{F}\left(\mathbf{e}, \mathbf{x}_{1_R}\right) + \mathbf{G}^* \mathbf{e_f} \\
\dot{\mathbf{e}}_\mathbf{f} &= \mathbf{H}\left(\mathbf{e_f}\right)
\end{aligned}
\tag{2.91}
$$

where the second subsystem represents the dynamics of the Least Squares - Sliding Mode estimation error.

Theorem 2.2. *Consider the system* (2.91). *Let S be a set with the property that, for any $\bar{\mathbf{e}}^o \in S$, the integral curve $\dot{\bar{\mathbf{e}}}(t) = \mathbf{F}\left(\bar{\mathbf{e}}, \mathbf{x}_{1_R}\right)$ satisfying $\bar{\mathbf{e}}(0) = \bar{\mathbf{e}}^o$ is defined for all $t \geq 0$ and is such that $\lim_{t\to\infty} \bar{\mathbf{e}}(t) = \mathbf{0}$.*

Pick any $\mathbf{e}_\mathbf{f}^o$ and let $\mathbf{e}_\mathbf{f}^o(t)$ denote the integral curve of $\dot{\mathbf{e}}_\mathbf{f} = \mathbf{H}\left(\mathbf{e_f}\right)$ satisfying $\mathbf{e}_\mathbf{f}^o(0) = \mathbf{e}_\mathbf{f}^o$.

Pick any $\mathbf{e}^o \in S$ and let $\mathbf{e}^o(t)$ denote the integral curve of $\dot{\mathbf{e}}(t) = \mathbf{F}\left(\mathbf{e}, \mathbf{x}_{1_R}\right) + \mathbf{G}^* \mathbf{e}_\mathbf{f}^o$.

The following hold:

$$
\lim_{t\to\infty} \mathbf{e}^o(t) = \mathbf{0}
\tag{2.92}
$$

Proof The proof start by showing that the for any $\mathbf{e}^o \in S$, $\mathbf{e}^o(t)$ is defined for all $t \geq 0$, us bounded and is such that $\mathbf{e}^o(t) \in S$ for all $t \geq 0$. Using the theorem of "total stability" (see [83]), it's easy to prove that, since the equilibrium $\mathbf{e} = \mathbf{0}$ of $\dot{\mathbf{e}}(t) = \mathbf{F}\left(\mathbf{e}, \mathbf{x}_{1_R}\right)$ is locally asymptotically stable, given any ε, there exist δ_1 and δ_2 such that, if $||\mathbf{e}^o|| \leq \delta_1$ and $||\mathbf{e}_\mathbf{f}^o|| \leq \delta_2$ for all $t \geq 0$, the solution $\bar{\mathbf{e}}$ of $\dot{\mathbf{e}}(t) = \mathbf{F}\left(\mathbf{e}, \mathbf{x}_{1_R}\right) + \mathbf{G}^* \mathbf{e_f}$ satisfying $\bar{\mathbf{e}}(0) = \bar{\mathbf{e}}^o$ is such that $||\bar{\mathbf{e}}(t)|| \leq \varepsilon$ for all $t \geq 0$. This has been proved in the demonstration of Theorem 2.1.

Now, the proof exactly continues by following the proof of Theorem 10.3.1 in [83]. $\square$

2.2.2   Active Composite Controller

This controller has been investigated because the need of fulfill the validity hypothesis at the base of the Detection and Isolation scheme relying on the singular perturbations approximation. Here, a brief SP theory sketch is given for input affine models, whereas, for a complete description see [66]. A singularly perturbed system can be generally expressed in terms of fast and slow variables in the following way:

$$
\begin{cases}
\dot{\mathbf{x}}_1 &= \mathbf{f}_1(\mathbf{x}_1, \mathbf{x}_2, \varepsilon) + \mathbf{g}_1(\mathbf{x}_1, \mathbf{x}_2, \varepsilon)\mathbf{u}_a \\
\varepsilon\dot{\mathbf{x}}_2 &= \mathbf{f}_2(\mathbf{x}_1, \mathbf{x}_2, \varepsilon) + \mathbf{g}_2(\mathbf{x}_1, \mathbf{x}_2, \varepsilon)\mathbf{u}_a \\
\mathbf{y}_1 &= \mathbf{x}_1 \\
\mathbf{y}_2 &= \mathbf{x}_2
\end{cases}
\tag{2.93}
$$

where $\mathbf{x}_1 \in \mathbb{R}^{n_1}$ is the vector of slow variables, $\mathbf{x}_2 \in \mathbb{R}^{n_2}$ is the vector of fast variables, and $\mathbf{u}_a \in \mathbb{R}^p$ is the input vector. The term, ε, is the small positive perturbation parameter, called *singular*. By assuming $\varepsilon = 0$ the state-space dimension shrinks from $n_1 + n_2$ to n_1 because the second relation in (2.93) degenerates to an algebraic equation:

$$
\begin{cases}
\dot{\bar{x}}_1 &= \mathbf{f}_1(\bar{\mathbf{x}}_1, \bar{\mathbf{x}}_2, 0) + \mathbf{g}_1(\mathbf{x}_1, \mathbf{x}_2, 0)\mathbf{u}_a \\
0 &= \mathbf{f}_2(\bar{\mathbf{x}}_1, \bar{\mathbf{x}}_2, 0) + \mathbf{g}_1(\mathbf{x}_1, \mathbf{x}_2, 0)\mathbf{u}_a
\end{cases}
\tag{2.94}
$$

Equations (2.94) represent the *reduced model*.

Remark 4. The system in (2.93) is said to be in the *standard form* if the algebraic equation $0 = \mathbf{f}_2(\mathbf{x}_1, \mathbf{x}_2, 0) + \mathbf{g}_1(\mathbf{x}_1, \mathbf{x}_2, 0)\mathbf{u}_a$ admits at least one isolated root. If $\mathbf{x}_{2_\mathcal{M}} = \mathbf{h}(\bar{\mathbf{x}}_1, \mathbf{u}_a)$ is an isolated root of $0 = \mathbf{f}_2(\mathbf{x}_1, \mathbf{x}_2, 0) + \mathbf{g}_1(\mathbf{x}_1, \mathbf{x}_2, 0)\mathbf{u}_a$, satisfying conditions in Tikhonov's theorem, then it describes an $n_1 + p$ dimension invariant manifold for the system (2.94), see [66].

On the other hand, while fast variables are moving, it isn't wrong to treat slow variables as parameters. Thanks to a time scale change, made by defining $\tau = (t - t_0)/\varepsilon$, it's possible to define apex derivatives as $\mathbf{x}' = d\mathbf{x}/d\tau$. As previously made, by assuming $\varepsilon = 0$, the dynamic order of the system is reduced from $n_1 + n_2$ to n_2:

$$
\begin{cases}
\mathbf{x}_1' &= 0 \\
\mathbf{x}_2' &= \mathbf{f}_2(\mathbf{x}_1, \mathbf{x}_2, 0) + \mathbf{g}_1(\mathbf{x}_1, \mathbf{x}_2, 0)\mathbf{u}_a
\end{cases}
\tag{2.95}
$$

Equations (2.95) represent the *boundary–layer model*. Finally, if Tikhonov's theorem is verified, the actual system dynamics (2.93) can be approximated by:

$$
\begin{cases}
\dot{\mathbf{x}}_1 &= \mathbf{f}_1(\bar{\mathbf{x}}_1, \mathbf{h}(\bar{\mathbf{x}}_1, \mathbf{u}_a), 0) + \mathbf{g}_1(\bar{\mathbf{x}}_1, \mathbf{h}(\bar{\mathbf{x}}_1, \mathbf{u}_a), 0)\mathbf{u}_a \\
\mathbf{x}_2' &= \mathbf{f}_2(\bar{\mathbf{x}}_1, \mathbf{x}_2, 0) + \mathbf{g}_1(\bar{\mathbf{x}}_1, \mathbf{x}_2, 0)\mathbf{u}_a
\end{cases}
\tag{2.96}
$$

As will be presented in the following, several advantages can be achieved by adopting the above described SP strategy both in the design of the controller and in the FDD module synthesis.

2.2.2.1 Generalized Faults Scenario

As introduced in Section 2.1.1.3, $\mathbf{f}_s$ considers additive non concurrent multiple faults, modeled by step time functions, affecting both actuators and sensors. The fault scenario is modeled by the following equations:

$$
\begin{aligned}
\mathbf{y}_1 &= \mathbf{x}_1 + \mathbf{f}_{\mathbf{y}_1} \\
\mathbf{y}_2 &= \mathbf{x}_2 + \mathbf{f}_{\mathbf{y}_2} \\
\mathbf{u}_a &= \mathbf{u} + \mathbf{f}_u
\end{aligned}
\tag{2.97}
$$

where $\mathbf{y}_1$, $\mathbf{y}_2$, $\mathbf{u}_a$ respectively represent the slow variable output, the fast variable output and the actual actuator input. The terms $\mathbf{f}_{\mathbf{y}_1}$, $\mathbf{f}_{\mathbf{y}_2}$ and $\mathbf{f}_u$ represent the vectors of physical faults acting on output sensors and actuator inputs. Let's denote with s the number of physical faults affecting sensors whereas p is the number of actuator faults. Can be useful remembering that, being the system nonlinear, additive faults can destabilize the system pushing the state out from the local attraction domain. Furthermore additive faults are very suitable both for the model of a class of faults more general than the multiplicative ones, and for the Diagnosis module design, see [84]. Finally, define the fault vector as $\mathbf{f}_s = [f_1, ..., f_{\nu_s}]^T = [\mathbf{f}_{\mathbf{y}_1}^T, \mathbf{f}_{\mathbf{y}_2}^T, \mathbf{f}_u^T]^T$.

2.2.2.2 Modeling the faulty plant

Given a sufficiently smooth, bounded, time-varying trajectory, $\mathbf{x}_{1_R}(t)$, define the state tracking error as $\mathbf{e}_1 = \mathbf{x}_1 - \mathbf{x}_{1_R}$ and rewrite the system (2.93) in the errors form:

$$
\begin{aligned}
\dot{\mathbf{e}}_1 &= \dot{\mathbf{x}}_1 - \dot{\mathbf{x}}_R = \\
&= \mathbf{f}_1(\mathbf{e}_1 + \mathbf{x}_{1_R}, \mathbf{e}_2 + \mathbf{x}_{2_\mathcal{M}}, \varepsilon) + \mathbf{g}_1(\mathbf{e}_1 + \mathbf{x}_{1_R}, \mathbf{e}_2 + \mathbf{x}_{2_\mathcal{M}}, \varepsilon)\mathbf{u}_a - \dot{\mathbf{x}}_R = \\
&= \mathbf{F}_1(\mathbf{e}_1, \mathbf{e}_2, \mathbf{x}_{1_R}, \mathbf{u}_a, \varepsilon) - \dot{\mathbf{x}}_R \\
\varepsilon\dot{\mathbf{e}}_2 &= \varepsilon\dot{\mathbf{x}}_2 - \varepsilon\dot{\mathbf{x}}_{2_\mathcal{M}} = \\
&= \mathbf{f}_2(\mathbf{e}_1 + \mathbf{x}_{1_R}, \mathbf{e}_2 + \mathbf{x}_{2_\mathcal{M}}, \varepsilon) + \mathbf{g}_2(\mathbf{e}_1 + \mathbf{x}_{1_R}, \mathbf{e}_2 + \mathbf{x}_{2_\mathcal{M}}, \varepsilon)\mathbf{u}_a - \varepsilon\dot{\mathbf{x}}_{2_\mathcal{M}} = \\
&= \mathbf{F}_2(\mathbf{e}_1, \mathbf{e}_2, \mathbf{x}_{1_R}, \mathbf{u}_a, \varepsilon) - \varepsilon\dot{\mathbf{x}}_{2_\mathcal{M}}
\end{aligned}
\tag{2.98}
$$

where the definition of $\mathbf{F}_1$ and $\mathbf{F}_2$ is obvious. The state tracking error $\mathbf{e}_2$ is defined as $\mathbf{e}_2 = \mathbf{x}_2 - \mathbf{x}_{2_\mathcal{M}}$. The term

$$
\mathbf{x}_{2_\mathcal{M}} := \mathbf{f}_2(\mathbf{x}_1, \mathbf{x}_{2_\mathcal{M}}, \mathbf{u}, 0) = \mathbf{0}
\tag{2.99}
$$

constitutes an isolated solution of the faultless equation $\mathbf{f}_2(\mathbf{x}_1, \mathbf{x}_{2_\mathcal{M}}, \mathbf{u}, 0) = \mathbf{0}$. Let's define the manifold of (2.98) as the solution of $0 = \mathbf{F}_2(\mathbf{e}_1, \mathbf{e}_2, \mathbf{x}_{1_R}, \mathbf{u}_a, 0)$, *i.e.* $\mathbf{e}_{2_\mathcal{M}} = \mathbf{H}(\mathbf{e}_1, \mathbf{u}_a, \mathbf{x}_{1_R})$. It is worth nothing that $\mathbf{e}_{2_\mathcal{M}}|_{\mathbf{u}_a=\mathbf{u}} = \mathbf{e}_2|_{\mathbf{x}_2=\mathbf{x}_{2_\mathcal{M}}} = \mathbf{0}$; it means that in absence of actuator faults

the boundary layer system lives on the nominal manifold. Finally, the reference state, $\mathbf{x}_R$, is $\mathbf{x}_R = \left[\mathbf{x}_{1_R}^T \ \mathbf{x}_{2_{\mathcal{M}}}^T \right]^T$.

2.2.2.3 Control problem formulation and solution

Problem 6. **Active Composite Control**. Given the system (2.98) find a time varying error–feedback control law

$$\mathbf{u} = \mathbf{u}\left(\mathbf{e}_1, \mathbf{e}_2, \mathbf{x}_{1_R}, \dot{\mathbf{x}}_{1_R}, \ddot{\mathbf{x}}_{1_R}, \mathbf{f}_u\right)$$

such that the origin of the closed-loop system is a locally exponentially stable (LES) equilibrium point.

Remark 5. Normally, any feedback design will suffer from high dimensions and ill-conditioned systems resulting from the interaction of slow and fast dynamics. The singular perturbation state-feedback design technique yields to a composite feedback (sum of two time scaled control laws) that take advantages from decomposition of the original ill-conditioned system into two well-conditioned subsystems in separate time scales. Then, a particularly suitable solution to Problem 6 can be found in a composite error–feedback control law.

Proposition 2.3. *The composite error-feedback control law,* $\mathbf{u} = \mathbf{\Gamma}_1 + \mathbf{\Gamma}_2$*, obtained by the following procedure, solves the Problem 6, see Theorem 11.4 in [66].*

Procedure 1. **- Composite Controller Design**

Assume that the fast control law

$$\mathbf{\Gamma}_2 = \mathbf{\Gamma}_2\left(\mathbf{e}_1, \mathbf{e}_2, \mathbf{f}_u, \mathbf{x}_{1_R}\right) \tag{2.100}$$

is such that:

- the feedback control law, $\mathbf{u}$, when applied to (2.98), still results in a singularly perturbed system;

- the input $\mathbf{\Gamma}_2 + \mathbf{f}_u$ is *inactive* for $\mathbf{e}_2 = \mathbf{H}\left(\mathbf{e}_1, \mathbf{\Gamma}_1, \mathbf{x}_{1_R}\right) = \mathbf{0}$, *i.e.*

$$\mathbf{\Gamma}_2\left(\mathbf{e}_1, \mathbf{0}, \mathbf{f}_u, \mathbf{x}_{1_R}\right) + \mathbf{f}_u = \mathbf{0} \tag{2.101}$$

Then:

1. Design a control law, $\mathbf{\Gamma}_1 = \mathbf{\Gamma}_1\left(\mathbf{e}_1, \mathbf{x}_{1_R}, \dot{\mathbf{x}}_R, \ddot{\mathbf{x}}_R\right)$, for the reduced model such that the origin of this subsystem is LES;

2. With the knowledge of $\mathbf{\Gamma}_1$ design a control law, $\mathbf{\Gamma}_2$, satisfying the above mentioned assumptions and such that $\mathbf{e}_2 = \mathbf{0}$ for the closed–loop system

$$\mathbf{e}_2' = \mathbf{F}_2(\mathbf{e}_1, \mathbf{e}_2, \mathbf{x}_{1_R}, \mathbf{\Gamma}_1 + \mathbf{\Gamma}_2 + \mathbf{f}_u, 0) \tag{2.102}$$

is the unique LES equilibrium point uniformly in $(\mathbf{e}_1, \mathbf{x}_{1_R})$.

Remark 6. Theorem 11.4 in [66] demonstrates the existence and determines the value of an $\varepsilon*$ such that $\forall \varepsilon < \varepsilon*$ the origin of the actual system (2.98) is locally exponentially stable.

Remark 7. If the stability requirements at the procedural steps (1) and (2) regard only asymptotic stability these two steps became necessary but not sufficiency conditions to assure the asymptotic stability required in the Problem 6. In this case a third step, consisting in verifying interconnection conditions as in [85], is needed to fulfill sufficiency.

Remark 8. Thanks to the condition (2.101) the slow control law, $\mathbf{\Gamma}_1$, can be designed in a fault scenario without actuator faults.

Remark 9. The controller design procedure has to be completed by taking into account the fact that the state errors $\mathbf{e}_1$ and $\mathbf{e}_2$ as well the faults are unknown. Let's define the *measured* errors as $\mathbf{e}_{y_1} = \mathbf{y}_1 - \mathbf{x}_{1_R}$ and $\mathbf{e}_{y_2} = \mathbf{y}_2 - \mathbf{x}_{2_{\mathcal{M}}}$. It's easy to see that $\mathbf{e}_1 = \mathbf{e}_{y_1} - \mathbf{f}_{\mathbf{y}_1}$ and $\mathbf{e}_2 = \mathbf{e}_{y_2} - \mathbf{f}_{\mathbf{y}_2}$. Thanks to the previous change of variables it's possible to rewrite the nominal controller and to highlighting its dependence on faults:

$$\begin{aligned} \mathbf{u} = \ & \mathbf{\Gamma}_1 \left(\mathbf{e}_{y_1} - \mathbf{f}_{\mathbf{y}_1}, \mathbf{x}_{1_R}, \dot{\mathbf{x}}_{1_R}, \ddot{\mathbf{x}}_{1_R} \right) + \\ & + \mathbf{\Gamma}_2 \left(\mathbf{e}_{y_1} - \mathbf{f}_{\mathbf{y}_1}, \mathbf{e}_{y_2} - \mathbf{f}_{\mathbf{y}_2}, \mathbf{f}_u, \mathbf{x}_{1_R} \right) \end{aligned} \tag{2.103}$$

The last step is the substitution of faults $\mathbf{f}_{\mathbf{y}_1}$, $\mathbf{f}_{\mathbf{y}_2}$ and $\mathbf{f}_u$ with their estimation $\hat{\mathbf{f}}_{\mathbf{y}_1}$, $\hat{\mathbf{f}}_{\mathbf{y}_2}$ and $\hat{\mathbf{f}}_u$ respectively. Then, the real controller is described by the following equation:

$$\begin{aligned} \mathbf{u} = \ & \mathbf{\Gamma}_1 \left(\mathbf{e}_{y_1} - \hat{\mathbf{f}}_{\mathbf{x}_1}, \mathbf{x}_{1_R}, \dot{\mathbf{x}}_{1_R}, \ddot{\mathbf{x}}_{1_R} \right) + \\ & + \mathbf{\Gamma}_2 \left(\mathbf{e}_{y_1} - \hat{\mathbf{f}}_{\mathbf{y}_1}, \mathbf{e}_{y_2} - \hat{\mathbf{f}}_{\mathbf{x}_2}, \hat{\mathbf{f}}_u, \mathbf{x}_{1_R} \right) \end{aligned} \tag{2.104}$$

2.2.2.4 Feedback Linearization for the Reduced Errors Model

Starting from the *inactivity* properties of $\mathbf{\Gamma}_2 + \mathbf{f}_u$ on the manifold, it's possible to describe the reduced system of (2.98) as follows:

$$\dot{\mathbf{e}}_1 = \mathbf{F}_1(\mathbf{e}_1, \mathbf{H}\left(\mathbf{e}_1, \mathbf{\Gamma}_1, \mathbf{x}_{1_R}\right), \mathbf{x}_{1_R}) - \dot{\mathbf{x}}_{1_R} \tag{2.105}$$

which is non affine in $\boldsymbol{\Gamma}_1$. In order to fulfill the requirements at the step (1) of the Procedure 1, the following controller, obtained by *dynamic extension*, see [86], can be used:

$$
\begin{cases}
\dot{\boldsymbol{\Gamma}}_1 &= \boldsymbol{\Phi}_1 \\
\boldsymbol{\Phi}_1 &= \mathbf{A}_1^{-1}\left(\mathbf{e}_1, \mathbf{x}_{1_R}\right)\left[-\mathbf{b}_1\left(\mathbf{e}_1, \mathbf{x}_{1_R}\right) + \right. \\
&\quad \left. +\mathbf{v}_1\left(\mathbf{e}_1, \mathbf{x}_{1_R}, \dot{\mathbf{x}}_{1_R}, \ddot{\mathbf{x}}_{1_R}\right)\right]
\end{cases}
\tag{2.106}
$$

where the first term in (2.106), $-\mathbf{A}_1^{-1}\mathbf{b}_1$, linearises the system (2.105) and makes the origin an equilibrium point which is exponentially stabilised, with arbitrary decay rate, by means of the second term, $\mathbf{A}_1^{-1}\mathbf{v}_1$. It's worth observing that $\boldsymbol{\Phi}_1$ can be considered as a new input respect to which the sum of the relative degree (total relative degree) have to be evaluated: if it is maximum, it is possible to obtain an *exact* feedback linearisation such that the controlled system, (2.105)–(2.106), has not *zero dynamics*, see [86]. The controller design is completed by procedures stated in Remark 9.

2.2.2.5 Feedback Linearization for the Boudary–Layer Error Model

The model (2.102) is input affine (see (2.98) indeed) and, if the total relative degree is maximum, an exact feedback linearisation is obtained by means of the following control law, otherwise a zero-dynamics occurs:

$$
\begin{aligned}
\boldsymbol{\Gamma}_2 &= \mathbf{A}_2^{-1}\left(\mathbf{e}_1, \mathbf{e}_2, \mathbf{x}_{1_R}\right)\left[-\mathbf{b}_2\left(\mathbf{e}_1, \mathbf{e}_2, \mathbf{x}_R\right) + \right. \\
&\quad \left. + \mathbf{v}_2\left(\mathbf{e}_1, \mathbf{e}_2, \mathbf{x}_{1_R}\right)\right] - \mathbf{f}_u
\end{aligned}
\tag{2.107}
$$

where, analogously to (2.106), if the feedback linearization is exact the origin is an exponentially stable equilibrium point. Let's use what stated in Remark 9 to implement the controller.

2.2.2.6 Stability analysis of the Active Fault Tolerant Composite Control

As described in Section 2.1.1.3, the main task of the nominal controller is the stabilization of the system during all working phases, *i.e.* in nominal conditions, in presence of fault during the detection and isolation and, finally, during the fault accommodation (including the estimation transient). If the stability in presence of fault is lost, the detection and isolation scheme is not more applicable and the entire active control fails.

Whereas the stability of the nominal aircraft (no faults), under the control action, has been established by design, see previous Sections, in this Section the stability during the fault isolation and identification process will be proved as well as the stability of the overall AFTC, after the FDI phase, with the fault estimation feedback.

Stability during the Fault Detection and Isolation process

In this section the problem of the stability during the (short but methodologically important) fault detection and isolation time will be analyzed. In particular, the plant, affected by the fault, $\mathbf{f}_s$, is controlled by the non-nominal controller (the fault estimation feedback is not activated yet), $\mathbf{u}_{nn} = \mathbf{u}_a|_{\hat{\mathbf{f}}_s=\mathbf{0}}$:

$$
\begin{aligned}
\mathbf{u}_{nn} &= \boldsymbol{\Gamma}_1\left(\mathbf{e}_{y_1} - \mathbf{0}, \mathbf{x}_{1_R}, \dot{\mathbf{x}}_{1_R}, \ddot{\mathbf{x}}_{1_R}\right) + \\
&\quad + \boldsymbol{\Gamma}_2\left(\mathbf{e}_{y_1} - \mathbf{0}, \mathbf{e}_{y_2} - \mathbf{0}, \mathbf{0}, \mathbf{x}_{1_R}\right) = \\
&= \boldsymbol{\Gamma}_1\left(\mathbf{e}_1 + \mathbf{f}_{\mathbf{y}_1}, \mathbf{x}_{1_R}, \dot{\mathbf{x}}_{1_R}, \ddot{\mathbf{x}}_{1_R}\right) + \\
&\quad + \boldsymbol{\Gamma}_2\left(\mathbf{e}_1 + \mathbf{f}_{\mathbf{y}_1}, \mathbf{e}_2 + \mathbf{f}_{\mathbf{y}_2}, \mathbf{0}, \mathbf{x}_{1_R}\right) = \\
&= \boldsymbol{\Gamma}_{1_n} + \boldsymbol{\Gamma}_{2_n} + \boldsymbol{\Delta\Gamma}_1 + \boldsymbol{\Delta\Gamma}_2 = \mathbf{u}_n + \boldsymbol{\Delta u}
\end{aligned}
\tag{2.108}
$$

where

$$
\begin{aligned}
\mathbf{u}_n &= \boldsymbol{\Gamma}_{1_n} + \boldsymbol{\Gamma}_{2_n} \\
\boldsymbol{\Delta u} &= \boldsymbol{\Delta\Gamma}_1 + \boldsymbol{\Delta\Gamma}_2 \\
\boldsymbol{\Gamma}_{1_n} &= \boldsymbol{\Gamma}_1\left(\mathbf{e}_1, \mathbf{x}_{1_R}, \dot{\mathbf{x}}_{1_R}, \ddot{\mathbf{x}}_{1_R}\right) \\
\boldsymbol{\Gamma}_{2_n} &= \boldsymbol{\Gamma}_2\left(\mathbf{e}_1, \mathbf{e}_2, \mathbf{0}, \mathbf{x}_{1_R}\right) \\
\boldsymbol{\Delta\Gamma}_1 &= \boldsymbol{\Gamma}_1\left(\mathbf{e}_1 + \mathbf{f}_{\mathbf{y}_1}, \mathbf{x}_{1_R}, \dot{\mathbf{x}}_{1_R}, \ddot{\mathbf{x}}_{1_R}\right) - \boldsymbol{\Gamma}_{1_n} \\
\boldsymbol{\Delta\Gamma}_2 &= \boldsymbol{\Gamma}_2\left(\mathbf{e}_1, \mathbf{e}_2 + \mathbf{f}_{\mathbf{y}_2}, \mathbf{0}, \mathbf{x}_{1_R}\right) - \boldsymbol{\Gamma}_{2_n}
\end{aligned}
\tag{2.109}
$$

The overall aircraft model (2.98), under the action of the non nominal controller, $\mathbf{u}_{nn}$, and the fault, $\mathbf{F}$, is represented by the following nonlinear system:

$$
\begin{aligned}
\dot{\mathbf{e}}_1 &= \mathbf{F}_1(\mathbf{e}_1, \mathbf{e}_2, \mathbf{x}_{1_R}, \mathbf{u}_n, \varepsilon) - \dot{\mathbf{x}}_R + \boldsymbol{\Delta F}_1 \\
\varepsilon \dot{\mathbf{e}}_2 &= \mathbf{F}_2(\mathbf{e}_1, \mathbf{e}_2, \mathbf{x}_{1_R}, \mathbf{u}_n, \varepsilon) - \varepsilon \dot{\mathbf{x}}_{2_{\mathcal{M}}} + \boldsymbol{\Delta F}_2
\end{aligned}
\tag{2.110}
$$

where

$$
\begin{aligned}
\boldsymbol{\Delta F}_1 &= \mathbf{F}_1(\mathbf{e}_1, \mathbf{e}_2, \mathbf{x}_{1_R}, \mathbf{u}_{nn}, \varepsilon) - \mathbf{F}_1(\mathbf{e}_1, \mathbf{e}_2, \mathbf{x}_{1_R}, \mathbf{u}_n, \varepsilon) \\
\boldsymbol{\Delta F}_2 &= \mathbf{F}_2(\mathbf{e}_1, \mathbf{e}_2, \mathbf{x}_{1_R}, \mathbf{u}_{nn}, \varepsilon) - \mathbf{F}_2(\mathbf{e}_1, \mathbf{e}_2, \mathbf{x}_{1_R}, \mathbf{u}_n, \varepsilon)
\end{aligned}
\tag{2.111}
$$

Finally, the system (2.110) is rewritten as the sum of a nominal part (without faults) and a perturbed part (comprehensive of faults):

$$
\dot{\mathbf{e}} = \mathbf{f}\left(\mathbf{e}, \mathbf{x}_{1_R}, \dot{\mathbf{x}}_{1_R}, \mathbf{u}_n, \varepsilon\right) + \boldsymbol{\Delta f}\left(\mathbf{e}, \mathbf{x}_{1_R}, \mathbf{u}_n, \varepsilon, \mathbf{f}_s\right)
\tag{2.112}
$$

where

$$
\mathbf{e} = \begin{bmatrix} \mathbf{e}_1 \\ \varepsilon \mathbf{e}_2 \end{bmatrix} \quad \boldsymbol{\Delta f} = \begin{bmatrix} \boldsymbol{\Delta F}_1 \\ \boldsymbol{\Delta F}_2 \end{bmatrix}
$$

$$
\mathbf{f} = \begin{bmatrix} \mathbf{F}_1(\mathbf{e}_1, \mathbf{e}_2, \mathbf{x}_{1_R}, \mathbf{u}_n) - \dot{\mathbf{x}}_R \\ \mathbf{F}_2(\mathbf{e}_1, \mathbf{e}_2, \mathbf{x}_{1_R}, \mathbf{u}_n, \varepsilon) - \varepsilon \dot{\mathbf{x}}_{2_{\mathcal{M}}} \end{bmatrix}
\tag{2.113}
$$

Hypothesis 4. The single fault f_i with $i \in \{1, ..., \nu_s\}$ is such that the function $\mathbf{\Delta f}|_{\mathbf{f}_s = f_i}$ is piecewise continuous and satisfies a Lipschitz condition

$$||\mathbf{\Delta f}\left(\mathbf{e}', \mathbf{x}_{1_R}, \mathbf{u}_n, \varepsilon, f_i\right) - \mathbf{\Delta f}\left(\mathbf{e}'', \mathbf{x}_{1_R}, \mathbf{u}_n, \varepsilon, f_i\right)|| < L||\mathbf{e}' - \mathbf{e}''|| \tag{2.114}$$

for all $\mathbf{e}'$, $\mathbf{e}''$ in some neighborhood U of the origin, $\mathbf{e} = \mathbf{0}$.

Theorem 2.4. *Taken the model* (2.113)*, if the Hypothesis* 1 *and* 4 *are verified, then* $\forall \, d > 0 \; \exists$ $\delta_1 > 0$ *and* $\delta_2 > 0$ *(both possibly dependent on d) such that if:*

$$||\mathbf{e}^o|| < \delta_1$$
$$||\mathbf{\Delta f}\left(\mathbf{e}, \mathbf{x}_{1_R}, \mathbf{u}_n, \varepsilon, f_i\right)|| < \delta_2 \quad \forall \, ||\mathbf{e}|| < d \tag{2.115}$$

the solution, $\mathbf{e}(t)$*, of the differential equation* (2.113)*, satisfying* $\mathbf{e}(0) = \mathbf{e}^o$*, is such that*

$$||\mathbf{e}(t)|| < d \tag{2.116}$$

for all $t > 0$. ◇

Proof The proof is based on the fundamental result of the so called *theorem of global stability* in [83]. Thanks to the controller design procedure, the origin is an equilibrium point for the unperturbed system

$$\dot{\mathbf{e}} = \mathbf{f}\left(\mathbf{e}, \mathbf{x}_{1_R}, \dot{\mathbf{x}}_{1_R}, \mathbf{u}_n, \varepsilon\right) \tag{2.117}$$

Furthermore, the origin of (2.117) is also locally exponentially stable, see Section 2.2.2.3, Remark 6. Then, a Lyapunov function, $V(\mathbf{e}) : B_d \rightarrow \mathbb{R}$, $V \in C^1$, exists and, for some some $\mathcal{K}$-class functions $\underline{\alpha}(\cdot), \alpha(\cdot), \bar{\alpha}(\cdot)$ defined in $[0, d)$, it is such that:

$$\underline{\alpha}(||\mathbf{e}||) \leq V(\mathbf{e}) \leq \bar{\alpha}(||\mathbf{e}||)$$
$$\frac{\partial V}{\partial \mathbf{e}} \mathbf{f}\left(\mathbf{e}, \mathbf{x}_{1_R}, \dot{\mathbf{x}}_{1_R}, \mathbf{u}_n, \varepsilon\right) \leq -\alpha(||\mathbf{e}||) \tag{2.118}$$
$$\forall ||\mathbf{e}|| < d$$

Since the $\frac{\partial V}{\partial \mathbf{e}}$ is C^0, there exists a real number $M > 0$ such that:

$$||\frac{\partial V}{\partial \mathbf{e}}|| \leq M \tag{2.119}$$

for all $\mathbf{e} \in U$. Suppose that $d > 0$ is such that $B_d \subset U$ and let $c > 0$ be such that $c \leq \underline{\alpha}(d)$. Choose δ_2 such that:

$$-\alpha\left(\bar{\alpha}^{-1}(c)\right) + M\delta_2 < 0 \tag{2.120}$$

Let's define

$$\Omega_c = \{\mathbf{e} \in \mathbb{R}^n : V(\mathbf{e}) \leq c\} \tag{2.121}$$

By construction, $\mathbf{e} \in \Omega_c$ implies

$$||\mathbf{e}|| \leq d \tag{2.122}$$

In fact,

$$\underline{\alpha}(||\mathbf{e}||) \leq V(\mathbf{e}) \leq c \tag{2.123}$$

implies

$$||\mathbf{e}|| \leq \underline{\alpha}^{-1}(c) \leq \underline{\alpha}^{-1}(\underline{\alpha}(d)) = d \tag{2.124}$$

Also, at each point $\mathbf{e}$ of the boundary of Ω_c,

$$\alpha(||\mathbf{e}||) \geq \alpha(\bar{\alpha}^{-1}(V(||\mathbf{e}||))) = \alpha(\bar{\alpha}^{-1}(c)) \tag{2.125}$$

As a consequence, at each point $\mathbf{e}$ of the boundary of Ω_c,

$$\frac{\partial V}{\partial \mathbf{e}} \left[\mathbf{f}\left(\mathbf{e}, \mathbf{x}_{1_R}, \dot{\mathbf{x}}_{1_R}, \mathbf{u}_n, \varepsilon\right) + \mathbf{\Delta f}\left(\mathbf{e}, \mathbf{x}_{1_R}, \mathbf{u}_n, \varepsilon, f_i\right) \right] \leq \\ -\alpha(||\mathbf{e}||) + ||\frac{\partial V}{\partial \mathbf{e}}||\delta_2 \leq -\alpha(\bar{\alpha}^{-1}(c)) + M\delta_2 < 0 \tag{2.126}$$

From this, it can be concluded that, for any initial condition in the interior of Ω_c, the solution $\mathbf{e}$ of (2.113) is defined for all $t \geq 0$ and is such that $\mathbf{e}(t) \in \Omega_c$ for all $t \geq 0$. To complete the proof it is suffices to choose $\delta_1 < \bar{\alpha}^{-1}(c)$, for this guarantees that $\mathbf{e}^o$ is in the interior of Ω_c. In fact:

$$\bar{\alpha}^{-1}\left(V(\mathbf{e}^o)\right) \leq ||\mathbf{e}^o|| \leq \delta_1 < \bar{\alpha}^{-1}(c) \tag{2.127}$$

implies $V(\mathbf{e}^o) < c$. $\square$

Stability of the Active Fault Tolerant Control system

In this section the stability proof of the overall Active Fault Tolerant Composite Control based on Singular Perturbation will be shown. It will be demonstrated that the plant with the nominal controller and fault estimation feedback has a locally exponentially stable equilibrium point and that, furthermore, this point coincides with the nominal reference trim point.

Before stating the stability proof can be useful to introduce some definitions. Define as *estimated* state errors the terms:

$$\begin{aligned} \mathbf{e}_{1_{EST}} &= \mathbf{e}_{y_1} - \hat{\mathbf{f}}_{\mathbf{y}_1} \\ \mathbf{e}_{2_{EST}} &= \mathbf{e}_{y_2} - \hat{\mathbf{f}}_{\mathbf{y}_2} \end{aligned} \tag{2.128}$$

where, for $\# \in \{1, 2\}$, $\mathbf{e}_{y_\#}$ are the actual output error and $\hat{\mathbf{f}}_{\mathbf{y}_\#}$ are the estimation of physical fault on output sensors. On the other hand, the *actual* state errors can be written as follow

$$\begin{aligned} \mathbf{e}_1 &= \mathbf{e}_{y_1} - \mathbf{f}_{\mathbf{y}_1} \\ \mathbf{e}_2 &= \mathbf{e}_{y_2} - \mathbf{f}_{\mathbf{y}_2} \end{aligned} \tag{2.129}$$

where, for $\# \in \{1, 2\}$, $\mathbf{f}_{\mathbf{y}_\#}$ are the physical fault acting on output sensors. Then, combining the last two sets of equations, it is possible to write:

$$
\begin{aligned}
\mathbf{e}_{1_{EST}} &= \mathbf{e}_1 + \left(\mathbf{f}_{\mathbf{y}_1} - \hat{\mathbf{f}}_{\mathbf{y}_1}\right) = \mathbf{e}_1 - \mathbf{e}_{\mathbf{f}_{\mathbf{y}_1}} \\
\mathbf{e}_{2_{EST}} &= \mathbf{e}_2 + \left(\mathbf{f}_{\mathbf{y}_2} - \hat{\mathbf{f}}_{\mathbf{y}_2}\right) = \mathbf{e}_2 - \mathbf{e}_{\mathbf{f}_{\mathbf{y}_2}}
\end{aligned}
\tag{2.130}
$$

where, for $\# \in \{1, 2\}$, $\mathbf{e}_{\mathbf{f}_{\mathbf{y}_\#}}$ represent the output sensor fault estimation errors. It is possible to introduce also the actuator fault estimation error, $\mathbf{e}_{\mathbf{f}_u}$, as:

$$
\hat{\mathbf{f}}_u = \mathbf{f}_u + \left(\hat{\mathbf{f}}_u - \mathbf{f}_u\right) = \mathbf{f}_u + \mathbf{e}_{\mathbf{f}_u}
\tag{2.131}
$$

For clarity purpose can be useful recall the expressions of control law, $\mathbf{u}$:

$$
\begin{aligned}
\mathbf{u} &= \mathbf{\Gamma}_1\left(\mathbf{e}_{y_1} - \hat{\mathbf{f}}_{\mathbf{y}_1}, \mathbf{x}_{1_R}, \dot{\mathbf{x}}_{1_R}, \ddot{\mathbf{x}}_{1_R}\right) + \\
&\quad +\mathbf{\Gamma}_2\left(\mathbf{e}_{y_1} - \hat{\mathbf{f}}_{\mathbf{y}_1}, \mathbf{e}_{y_2} - \hat{\mathbf{f}}_{\mathbf{y}_2}, \hat{\mathbf{f}}_u, \mathbf{x}_{1_R}\right)
\end{aligned}
\tag{2.132}
$$

Substitute now equations (2.128)-(2.131) in (2.132):

$$
\begin{aligned}
\mathbf{u} &= \mathbf{\Gamma}_1\left(\mathbf{e}_1 - \mathbf{e}_{\mathbf{f}_{\mathbf{y}_1}}, \mathbf{x}_{1_R}, \dot{\mathbf{x}}_{1_R}, \ddot{\mathbf{x}}_{1_R}\right) + \\
&\quad +\mathbf{\Gamma}_2\left(\mathbf{e}_1 - \mathbf{e}_{\mathbf{f}_{\mathbf{y}_1}}, \mathbf{e}_2 - \mathbf{e}_{\mathbf{f}_{\mathbf{y}_2}}, \mathbf{f}_u + \mathbf{e}_{\mathbf{f}_u}, \mathbf{x}_{1_R}\right)
\end{aligned}
\tag{2.133}
$$

Remark 10. When no fault estimation errors are present, *i.e.* $\mathbf{e}_{\mathbf{f}_{\mathbf{y}_1}}$, $\mathbf{e}_{\mathbf{f}_{\mathbf{y}_2}}$ and $\mathbf{e}_{\mathbf{f}_u}$ are zero, the control law, $\mathbf{u}$, is the nominal one and the LES of the origin of the state–space error is guaranteed, thanks to the controller design procedure.

The Detection and Isolation module needs a small amount of time, namely t_0, to correctly detect and isolate faults. After this modest amount of time the fault estimation filter, designed for the isolated fault, is switched-on.

Making the fault estimator dynamics faster than the fastest plant dynamics, it's possible to complete the overall AFTC system with a further equation representing the dynamics of the estimation filter (2.31)-(2.32)-(2.33):

$$
\begin{aligned}
\varphi \dot{e}_{f_i} &= \varphi \dot{\hat{f}}_i - \varphi \dot{f}_i = \\
&= F_3(\mathbf{e}_1, \mathbf{e}_2, \mathbf{x}_{1_R}, \mathbf{u}, e_{f_i}) \\
e_{f_i}(t_0) &= -f_i(t_0)
\end{aligned}
\tag{2.134}
$$

where $i \in \{1, ..., \nu_s\}$ and φ is a singular parameter such that $0 < \varphi \ll \varepsilon \ll 1$.

On the other hand, for all $j \neq i$ and $j \in \{1, ..., \nu_s\}$ the other filters are not activated and their relative physical faults are not present then, all $e_{f_j} \equiv 0$ for all $j \neq i$ and $j \in \{1, ..., \nu_s\}$. Let's

define $\mathbf{e_f}$ as the vector of the estimation errors:

$$\mathbf{e_f^T} = \begin{bmatrix} \mathbf{e}_{f_{\mathbf{y_1}}}^T & \mathbf{e}_{f_{\mathbf{y_2}}}^T & \mathbf{e}_{f_{\mathbf{u}}}^T \end{bmatrix}^T \tag{2.135}$$

Finally, the overall Active Fault Tolerant Control system becomes:

$$
\begin{aligned}
plant & \quad \begin{cases} \dot{\mathbf{e}}_1 &= \mathbf{F}_1(\mathbf{e}_1, \mathbf{e}_2, \mathbf{x}_{1_R}, \mathbf{u}) - \dot{\mathbf{x}}_R \\ \varepsilon\dot{\mathbf{e}}_2 &= \mathbf{F}_2(\mathbf{e}_1, \mathbf{e}_2, \mathbf{x}_{1_R}, \mathbf{u}, \varepsilon) - \varepsilon\dot{\mathbf{x}}_{2_{\mathcal{M}}} \end{cases} \\
fault\,estimator & \quad \begin{cases} \varphi\dot{e}_{f_i} &= F_3(\mathbf{e}_1, \mathbf{e}_2, \mathbf{x}_{1_R}, \mathbf{u}, e_{f_i}) \end{cases}
\end{aligned}
\tag{2.136}
$$

where

$$
\begin{aligned}
\mathbf{u} = & \ \mathbf{\Gamma}_1\left(\mathbf{e}_1 - \mathbf{e}_{\mathbf{f_{y_1}}}, \mathbf{x}_{1_R}, \dot{\mathbf{x}}_{1_R}, \ddot{\mathbf{x}}_{1_R}\right) + \\
& + \mathbf{\Gamma}_2\left(\mathbf{e}_1 - \mathbf{e}_{\mathbf{f_{y_1}}}, \mathbf{e}_2 - \mathbf{e}_{\mathbf{f_{y_2}}}, \mathbf{f}_u + \mathbf{e}_{\mathbf{f}_u}, \mathbf{x}_{1_R}\right)
\end{aligned}
$$

By approaching the problem in the sense of the Singular Perturbations it is possible to select φ as perturbation parameter of *fault estimation* subsystem (fast dynamics). In this way the plant can be considered characterized by a slow dynamics (slower than that relative to the fault estimator). Consider the boundary-layer subsystem, here defined as:

$$e'_{f_i} = F_3(\mathbf{e}_1, \mathbf{e}_2, \mathbf{x}_{1_R}, \mathbf{u}, e_{f_i}) \tag{2.137}$$

Theorem 2.5. *The origin of the boundary-layer subsystem defined in* (2.137) *is an exponentially stable equilibrium point uniformly in* $(\mathbf{e}_1, \mathbf{e}_2, \mathbf{x}_{1_R}, \mathbf{u})$.⋄

Proof If the Hypothesis 2 is verified then the origin of (2.137) is uniformly LES in $(\mathbf{e}_1, \mathbf{e}_2, \mathbf{x}_{1_R}, \mathbf{u})$. In fact, the Hypothesis 2 requires $M_1(t)$ having some properties for each time $t > 0$, but the term $M_1(t)$ is:

$$M_1(t) = M_1\left(\mathbf{e}_1(t), \mathbf{e}_2(t), \mathbf{x}_{1_R}(t), \mathbf{u}(t)\right) \tag{2.138}$$

which means that for each time $t > 0$, the quadruple $(\mathbf{e}_1(t), \mathbf{e}_2(t), \mathbf{x}_{1_R}(t), \mathbf{u}(t))$ is such that the Hypothesis 2 is verified. In turn, if the Hypothesis 2 is verified the origin is LES for each time $t > 0$ independently on the particular value of each variable in the quadruple $(\mathbf{e}_1(t), \mathbf{e}_2(t), \mathbf{x}_{1_R}(t), \mathbf{u}(t))$, see Section 2.1.4.1. □

Theorem 2.6. *Consider the perturbed system described in* (2.136). *If all the following assumptions are verified then, there exists* $\varphi* > 0$ *such that for all* $\varphi < \varphi*$, *the origin of system* (2.136) *is locally exponentially stable.*

Assumptions:

1) the origin of system $(\mathbf{e}_1 = \mathbf{0}, \mathbf{e}_2 = \mathbf{0}, \mathbf{e_f} = \mathbf{0})$ *is an isolated equilibrium point and the functions* $\mathbf{L}_1 = \mathbf{F}_1 - \dot{\mathbf{x}}_R$, $\mathbf{L}_2 = \mathbf{F}_2 - \varepsilon\dot{\mathbf{x}}_{2_{\mathcal{M}}}$ *and* $L_3 = F_3$ *are locally Lipschitz in a domain that contain the*

origin. Hence,

$$
\begin{cases}
\mathbf{F}_1(\mathbf{0}, \mathbf{0}, \mathbf{x}_{1_R}, \mathbf{u}, \varepsilon) - \dot{\mathbf{x}}_R = \mathbf{0} \\
\mathbf{F}_2(\mathbf{0}, \mathbf{0}, \mathbf{x}_{1_R}, \mathbf{u}, \varepsilon) - \varepsilon \dot{\mathbf{x}}_{2_{\mathcal{M}}} = \mathbf{0} \\
F_3(\mathbf{0}, \mathbf{0}, \mathbf{x}_{1_R}, \mathbf{u}, 0) = 0
\end{cases}
\tag{2.139}
$$

where

$$
\begin{aligned}
\mathbf{u} &= \boldsymbol{\Gamma}_1\left(0, \mathbf{x}_{1_R}, \dot{\mathbf{x}}_{1_R}, \ddot{\mathbf{x}}_{1_R}\right) + \boldsymbol{\Gamma}_2\left(0, 0, \mathbf{F}_u, \mathbf{x}_{1_R}\right) = \\
&= \boldsymbol{\Gamma}_1\left(0, \mathbf{x}_{1_R}, \dot{\mathbf{x}}_{1_R}, \ddot{\mathbf{x}}_{1_R}\right) - \mathbf{F}_u
\end{aligned}
$$

2) the equation

$$
F_3(\mathbf{e}_1, \mathbf{e}_2, \mathbf{x}_{1_R}, \mathbf{u}, e_{f_i}) = 0
\tag{2.140}
$$

has an isolated root $e_{f_{i_{\mathcal{M}}}} = H_3(\mathbf{e}_1, \mathbf{e}_2, \mathbf{x}_{1_R}, \mathbf{u})$ such that:

$$
H_3(\mathbf{0}, \mathbf{0}, \mathbf{x}_{1_R}, \mathbf{u}) = 0;
\tag{2.141}
$$

3) the origin the reduced system (aircraft)

$$
\begin{aligned}
\dot{\mathbf{e}}_1 &= \mathbf{F}_1(\mathbf{e}_1, \mathbf{e}_2, \mathbf{x}_{1_R}, \mathbf{u}) - \dot{\mathbf{x}}_R \\
\varepsilon \dot{\mathbf{e}}_2 &= \mathbf{F}_2(\mathbf{e}_1, \mathbf{e}_2, \mathbf{x}_{1_R}, \mathbf{u}, \varepsilon) - \varepsilon \dot{\mathbf{x}}_{2_{\mathcal{M}}}
\end{aligned}
\tag{2.142}
$$

is exponentially stable;

4) the origin of boundary-layer system (fault estimation)

$$
e'_{f_i} = F_3(\mathbf{e}_1, \mathbf{e}_2, \mathbf{x}_{1_R}, \mathbf{u}, e_{f_i})
\tag{2.143}
$$

is exponentially stable, uniformly in $(\mathbf{e}_1, \mathbf{e}_2, \mathbf{x}_{1_R}, \mathbf{u})$.◇

Proof The proof starts by noting that the origin of the reduced system (plant)

$$
\begin{aligned}
\dot{\mathbf{e}}_1 &= \mathbf{F}_1(\mathbf{e}_1, \mathbf{e}_2, \mathbf{x}_{1_R}, \mathbf{u}, \varepsilon) - \dot{\mathbf{x}}_R \\
\varepsilon \dot{\mathbf{e}}_2 &= \mathbf{F}_2(\mathbf{e}_1, \mathbf{e}_2, \mathbf{x}_{1_R}, \mathbf{u}, \varepsilon) - \varepsilon \dot{\mathbf{x}}_{2_{\mathcal{M}}}
\end{aligned}
\tag{2.144}
$$

with $\mathbf{u} = \boldsymbol{\Gamma}_1\left(\mathbf{e}_1, \mathbf{x}_{1_R}, \dot{\mathbf{x}}_{1_R}, \ddot{\mathbf{x}}_{1_R}\right) + \boldsymbol{\Gamma}_2\left(\mathbf{e}_1, \mathbf{e}_2, \mathbf{f}_u, \mathbf{x}_{1_R}\right)$ is exponentially stable by design. The control law is such that, when in absence of fault estimation error, the origin of state-space error of plant subsystem is exponentially stable, see Section 2.2.2.3, indeed.

Furthermore, as proved in this section, also the origin of the boundary-layer subsystem (fault estimation) is exponentially stable and the boundary-layer manifold solution is an isolated root and corresponds to the origin.

Starting from above results, which verify all the assumptions in Theorem 2.6, the proof proceeds by following the same steps in the proof of Theorem 11.4 in [66]. □

Chapter 3

Case Studies

T his Section presents several applications of the proposed Active Control for aerospace
systems. The systems under investigation are aircraft, fixed wind unmanned aerial
vehicles, satellites and quadrotors. Their models share the same basic equations
and this is a fundamental aspect that allows the application of the proposed active
control strategy to all these systems. These examples cover different applications in terms of
active fault tolerant control, active disturbance rejection control and indirect adaptive control.

The motion of all aerospace systems, considered in this work, is described by two fundamental
groups of equations, see [87]. The first group is referred to the translational dynamics whereas
the second one describes the rotational dynamics. The equations describing the dynamics of
aircraft, UAV, satellite and quad-rotors have been written in an opportune body frame, selected
on the case, usually located in the center of gravity. Furthermore, all these systems are considered
rigid bodies, subject to the gravity (due the their mass) and external forces and momentums
generated by actuators (engines, momentum wheels, propellers, . . .) and by the interaction with
the environment (aerodynamics, solar pressure, . . .).

This thesis investigates methodologies, based on aerospace plants dynamics model, with a "short"
time horizon: the time windows during which the detection, isolation, estimation and the suc-
cessive control action evolve is short when in caparison with the entire mission of that system.
Thanks to these considerations the mass properties of the considered plants can be assumed as
constants.

The dynamics of a rigid body, in an inertial reference frame, expressed in body axes, is:

$$
\begin{aligned}
m\dot{\mathbf{V}}_{I,B} + \mathbf{\Omega}_B \times m\mathbf{V}_{I,B} &= \sum \mathbf{F}_B \\
\mathbf{I}\dot{\mathbf{\Omega}}_B + \mathbf{\Omega}_B \times \mathbf{I}\mathbf{\Omega}_B &= \sum \mathbf{M}_B
\end{aligned}
\tag{3.1}
$$

where m and $\mathbf{I}$ represent the mass and the inertia matrix respect to the center of gravity, $\mathbf{V}_{I,B}$ is the translational speed respect to the inertial frame and expressed in body axes, $\mathbf{\Omega}_B$ depicts the rotational speed vector in body axes, and finally, $\mathbf{F}_B$ and $\mathbf{M}_B$ respectively are the external forces and momentums expressed in body axes.

The description of the motion of a rigid body is completed by the kinematic equations, also, divisible in rotational and translational quantities:

$$
\begin{aligned}
\dot{\mathbf{P}}_I &= \mathbf{R}_{B\to I}\mathbf{V}_{I,B} \\
\dot{\mathbf{R}}_{B\to I} &= \mathbf{S}\left(\mathbf{\Omega}_B\right)\mathbf{R}_{B\to I}
\end{aligned}
\tag{3.2}
$$

where $\mathbf{P}_I$ represents the inertial position and $\mathbf{R}_{B\to I}$ is the rotation matrix from the body frame to the inertial frame and describes the attitude of the rigid body relative to the inertial frame.

The next Sections describe, for each of the considered aerospace systems, the external forces and momentums and the interaction with the environment.

Equations (3.1)-(3.2) describe the physical model of the system, particularly suitable for simulation goal, and for this called "simulation" model. The simulation model is completed by identifying which are the manipulable inputs, the disturbances and the available outputs leading, in this way, to the determination of the so called "synthesis" model, *i.e.* the model used for design. Often, due to the model high complexity, some simplifications are introduced in order to make the synthesis model practically exploitable during the design process.

3.1 Aircraft

The aircraft mathematical model is obtained by completing the equations (3.1)-(3.2) with the description of the external forces and momentums, $\mathbf{F}_B$ and $\mathbf{M}_B$. This work considers as "inertial" frame a frame located on the earth surface and oriented along the North-East-Down directions (NED). The external forces are due to the gravity acceleration, the aerodynamics and engine thrust, see [88]:

$$
\begin{aligned}
\mathbf{F}_B &= \mathbf{F}_{B,g} + \mathbf{F}_{B,a} + \mathbf{F}_{B,e} \\
\mathbf{F}_{B,g} &= \mathbf{R}_{I \to B}\, \mathbf{e}_z\, m\, g \\
\mathbf{F}_{B,a} &= \tfrac{1}{2}\, \rho\, S\, V_a^2 \begin{bmatrix} C_x \\ C_y \\ C_z \end{bmatrix} \\
\mathbf{F}_{B,e} &= \mathbf{F}_{B,e}\,(V_a, RPM, \rho, \delta_{th})
\end{aligned}
\tag{3.3}
$$

The force due to the gravity acceleration, g, is represented by $\mathbf{F}_{B,g}$ where $\mathbf{R}_{I \to B}$ is the rotation matrix from inertial to body axes and $\mathbf{e}_z$ indicates the unitary vector along the *Down* axes of the NED reference frame.

The aerodynamic forces $\mathbf{F}_{B,a}$ are function of the True AirSpeed, V_a, *i.e.* the aircraft speed relative to the air, the air density ρ and the reference wing surface S. Furthermore, the aerodynamic force components are modulated by three aerodynamic coefficients C_x, C_y and C_z. Usually, they are functions of the airspeed vector components and their first time derivatives, the air relative rotational speed and the control surface deflections:

$$
C_\# = C_\# \left(\mathbf{V}_{a,B},\, \dot{\mathbf{V}}_{a,B},\, \mathbf{\Omega}_{a,B},\, \boldsymbol{\delta} \right)
\tag{3.4}
$$

with $\# \in \{x, y, z\}$,

$$
\begin{aligned}
\mathbf{V}_{a,B} &= \mathbf{V}_{I,B} - \mathbf{W}_{I,B} \\
|\mathbf{V}_{a,B}| &= V_a \\
\mathbf{\Omega}_{a,B} &= \mathbf{\Omega}_B - \mathbf{\Omega}_{W_{I,B}}
\end{aligned}
\tag{3.5}
$$

where $\mathbf{V}_{a,B}$ is the airspeed vector, $\mathbf{W}_{I,B}$ represents the wind velocity respect to the inertial frame, $\mathbf{\Omega}_{a,B}$ indicates the rotational speed relative to the air and, finally, $\mathbf{\Omega}_{W_{I,B}}$ depicts the wind rotational field. The aerodynamic surfaces deflections are represented by $\boldsymbol{\delta} = [\delta_e,\, \delta_a,\, \delta_r]^T$ for elevator, aileron and rudder respectively.

The engines provide the thrust force, $\mathbf{F}_{B,e}$ that usually is a function of the flight conditions both in terms of airspeed, V_a, and air density ρ. The available thrust also depends on the engine working condition, here summarized by the engine shaft rotational speed RPM, on lots of engine parameters (kind of propulsion system, size, ...) and as well as on the throttle valve opening value δ_{th}.

The external momentums, acting on the center of gravity of an aircraft, are composed by two contributes:

$$
\begin{aligned}
\mathbf{M}_B &= \mathbf{M}_{B,a} + \mathbf{M}_{B,e} \\
\mathbf{M}_{B,a} &= \tfrac{1}{2}\,\rho\,S\,V_a^2\,\bar{c}
\begin{bmatrix} C_l \\ C_m \\ C_n \end{bmatrix} \\
\mathbf{M}_{B,e} &= \mathbf{M}_{B,T}\,(V_a, RPM, \rho, \delta_{th})
\end{aligned} \tag{3.6}
$$

The momentums induced by the engine, $\mathbf{M}_{B,e}$, is due to the lever arm between the thrust and the gravity center, and to the propulsion system rotational momentum plus the gyroscopic effects.

The aerodynamic momentums reflect the same structure and the same dependencies of the aerodynamic forces but with a further dimensional term, $\bar{c}$, that is the mean aerodynamic chord.

The simulator in Figure 3.1 performs the updating of both the air density, ρ, and the gravity acceleration modulus, g, by implementing the reference [89] and [90] respectively. The aerodynamic surface deflection and throttle dynamics have been modeled as suggested in [88].
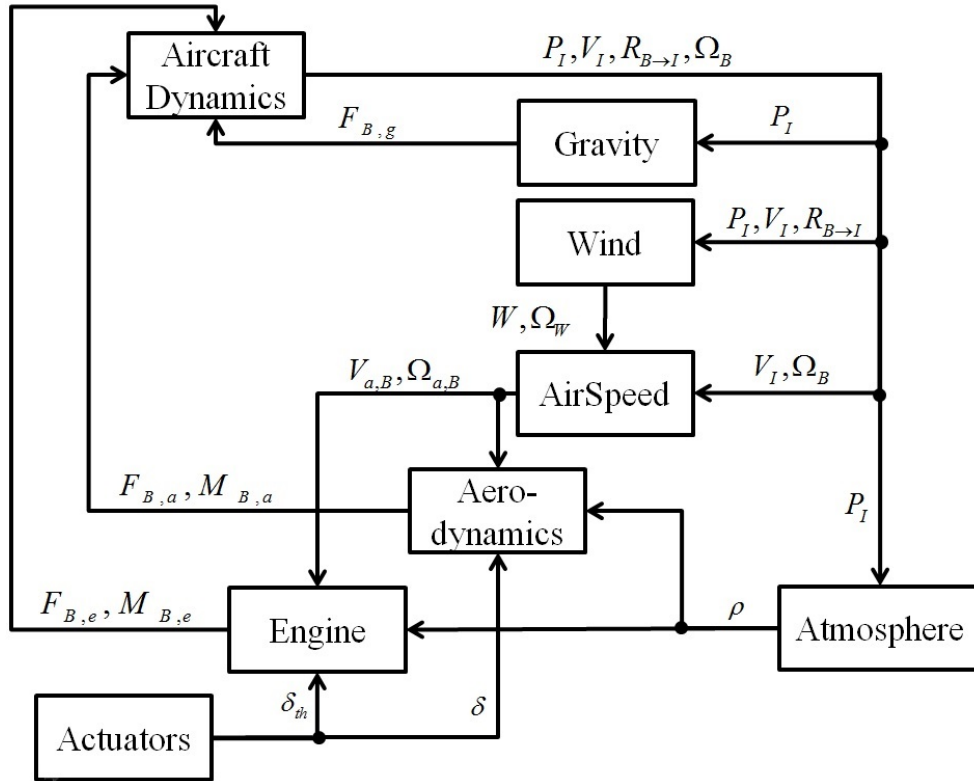
FIGURE 3.1: Aicraft simulator structure.

The simulator is comprehensive of different wind representations: constant wind, wind shear and turbulence. As suggested in [91], the wind shear can be modeled in inertial axes as function of spatial coordinates and then rotated to convenient axes, that in this work are the wind axes. In particular, the wind model proposed in [91], is relative to microburst and is the most detailed and

realistic analytical description for microburst presented nowadays in literature. In this work the microburst is described by its linear components as well as its rotational field. The microburst components are functions of the position and inertial speed of the aircraft:

$$
\begin{aligned}
\mathbf{W} &= \mathbf{W}\left(\mathbf{P}_I\right) \\
\mathbf{\Omega}_{W_I} &= \mathbf{\Omega}_{W_I}\left(\mathbf{P}_I\right)
\end{aligned}
\tag{3.7}
$$

Finally, also the Dryden turbulence model ([92] and [93]) (translational and rotational) has been implemented by using the "Dryden Wind Turbulence Model" in the "Aerospace Blockset" of Matlab–Simulink [94].

The simulator implements a model of the measurement system as follows:

- the command surface deflection angles are acquired by potentiometers whose errors are modeled as white noises;

- the angular rate measurements are given by 2 gyroscopes of an IMU (Inertial Measurement Unit). The corresponding errors take into account non unitary scale factor, alignment error (random), g–sensitivity, additive white noise, gyro drift;

- the attitude angle measurement is given by a digital filtering system of both angular rate and accelerations provided by the IMU. The corresponding errors are due to a systematic uncertainty generated by the apparent vertical and a colored noise due to the system structure and the environment influences;

- the angular rate measurements provided by a gyroscope unit different from gyroscope device estimating angular rates and characterized by small drift vs larger bandwidths;

- Air Data Computer (ADC):

  - Errors affecting the True AirSpeed are due to calibration error of differential pressure sensor, additive colored noise induced by wind gusts and atmospheric turbulence and additive white noise;

  - Errors affecting the altitude are the calibration error of the static pressure sensor and an additive white noise;

  - Uncertainties affecting the attack angle are calibration errors affecting the wing boom sensors and additive white noise.

A detailed description of the measurements used by the considered system can be found in [55].

Synthesis model

The model based on (3.1)-(3.6) is particularly suitable for simulations but, for both the diagnosis module and controller design, the use of a transformed set of equations expressed in the so called "wind" reference frame is preferred. In this new reference frame, all the quantities, referred to aerodynamic variables except for the body angular rates, are organized in a cascade structure particularly suitable for the application of the backstepping and singular perturbation control methodologies.

$$
\begin{bmatrix} \dot{X} \\ \dot{Y} \\ \dot{Z} \end{bmatrix} = \begin{bmatrix} V_a \cos\chi\cos\gamma \\ V_a \sin\chi\cos\gamma \\ -V_a \sin\gamma \end{bmatrix} + \mathbf{W}_I
\tag{3.8}
$$

$$
\begin{bmatrix} \dot{V}_a \\ \dot{\chi} \\ \dot{\gamma} \end{bmatrix} = \begin{bmatrix} -g\sin\gamma \\ 0 \\ -\frac{g}{V_a}\cos\gamma \end{bmatrix} + \frac{1}{m}\begin{bmatrix} 1 & 0 & 0 \\ 0 & -\frac{\cos\mu}{V_a\cos\gamma} & -\frac{\sin\mu}{V_a\cos\gamma} \\ 0 & \frac{\sin\mu}{V_a} & -\frac{\cos\mu}{V_a} \end{bmatrix}\begin{bmatrix} -D \\ Y \\ -L \end{bmatrix} + \varepsilon_{I\to W}^{-1}\dot{\mathbf{W}}_I +
$$
$$
+ \frac{1}{m}\begin{bmatrix} 1 & 0 & 0 \\ 0 & -\sin\mu\cos\beta\sec\gamma & \cos\mu\sec\gamma \\ 0 & -\cos\mu\cos\beta & -\sin\mu \end{bmatrix}\varepsilon_{B\to W}^{-1}\mathbf{F}_{B,e}
\tag{3.9}
$$

$$
\begin{bmatrix} \dot{\mu} \\ \dot{\alpha} \\ \dot{\beta} \end{bmatrix} = \begin{bmatrix} \sin\gamma+\cos\gamma\sin\mu\tan\beta & \cos\mu\tan\beta \\ -\cos\gamma\sin\mu\sec\beta & -\cos\mu\sec\beta \\ \cos\mu\cos\gamma & -\sin\mu \end{bmatrix}\begin{bmatrix} \dot{\chi} \\ \dot{\gamma} \end{bmatrix} +
$$
$$
+ \begin{bmatrix} \cos\alpha\sec\beta & 0 & \sin\alpha\sec\beta \\ -\cos\alpha\tan\beta & 1 & -\sin\alpha\tan\beta \\ \sin\alpha & 0 & -\cos\alpha \end{bmatrix}\mathbf{\Omega}_B
\tag{3.10}
$$

$$
\mathbf{I}\dot{\mathbf{\Omega}}_B + \mathbf{\Omega}_B \times \mathbf{I}\mathbf{\Omega}_B = \mathbf{M}_{B,a} + \mathbf{M}_{B,e}
\tag{3.11}
$$

where $\varepsilon_{I\to W}$ and $\varepsilon_{B\to W}$ are defined as follows:

$$
\varepsilon_{I\to W}(V_a,\chi,\gamma) = \begin{bmatrix} \cos\chi\cos\gamma & -V_a\sin\chi\cos\gamma & -V_a\cos\chi\cos\gamma \\ \sin\chi\cos\gamma & V_a\cos\chi\cos\gamma & -V_a\sin\chi\sin\gamma \\ -\sin\gamma & 0 & -V_a\cos\gamma \end{bmatrix}
\tag{3.12}
$$

$$
\varepsilon_{B\to W}(V_a,\alpha,\beta) = \begin{bmatrix} \cos\beta\cos\alpha & -V_a\sin\beta\cos\alpha & -V_a\cos\beta\sin\alpha \\ \sin\beta & V_a\cos\beta & 0 \\ \sin\alpha\cos\beta & -V_a\sin\beta\sin\alpha & V_a\cos\beta\cos\alpha \end{bmatrix}
\tag{3.13}
$$

The aerodynamic forces, expressed in wind axes, are represented by the vector

$$\begin{bmatrix} -D \\ Y \\ -L \end{bmatrix} = \frac{1}{2}\rho S V_a^2 \begin{bmatrix} -C_D\left(\alpha, \beta, \boldsymbol{\Omega}_a, \boldsymbol{\delta}\right) \\ C_Y\left(\alpha, \beta, \boldsymbol{\Omega}_a, \boldsymbol{\delta}\right) \\ -C_L\left(\alpha, \beta, \boldsymbol{\Omega}_a, \boldsymbol{\delta}\right) \end{bmatrix} \tag{3.14}$$

The same dependences can be written for the aerodynamic momentums:

$$\mathbf{M}_{B,a} = \frac{1}{2}\,\rho\,S\,V_a^2\bar{c} \begin{bmatrix} C_l\left(\alpha, \beta, \boldsymbol{\Omega}_a, \boldsymbol{\delta}\right) \\ C_m\left(\alpha, \beta, \boldsymbol{\Omega}_a, \boldsymbol{\delta}\right) \\ C_n\left(\alpha, \beta, \boldsymbol{\Omega}_a, \boldsymbol{\delta}\right) \end{bmatrix} \tag{3.15}$$

A common assumption sees the propulsion system producing only a thrust aligned with the x-body axes. In this scenario the following holds:

$$\begin{aligned} \mathbf{F}_{B,e} &= \begin{bmatrix} T & 0 & 0 \end{bmatrix}^T \\ \mathbf{M}_{B,e} &= \mathbf{d}_T \times \mathbf{F}_{B,e} \end{aligned} \tag{3.16}$$

where $\mathbf{d}_T$ represents the lever arm of the thrust respect to the aircraft center of gravity.

3.1.1 Active Fault Tolerant Control - Case 1

The simulated aircraft is a Piper PA-30 for which very detailed NASA and Lycoming technical data are available. NASA Technical Notes [95], [96] and [97] describing the aircraft and propeller aerodynamics and the engine manual [98] for engine model have been implemented for simulation purposes.

Considering only the longitudinal dynamics the scenario, relative to this case, is composed by two non-concurrent faults, $f_{u_{\delta_e}}$ and $f_{u_{th}}$, respectively on elevator and throttle actuators, whereas the vertical wind gust W_h represents the disturbance. In this contests the vectors $\mathbf{f}_s$ and $\mathbf{d}_s$ are identified by:

- for the isolation of $f_{u_{th}}$: $\mathbf{f}_{s_1} = f_{u_{th}}$ $\qquad \mathbf{d}_{s_1} = \begin{bmatrix} W_h, f_{u_{\delta_e}} \end{bmatrix}^T$

- for the isolation of $f_{u_{\delta_e}}$: $\mathbf{f}_{s_2} = f_{u_{\delta_e}}$ $\qquad \mathbf{d}_{s_2} = [W_h, f_{u_{th}}]^T$

The faults are assumed to be step functions of the time and the estimation algorithm selected for this scenario is the recursive Least Squares with forgetting factor.

All the details on the backstepping controller structure, the $\bar{\mathbf{x}}_1$-subsystems obtained by applying the NLGA procedure, the stability proofs can be found in [58].
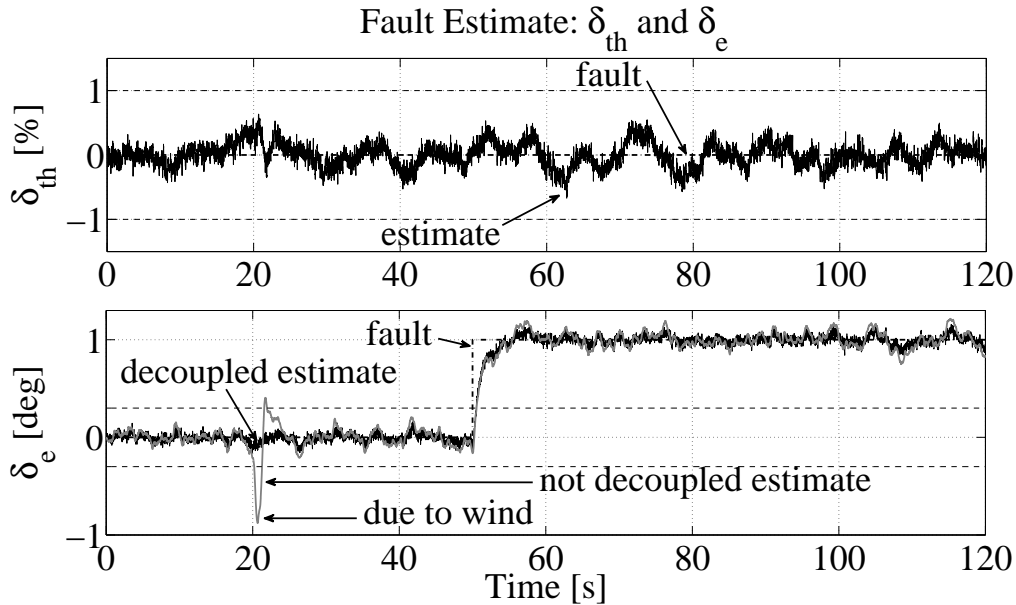
FIGURE 3.2: Estimate $\hat{f}_{\delta_e}$ of f_{δ_e} fault.

Simulation results

In this case study the filters are decoupled from both aerodynamic disturbances, *i.e.* the vertical wind gust, and the other fault. Figure 3.2 shows a fault on the elevator (dotted line) of size $f_{\delta_e} = 1^o$ and its estimate (black and gray) during an altitude hold flight phase. The fault is detected, isolated and estimated with a time delay smaller than the characteristic flight dynamics period and the convergence of the estimate to the actual fault size is observed. The fault commences at time $t = 50s$. Figure 3.2 shows that, via the NLGA design, the residual for the estimation of the throttle fault does not exceed its thresholds even in presence of elevator faults. The lower picture of Figure 3.2 shows also an elevator fault estimation (gray line) that is not decoupled from wind disturbances. It is clear how the wind gust (at time $20s$) affects the fault estimate (gray line) making it useless.

Figure 3.3 shows the accurate fault estimate for the case of a fault on the throttle of size $f_{\delta_{th}} = -10\%$.

The performance of the controlled aircraft with or without the estimated fault feedback are compared. In this way, the benefits of adopting the proposed AFTC scheme are highlighted in terms of state dynamics. The following simulations performed in presence of wind and noise on both input and output sensors serve to highlight the advantages of the fault recovery procedure obtained by using the fault estimate feedback. Since the fault is detected, isolated and estimated with a dynamics faster than the fastest aircraft dynamics, the flight proceed normally without loss of performance. Figure 3.4 is particularly meaningful because it compares the influence of a vertical wind gust and the effect of a not recovered elevator fault on the altitude. Similar considerations hold for Figure 3.5 that depicts the transient after the throttle fault occurrence. It
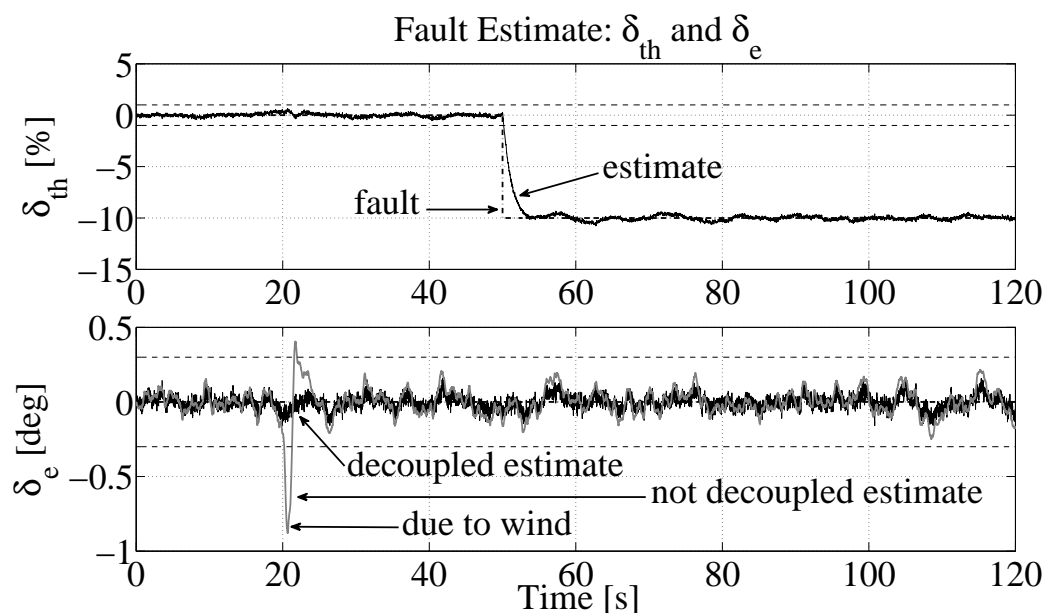
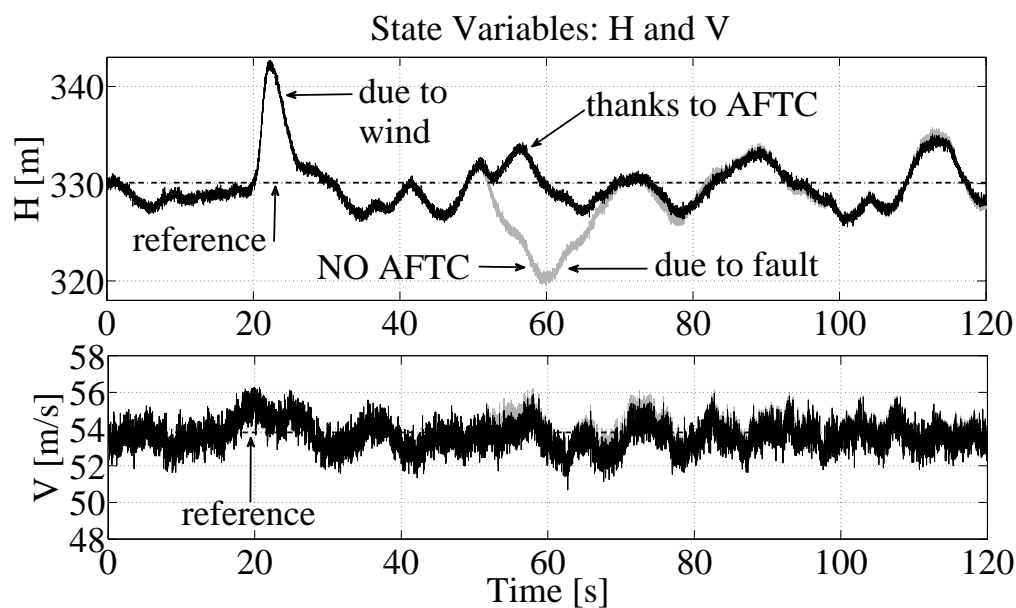FIGURE 3.3: Estimate $\hat{f}_{\delta_{th}}$ of $f_{\delta_{th}}$ fault.

FIGURE 3.4: Aircraft state with and without AFTC scheme: case of fault on δ_e.

is worth observing that the results refer to the same simulations conditions (noises, disturbances, *etc.*).

3.1.2 Active Fault Tolerant Control - Case 2

The scenario considered in this case regards an Active Fault Tolerant Control that allows an aircraft to land, even in presence of multiple and concurrent sinusoidal faults of both elevator
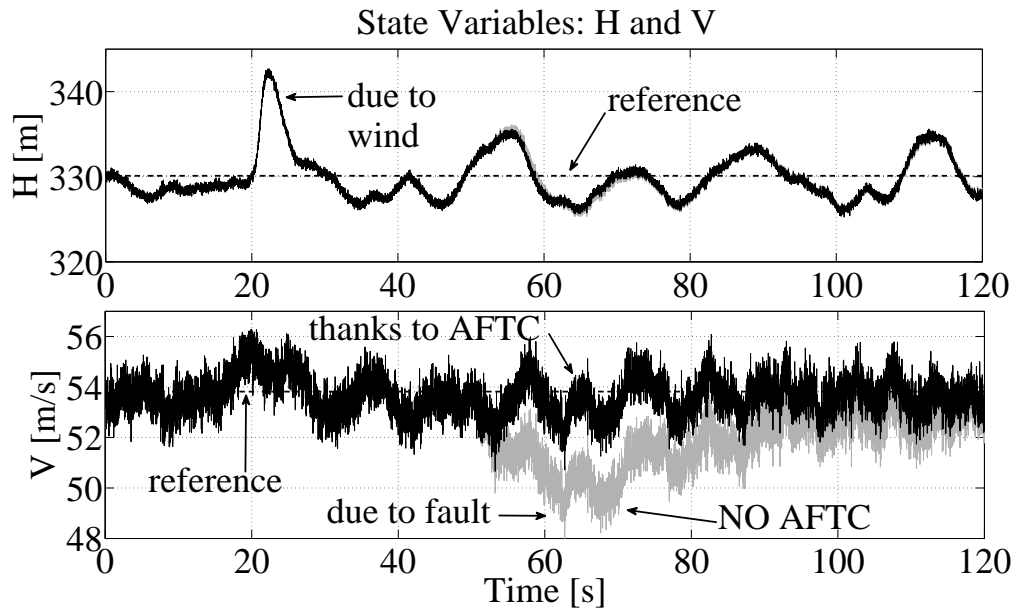
FIGURE 3.5: Aircraft state with and without AFTC scheme: case of fault on δ_{th}.

and throttle. The isolation module provides two distinct and independent activation signal for two dedicated estimation filters.

Differently from the kind of faults considered in Section 3.1.1, in this case the faults are characterized by a more general behavior and the recursive Least-Squares with forgetting factor is not the most appropriate estimation algorithm. In this case, a Radial Basis Functions Neural Network has been implemented because it allows the estimation of generic functions due to their approximation capabilities, see [73].

As in Section 3.1.1, only the longitudinal dynamics has been considered as methodologically representative example. All the details on the backstepping controller and on the Detection, Isolation and Estimation module are contained in [59].

Simulation results

In order to test the performances brought by the application of the proposed AFTFC scheme, an RQ-2 Pioneer UAV simulator has been considered. Whereas the simulator structure remain the same of Figure 3.1, the geometric and aerodynamic characteristics of the aircraft and the simulation parameters are those considered in [63] and [99]. Also a first order dynamic system has been introduced to simulate the engine response. The actual fault amplitude are $100N$ and $5deg$ with commencing time $100s$ and $200s$ for thrust and elevator faults respectively. Hence, after the time $t = 200s$ the faults are concurrent. The measurement noises are characterized by 3σ equal to 1 for V, γ and α in the proper dimensions m/s and deg, and 0.1 for q in deg/s.
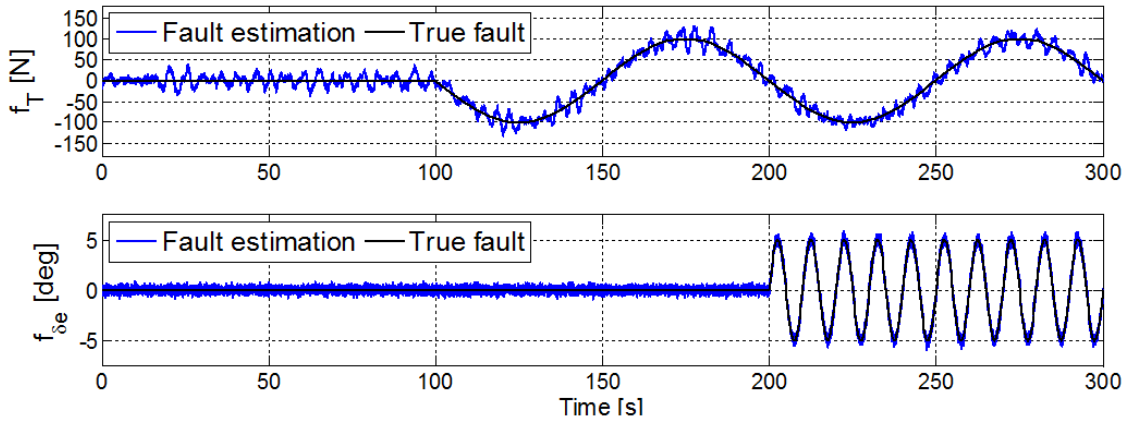
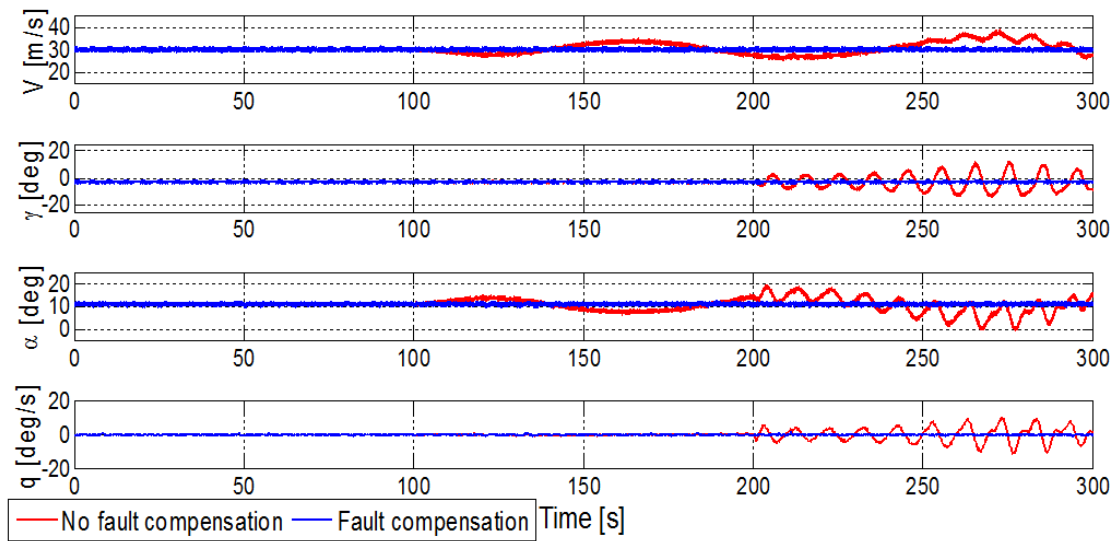FIGURE 3.6: Estimation of sinusoidal concurrent faults on δ_{th} and δ_e.

FIGURE 3.7: Aircraft state with and without AFTC scheme: case of concurrent faults on δ_{th} and δ_e.

In this case the backstepping controller, without fault estimates feedback, is not able to compensate the fault neither after a transient, as highlighted in Figures 3.7 and 3.8.

On the other hand, the proposed AFTFC, which exploits the accurate sinusoidal estimates for fault compensation, see Figure 3.6, yields to a very good aircraft behavior thus restoring a safe flight envelope. Finally, since in presence of sinusoidal fault, a threshold based on the fault size estimate cannot be defined, this work uses the mean of the absolute fault estimate on a sliding window as fault detection signal.
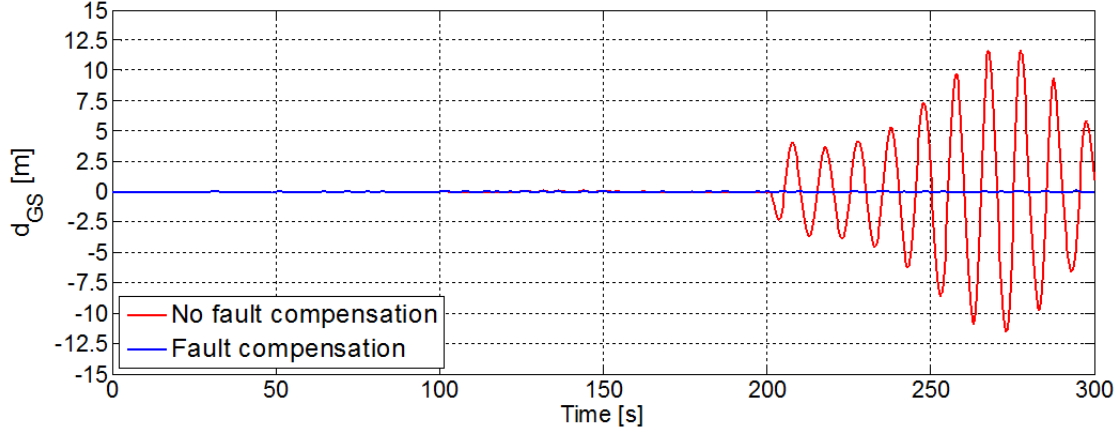
FIGURE 3.8: Distance from the glide slope with and without AFTC scheme: case of concurrent faults on δ_{th} and δ_e.

3.1.3 Active Fault Tolerant Control - Case 3

This case presents the most complex fault scenario of this thesis. Considering only the longitudinal dynamics of an aircraft, this case proposes a fault scenario composed by 8 non concurrent faults, 4 of them on the state sensors, 2 on the actuators state sensors and, finally, 2 on the actuators:

- output faults: $\mathbf{f}_y = [f_V, f_\gamma, f_\alpha, f_q, f_{y_e}, f_{y_T}]^T$;

- input faults; $\mathbf{f}_u = \left[f_{u_{\delta_e}}, f_{u_{\delta_T}} \right]^T$

The fault scenario is represented by $\mathbf{f} = [f_1, ..., f_8]^T = \left[\mathbf{f}_y^T \ \mathbf{f}_u^T \right]^T$ and 8 $\mathbf{f}_s$ and $\mathbf{d}_s$ can be identified with:

$$\mathbf{f}_{s_i} = f_i \quad \mathbf{d}_{s_i} = \mathbf{f} \setminus f_i \quad \forall i \in \{1, ..., 8\} \tag{3.17}$$

The Isolation logic works on the base of the Table 3.1, representing the Residual Matrix, RM.

TABLE 3.1: Isolation Logic Residual Matrix

Faults	r_1	r_2	r_3	r_4	r_5
f_V	1	1	1	0	0
f_γ	1	0	0	0	0
f_α	0	1	1	0	0
f_q	0	0	1	0	0
f_{y_T}	0	1	1	1	0
f_{y_e}	0	1	1	0	1
f_{u_T}	1	0	0	1	0
$f_{u_{\delta_e}}$	1	0	0	0	1
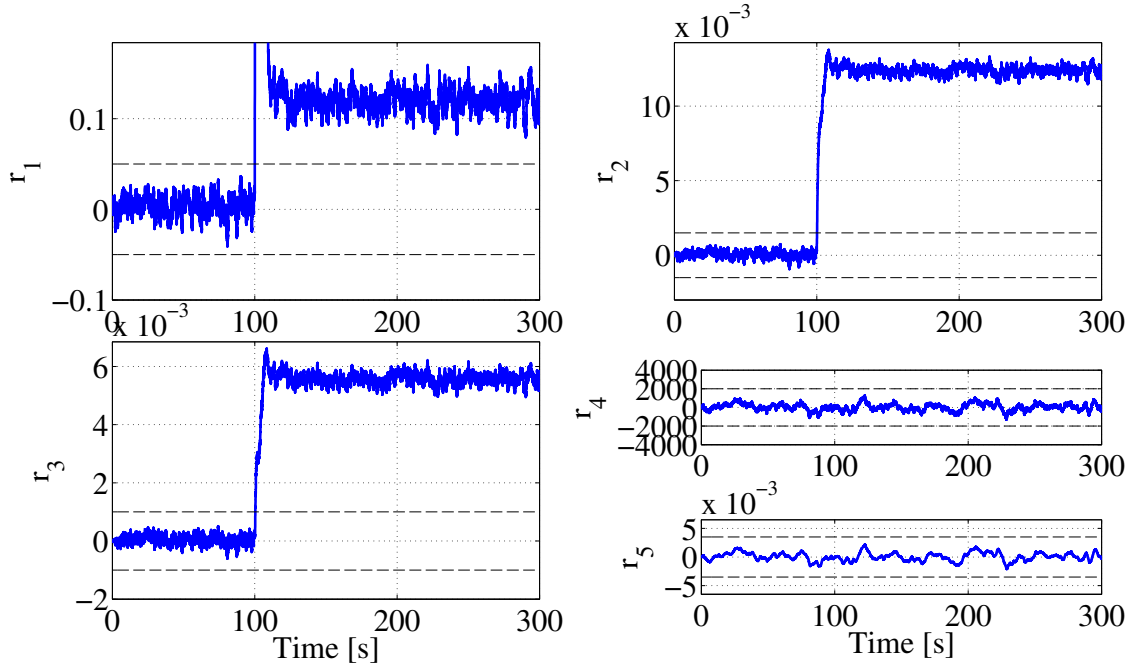
FIGURE 3.9: Detection residuals behavior: comparison for isolation.

The longitudinal dynamics of the aircraft is controlled by a "composite" controller, see Section 2.2.2, with the "slow" $\mathbf{x}_1$ and the "fast" $\mathbf{x}_2$ state variables identified as follows:

$$\mathbf{x}_1 = [V, \gamma]^T \quad \mathbf{x}_2 = [\alpha, q, \delta_e, T]^T \tag{3.18}$$

where the dynamics of the actuators has been classified as a "fast" dynamics. Finally, the errors $\mathbf{e}_1$ and $\mathbf{e}_2$ are defined as in 2.2.2. The details and results relative to this case have been presented in [56].

Simulation results

This section evaluates the performance of the AFTC in a fault scenario that take account of the presence of sensor noises. The guide and control performances are investigated by showing the state errors, $\mathbf{e}_1$ and $\mathbf{e}_2$, whereas the Diagnosis module performance is shown by the fault estimation behavior, $\hat{f}_i$. The simulated aircraft is a wide-body jet commercial airliner which aerodynamics and mass properties, listed in [100], have been implemented in the simulator of Figure 3.1. The reference trajectory is described by the constant vector $\mathbf{x}_{1_R} = [V_R, \gamma_R]^T = [67m/s, -3deg]^T$ which corresponds to a faultless manifold described by the constraint:

$$\mathbf{x}_{2_{\mathcal{M}}} = [\alpha_{\mathcal{M}}, q_{\mathcal{M}}, T_{\mathcal{M}}, \delta_{e_{\mathcal{M}}}]^T = \left[10.3deg, 0deg/s, 2.67 \cdot 10^5 N, 0deg\right]^T \tag{3.19}$$
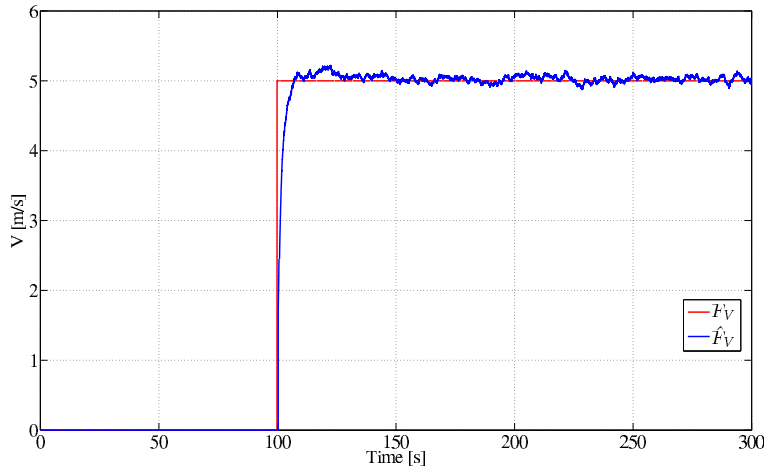
FIGURE 3.10: Fault Estimation: $\hat{F}_V$ estimates F_V.

The simulations are particularly meaningful since the slow and fast dynamics, for this class of aircrafts, are significantly coupled.

In Fig. 3.9 the residuals behavior has been showed in the case of airspeed sensor fault, f_V. The first three residuals overstep their threshold identifying, in this way, the configuration of the first row of Table 3.1. The isolation logic, in less than 1 second, recognizes the faulty sensor and activates the estimation filter, which is specifically designed to estimate the isolated fault. Fig. 3.10 shows the estimation of f_V with a settling time of about 4 seconds. Furthermore, in presence of the same fault f_V, Fig. 3.11 shows the state error as deviation from reference trajectory: the red line shows the controller performance when no fault compensation is engaged, *i.e.* when the fault estimation is not provided to the controller. The AFTC, that exploits the fault estimation (blue line), guarantees high performance levels similar to the case of faulty free scenario. Finally, it is worth nothing that without fault compensation the angle of attack, α, gets hazardously close to the stall angle.

3.1.4 Active Wind Rejection Control

In this scenario the problem is limited to the longitudinal dynamics of an aircraft that is flying along the glide path. During the final approach, a wind shear is encountered and the control goal is to let the aircraft continuing its mission (descent).

Two main wind contributions have been taken into account: the wind shear, modeled by a deterministic model, and the turbulences, well described by the Dryden statistic wind model. The wind shear model, suggested in [91], is relative to microburst and it is the most realistic analytical description for microburst presented till now. Furthermore the rotational wind field has been taken into account too. When the aircraft dynamics are expressed with respect to the
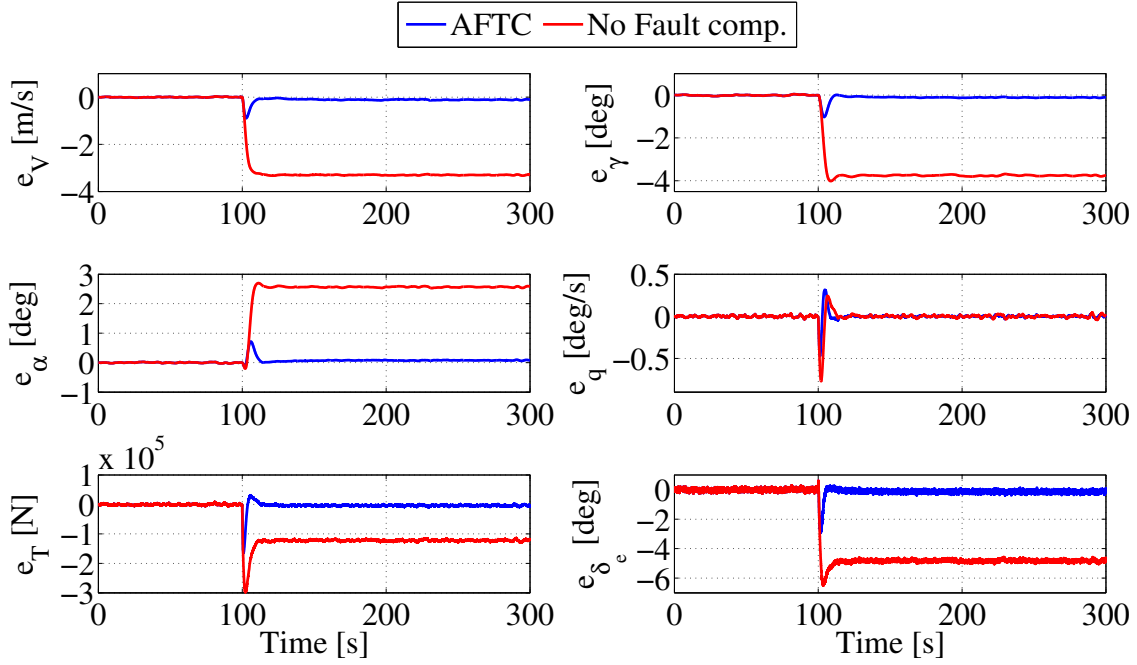
FIGURE 3.11: State error, $\mathbf{e} = [\mathbf{e}_1, \mathbf{e}_2]^T$: the designed AFTC, when engaged, guarantees faultless–like performance.

wind axes, the wind time derivatives arise as described in Section 3.1. Equation (3.9) contains also the first time derivative of the linear wind components. Since the wind shear modeled as in [91] is a space but time invariant function, its time derivative is formally obtained as:

$$\dot{\mathbf{W}}_I = \mathbf{J}\left(\mathbf{W}_I\right) \begin{bmatrix} \dot{X} \\ \dot{Y} \\ \dot{Z} \end{bmatrix} \tag{3.20}$$

where $\mathbf{J}\left(\mathbf{W}_I\right)$ represent the Jacobian matrix of $\mathbf{W}_I$. Even if the microburst is modeled as fixed with respect to the ground, aircraft flying through this wind experiment a different shape wind because of different trajectory in time–space coordinates. This fact has motivated the authors to find estimation filters for generic winds. The estimation algorithm implemented for this case is based on the Radial Bases Function Neural Network.

The implemented controller is a backstepping type and its details as well as the description of the $\bar{\mathbf{x}}_1$-subsystems are published in [64].

Simulation results

The adopted simulated aircraft is a wide-body airliner whose parameters are summarised in Table 3.2 of [64]. The nonlinear simulator is detailed with an accurate aerodynamics description and the implementation of the most advanced microburst model, as specified in [91]. The aircraft is
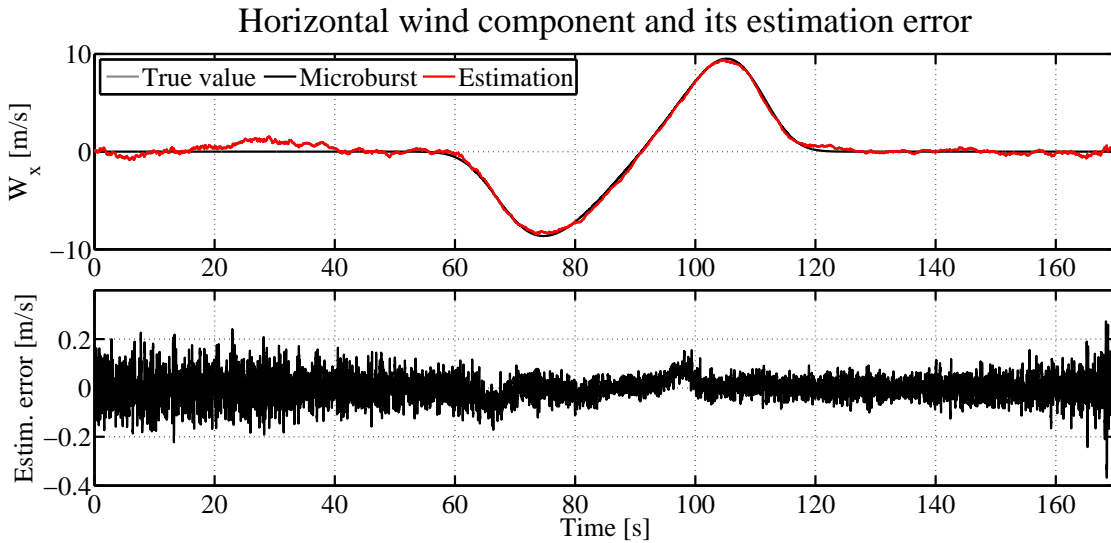
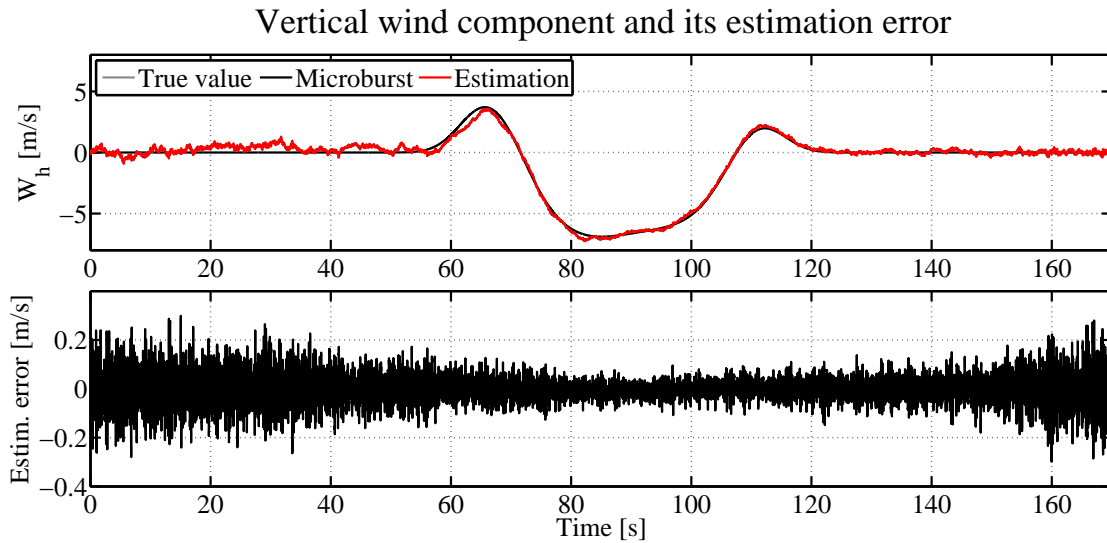FIGURE 3.12:   Comparison of the simulated and estimated horizontal wind component.

FIGURE 3.13:   Comparison of the simulated and estimated vertical wind component.

assumed to be in an approach configuration during the final segment of an instrumental landing trajectory.

The following figures show the performances of the designed NLGA RBF-NN adaptive filters providing the estimates of the wind disturbance components. Figures 3.12, 3.13 and 3.14 report the comparisons between the simulated wind components W_x, W_h and ω_q (gray lines) and their relative estimations $\hat{W}_x$, $\hat{W}_h$ and $\hat{\omega}_q$ (red lines).   Figures 3.15 and 3.16 show the estimates of the wind derivatives $\dot{W}_x$ and $\dot{W}_h$. In particular, they show the actual values of the overall wind derivatives (gray lines) comprehensive of Dryden turbulences, the actual values of the wind shear microburst derivatives only (black lines) and the corresponding estimates (red lines). The
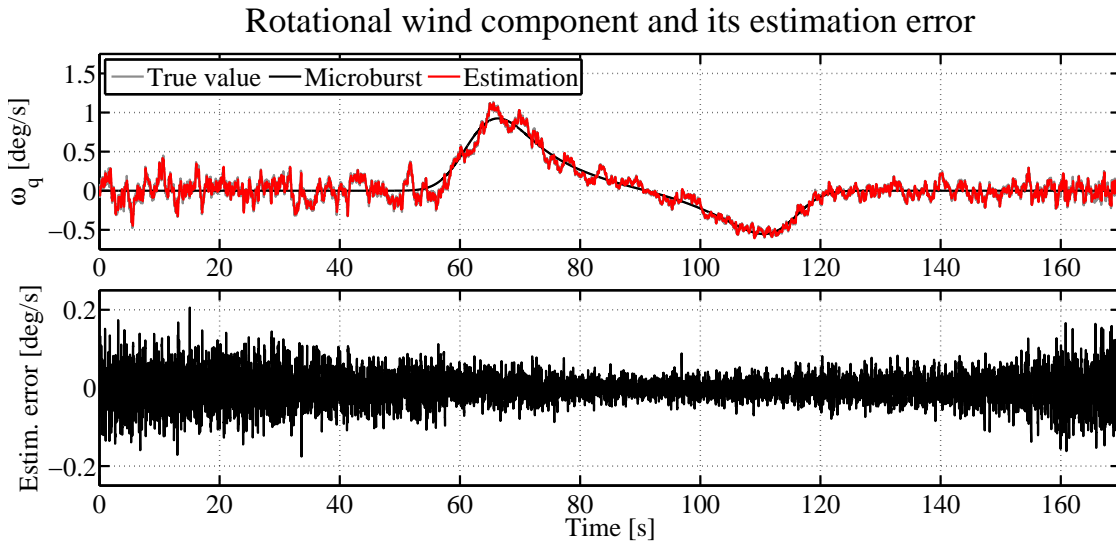
Rotational wind component and its estimation error

FIGURE 3.14:   Comparison of the simulated and estimated rotational wind component.

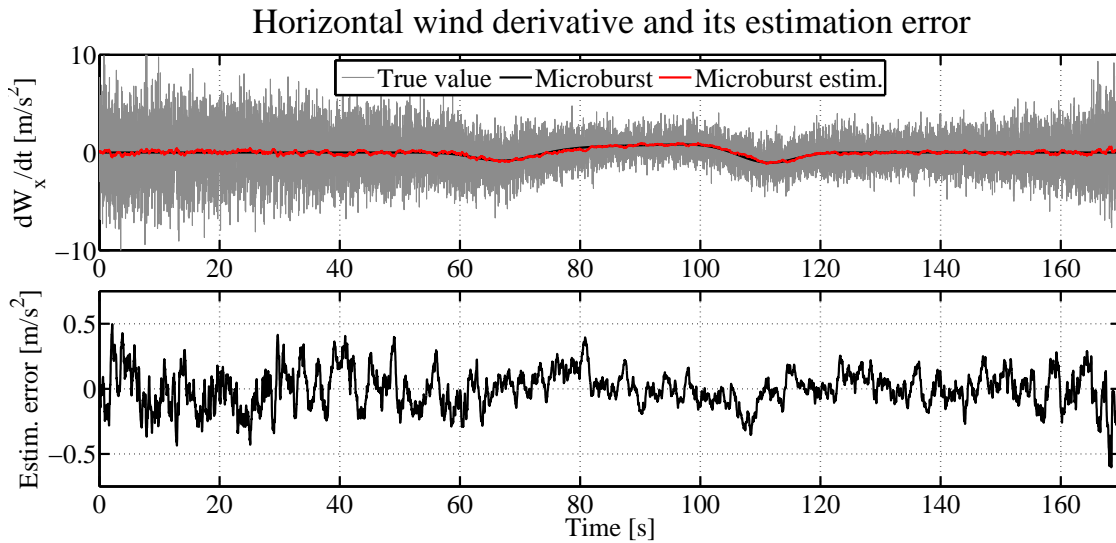## Horizontal wind derivative and its estimation error

FIGURE 3.15:   Comparison of the simulated and estimated horizontal wind derivative.

estimation goal is to provide a good and fast estimation of the microburst wind components only. It can be seen that the designed adaptive filters are able to estimate the evolution of the microburst wind derivatives by filtering the high frequency components due to the Dryden turbulence derivatives.

The wind estimates are exploited by the controller in order to compensate the wind effects and guarantee a safe flight during the glide slope path following. Figure 3.17 shows the distance (tracking error) from the glide path in presence of wind–shear microburst and Dryden turbulences, whose components have been described in Section 3.1.4. The benefits of a wind compensating controller, that allows a substantial reduction of the distance from the glide path,
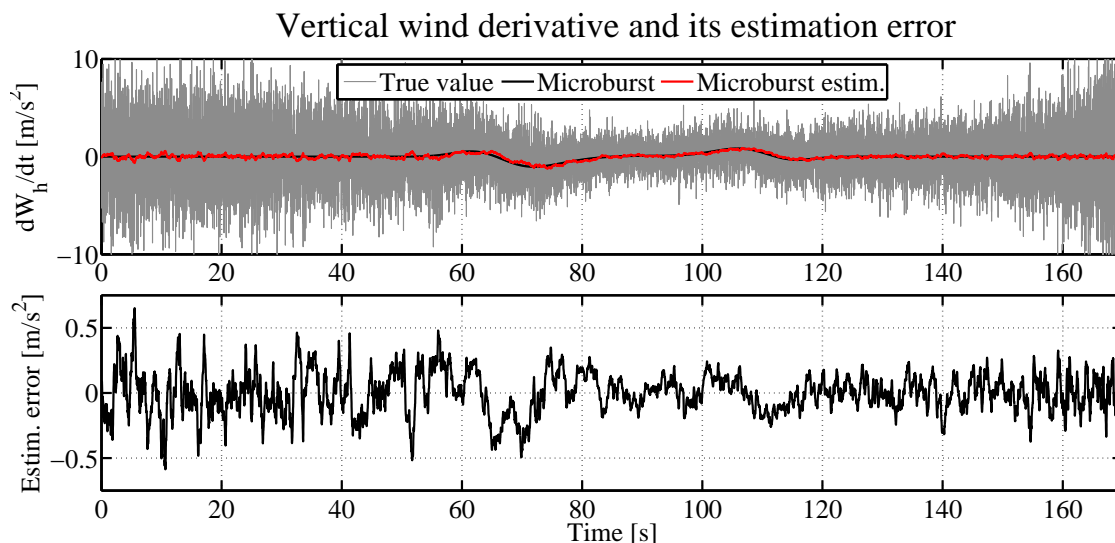
FIGURE 3.16:   Comparison of the simulated and estimated vertical wind derivative.
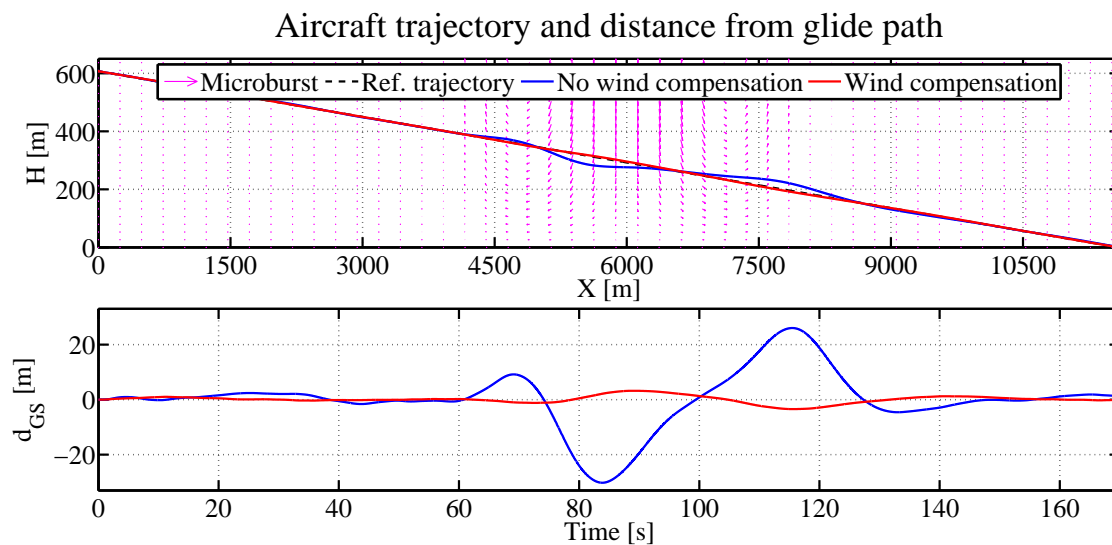

FIGURE 3.17:   Aircraft trajectory in the case of the controller with and without wind compensation.

are clear. In fact, the maximum tracking error is about 30 meters without wind shear compensation (blue line), while it reduces to about 3 m (red line) with the wind estimation. Figure 3.17 shows, in a clearly way, the trajectories of the controlled aircraft with (red line) and without (blue line) the wind compensation. Moreover, the profile of the wind–shear microburst is depicted through a schematic representation of the wind velocity and direction (magenta arrows). Finally, Figure 3.18 shows the dynamics of the main state variables (from an aeronautical point of view) V and α, for the controller without (blue lines) and with wind compensation (red lines). It is easy to see that, thanks to the wind compensation procedure, the attack angle, α, remains safely below its stall value. On the other hand, without wind estimation, the angle of attack
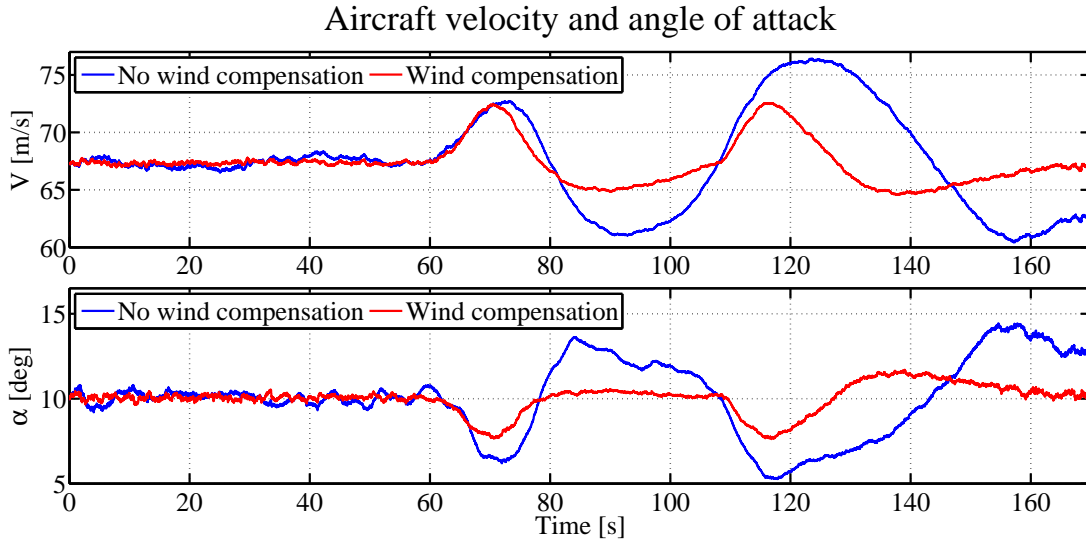
FIGURE 3.18: State evolutions in the case of the controller with and without wind compensation.

dangerously approaches the stall angle (15 deg). Therefore, the simulation results highlight the satisfactory performances achieved via the Active Control strategy relying on the NLGA RBF-NN wind estimation filters.

3.1.5 Flight Parameter Estimation for Extended Guidance Navigation and Control

This Section proposes an airspeed virtual sensor to extend the guidance navigation and control functions of an aircraft. The model exploited in this case is not in common with those depicted in (3.1)-(3.2) and will be detailed hereafter.

The main idea is to exploit the measurement (direct or indirect) of the aerodynamic forces applying on a control surface which are clearly related to the aircraft airspeed. Focusing on those aircraft equipped with a Fly By Wire system, at least one actuator is installed on each of the control surfaces; the actuators operate the surface by fighting against the aerodynamic forces. Generally speaking, aircraft are designed with a minimum set of control surfaces (one elevator, one rudder and two ailerons) but there are lots of examples of aircraft with redundant control surfaces. The possibility to exploit several measurements for the estimation of one flight parameter suggested the implementation of the "Least Squares – Sliding Mode" algorithm. This new virtual sensor, based on the NLGA and exploiting the $LS - SM$, has been applied to real aircraft flight data set leading to very encouraging preliminary results.

On each surface, the hinge momentum is constituted by the sum of momentums mainly due to the surface mass, surface inertia (movements), aerodynamics and frictions as well as actuator

TABLE 3.2: List of symbols

Symbol	Description	Dimensions
J	Surface Inertia	$kg \cdot m^2$
δ	Surface deflection	rad
M_a	Aerodynamic hinge momentum	Nm
M_{in}	Inertial hinge momentum	Nm
ΔP	Hydraulic chambers differential pressure	Pa
S	Piston reference area	m^2
F	Friction	N
l	Actuator lever arm	m
γ	Specific heat ratio	$-$
P_s	Static air pressure	Pa
M	Mach number	$-$
V	Surface reference volume	m^3
C_h	Aerodynamic hinge momentum coefficient	$-$
$\mathbf{d}$	Distance from the surface hinge to the surface center of gravity	m
$\mathbf{n}$	Load factor	$-$
m	Surface mass	kg
g	Gravity acceleration	m/s^2
R	Specific air constant	$J/(kgK)$
T_0	Temperature @ ISA sea level	K
P_{s_0}	Static pressure @ ISA sea level	Pa

torques. The aerodynamic momentum varies as the aircraft speed varies, so, the proposed solution exploits this relation to estimate the aircraft speed.

The following mathematical model represents the link between the hydraulic chambers of the n_j actuators installed to rotate the j-th aircraft control surface. For the description of all symbols, see Table 3.2:

$$J_j \ddot{\delta}_j \;=\; M_{a_j} + \sum_{i=1}^{n_j} \left(\Delta P_{i_j} S_{i_j} + F_{i_j} \right) l_{i_j} + M_{in_j} \tag{3.21}$$

where

$$\begin{aligned} M_{a_j} &= \tfrac{1}{2}\gamma P_s M^2 V_j C_{h_j} \\ M_{in_j} &= ||\mathbf{d}_j \times \mathbf{n}_j|| \, m_j g \end{aligned} \tag{3.22}$$

The aerodynamic hinge momentum coefficient, C_h, usually identified by flight test, is, in general, a complex function of the Mach number, aircraft attack angle and sideslip, surface deflection, aircraft angular rates, aircraft aerodynamic configuration, etc. A simplified expression for C_h is suggested in [100] and reported here:

$$C_h = C_{h_0} + C_{h_\alpha}\alpha^* + C_{h_\delta}\delta \tag{3.23}$$

where α^* represents the local angle of attack, δ is the surface deflection. Furthermore, the surface deflection, δ_j, and the hydraulic differential pressure, ΔP_{i_j}, are assume to be measured. The
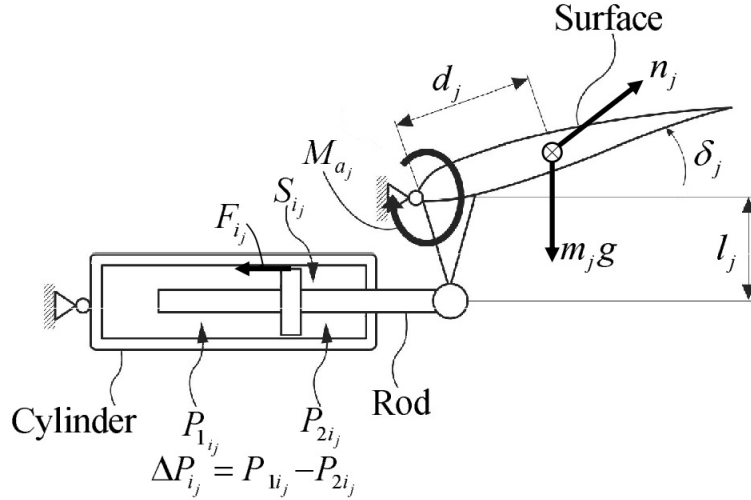
FIGURE 3.19: Surface – actuator: j-th system

actuators rod surface, S_j, the surface mass center, $\mathbf{d}_j$, and the lever arm, l_j, are known geometrical properties. Figure 3.19 depicts the system and its associated variables. With particular attention to the aileron, the local angle of attack is expressed as $\alpha^* = \alpha_{a/c} \pm p\, l_{\delta_a}/V_a$ where l_{δ_a} is the distance from the aircraft center line to the considered aileron. The V_a is the True AirSpeed that can be expressed as function of the Mach number: $V_a = M\,a$ where a is the (unknown) speed of sound. The sign $\pm$ indicates that, for right ailerons a positive roll rate increments the local angle of attack and, vice-versa, for left ailerons a positive roll rate decrements the local angle of attack. The complete model for the j-th right aileron is:

$$
\begin{aligned}
J_j \ddot{\delta}_j^{right} &= \tfrac{1}{2}\gamma P_s M^2 V_j \left\{ C_{h_{0_j}} + C_{h_{\alpha_j}}\left[\alpha_{a/c} + p\, l_{\delta_j}/(M\,a)\right] + C_{h_{\delta_j}}\delta_j^{right}\right\} + \\
&\quad + \sum_{i=1}^{n_j}\left(\Delta P_{i_j}^{right} S_{i_j} + F_{i_j}^{right}\right) l_{i_j}^{right} + \left\|\mathbf{d}_j \times \mathbf{n}_j^{right}\right\| m_j g \\
y_j^{right} &= \delta_j^{right}
\end{aligned}
\tag{3.24}
$$

The goal is the estimation of the Mach number, M, even during turns, *i.e.* for any roll rate, p. So, for the application of the NLGA, the following two quantities are defined:

$$
\mathbf{f}_s = M^2 \qquad \mathbf{d}_s = p
\tag{3.25}
$$

Assuming the presence of k left ailerons and k counterparts (right ailerons) the NLGA procedure generates k new variables identified by:

$$
\delta_j = \delta_j^{left} + \delta_j^{right} \quad \forall\, j \in \{1, ..., k\}
\tag{3.26}
$$

leading to the following $\bar{\mathbf{x}}_1$-subsystem:

$$
\begin{aligned}
\dot{\bar{\mathbf{x}}}_{1_1} &= \mathbf{M}_1(t)f_s + \mathbf{M}_2(t) \\
\dot{\bar{\mathbf{x}}}_{1_2} &= \bar{\mathbf{x}}_{1_1} \\
\bar{\mathbf{y}}_1 &= \bar{\mathbf{x}}_{1_2}
\end{aligned}
\tag{3.27}
$$

where

$$
\begin{aligned}
\mathbf{M}_1(t) &= \begin{bmatrix} M_{1_1} & ... & M_{1_k} \end{bmatrix}^T \\
\mathbf{M}_2(t) &= \begin{bmatrix} M_{2_1} & ... & M_{2_k} \end{bmatrix}^T
\end{aligned}
\tag{3.28}
$$

and

$$
M_{1_j} = \gamma P_s V_j \left(C_{h_{0_j}} + C_{h_{\alpha_j}} \alpha_{a/c} + \frac{1}{2} C_{h_{\delta_j}} \delta_j \right) \quad \forall\, j \in \{1, ..., k\}
\tag{3.29}
$$

$$
\begin{aligned}
M_{2_j} &= \sum_{i=1}^{n_j} \left(\Delta P_{i_j}^{right} S_{i_j} + F_{i_j}^{right} \right) l_{i_j}^{right} + \left\| \mathbf{d}_j \times \mathbf{n}_j^{right} \right\| m_j g + \\
&\quad + \sum_{i=1}^{n_j} \left(\Delta P_{i_j}^{left} S_{i_j} + F_{i_j}^{left} \right) l_{i_j}^{left} + \left\| \mathbf{d}_j \times \mathbf{n}_j^{left} \right\| m_j g \quad \forall\, j \in \{1, ..., k\}
\end{aligned}
\tag{3.30}
$$

It's with nothing that the system (3.27) is trivially dependent on the roll rate, p, but directly affected by the Mach number.

Simulation based on real flight data

The results depicted in this section are relative to the application of the proposed algorithm to a real aircraft flight data set. Figure 3.20(A) shows the real Mach number as measured by classical aircraft on board sensors (blue line), and the estimated Mach (in red). Finally the black line represents a filtered version of $\hat{M}$ added, only for presentation purposes, to highlight the behavior of the mean of the estimation. The Mach number can be converted in terms of Calibrated Air Speed (CAS), Figure 3.20(B), thanks to the classical formula:

$$CAS = \sqrt{\tfrac{2}{\gamma-1}}\sqrt{\gamma R T_0}\sqrt{\left\{\tfrac{P_s}{P_{s_0}}\left[\left(1+\tfrac{\gamma-1}{2}M^2\right)^{\frac{\gamma}{\gamma-1}}-1\right]+1\right\}^{\frac{\gamma}{\gamma-1}}-1} \qquad (3.31)$$

The estimation error is shown, in red, in Figure 3.20(C)-(D): for low CAS (*i.e.* for low dynamic pressures), $CAS < 300$ kts, the error is practically negligible and its mean is close to zero. On the other hand, at higher CAS, the Mach estimation error is limited, quite constant and less that 0.05. Error at high CAS, not found during preliminary simulations and discovered by flight test, is probably due to nonlinear phenomenon, not included in the synthesis model, such as the aeroelasiticty.
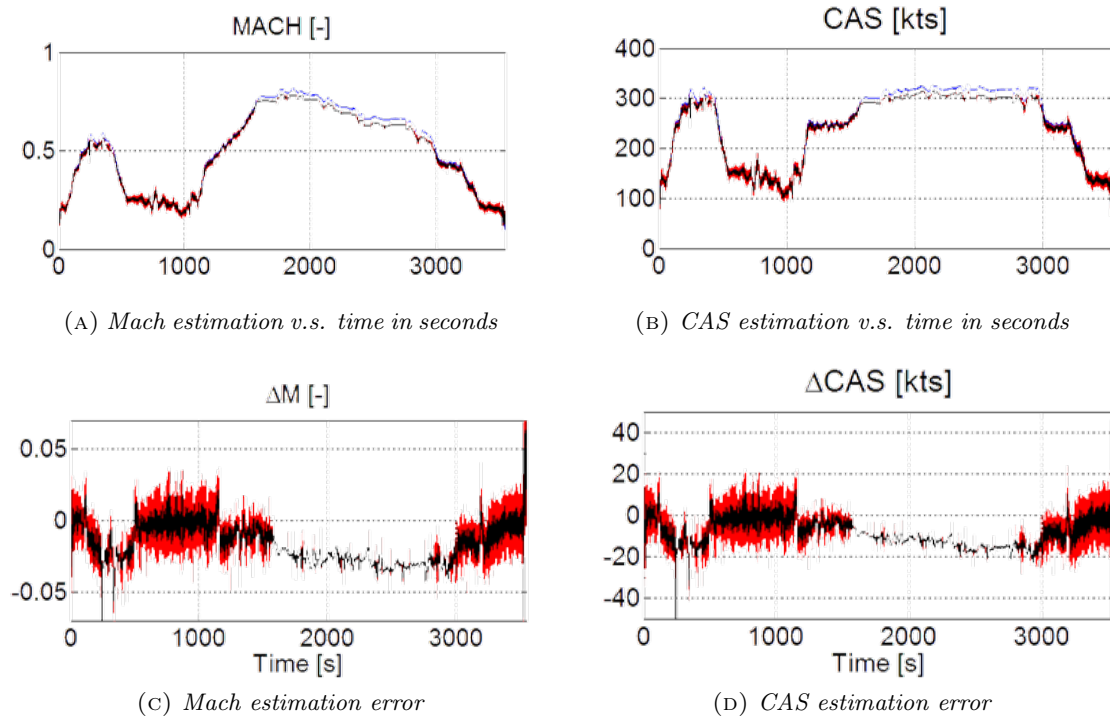

(A) *Mach estimation v.s. time in seconds*

(B) *CAS estimation v.s. time in seconds*

(C) *Mach estimation error*

(D) *CAS estimation error*

FIGURE 3.20: Airspeed Virtual Sensor: performance

3.2 Fixed Wing UAV

The model for the design of Active Control laws for fixed wing Unmanned Aerial Vehicles is obtained from the synthesis model of aircraft of Section 3.1, whereas the simulation models are the same, see Figure 3.1.

The application of the singular perturbation approximation to the model (3.8)-(3.11) is motivated by the different time scales relative to the rotational and translational dynamics. In particular, the rotational dynamics is faster than the translational one and, with a properly designed fast control law, the manifold $\mathbf{x}_{2_{\mathcal{M}}}$ is stable. With this in mind let's assume that the fast variables, such as α, β, μ exactly track their reference values α_R, β_R, μ_R, as well as the rotational speeds, *i.e.* $\boldsymbol{\Omega}_B = \boldsymbol{\Omega}_{B_R}$. The equilibrium of the angles impose $\boldsymbol{\Omega}_{B_R} = \mathbf{0}$ whereas, usually, the reference sideslip angle is imposed to zero, *i.e.* $\beta_R = 0$. So the model representing the reduces system is:

$$
\begin{bmatrix} \dot{V}_a \\ \dot{\chi} \\ \dot{\gamma} \end{bmatrix} = \begin{bmatrix} -g\sin\gamma \\ 0 \\ -\frac{g}{V_a}\cos\gamma \end{bmatrix} + \frac{1}{m}\begin{bmatrix} 1 & 0 & 0 \\ 0 & -\frac{\cos\mu_R}{V_a\cos\gamma} & -\frac{\sin\mu_R}{V_a\cos\gamma} \\ 0 & \frac{\sin\mu_R}{V_a} & -\frac{\cos\mu_R}{V_a} \end{bmatrix}\begin{bmatrix} -D \\ Y \\ -L \end{bmatrix} + \boldsymbol{\varepsilon}_{I\to W}^{-1}\dot{\mathbf{W}}_I +
$$
$$
+ \frac{1}{m}\begin{bmatrix} 1 & 0 & 0 \\ 0 & -\sin\mu_R\sec\gamma & \cos\mu_R\sec\gamma \\ 0 & -\cos\mu_R & -\sin\mu_R \end{bmatrix}\boldsymbol{\varepsilon}_{B\to W}^{-1}\mathbf{F}_{B,e}
$$
(3.32)

$$
\begin{bmatrix} -D \\ Y \\ -L \end{bmatrix} = \frac{1}{2}\rho S V_a^2 \begin{bmatrix} -C_D\left(\alpha_R, 0, \boldsymbol{\Omega}_a, \boldsymbol{\delta}\right) \\ C_Y\left(\alpha_R, 0, \boldsymbol{\Omega}_a, \boldsymbol{\delta}\right) \\ -C_L\left(\alpha_R, 0, \boldsymbol{\Omega}_a, \boldsymbol{\delta}\right) \end{bmatrix}
$$
(3.33)

Further useful approximation are introduced to reduce the model complexity while saving the model representativity:

- a common assumption is that the propulsion system provides a thrust mainly described by its x-body component, *i.e.* $\mathbf{F}_{B,e} = [T, 0, 0]^T$.

- the lift force, L, is n times the aircraft weight, *i.e.* $L = n\,mg$, where n represents the load factor;

- the aerodynamic drag, D, is approximated by the classical polar curve:

$$
D = \frac{1}{2}\rho V_a^2 S \left[C_{D_0} + K\frac{(n\,mg)^2}{\left(\frac{1}{2}\rho V_a^2 S\right)^2} \right]
$$
(3.34)

- the side force Y evaluated in $\beta = 0$ is negligible respect to the other forces.

The final synthesis model is:

$$
\begin{bmatrix} \dot{X} \\ \dot{Y} \\ \dot{Z} \end{bmatrix} = \begin{bmatrix} V_a \cos \chi \cos \gamma \\ V_a \sin \chi \cos \gamma \\ -V_a \sin \gamma \end{bmatrix} + \mathbf{W}_I \tag{3.35}
$$

$$
\begin{bmatrix} \dot{V}_a \\ \dot{\chi} \\ \dot{\gamma} \end{bmatrix} = \begin{bmatrix} -g \sin \gamma - \frac{1}{2m} \rho V_a^2 S C_{D_0} \\ 0 \\ -\frac{g}{V_a} \cos \gamma \end{bmatrix} + \frac{1}{m} \begin{bmatrix} T - K \frac{(n\,mg)^2}{\frac{1}{2}\rho V_a^2 S} \\ \frac{n\,mg \sin \mu_R}{V_a \cos \gamma} \\ \frac{n\,mg \cos \mu_R}{V_a} \end{bmatrix} + \varepsilon_{I \to W}^{-1} \dot{\mathbf{W}}_I \tag{3.36}
$$

3.2.1 Active Fault Tolerant Control

This application is particularly interesting because implements the "recursive" Detection and Isolation concept proposed in Section 2.1.1.4.

The inputs of model (3.35) - (3.36) are the thrust, T, the load factor, n, and the aerodynamic bank angle, μ. Two of these three inputs are considered subject to fault and, in particular, constant step functions are assumed to affect the thrust and the load factor, *i.e.* f_T and f_n. The strong nonlinearities don't allow the isolation of multiple concurrent faults on the thrust and the load factor: the standard NLGA procedure, in this case, effectively says that:

- it's possible to detect and isolate the load factor fault, independently from the thrust fault;

- it's not possible to detect and isolate thrust faults independently from faults affecting the load factor.

This conclusions would led to the possibility to detect and isolate only non concurrent faults. By introducing the concept of the "recursive" detection and isolation based on the estimation, once the load factor fault is estimated (so it becomes a known function) also the thrust fault can be estimated. The resulting Fault Detection and Diagnosis Module is depicted in Figure 3.21. The implemented estimation algorithm is the recursive Least Squares with forgetting factor whereas the controller has the typical backstepping structure where the mathematical peculiarity is the use of the dynamic extension to deal with the non input-affine synthesis model (3.35) - (3.36).

The details on the controller and on the Detection and Diagnosis module can be found in [57].

Simulation results

As shown in the following simulation results, the fault decoupling is perfect in steady–state conditions, and negligible in transient conditions, if the NLGA–AF is designed to provide a
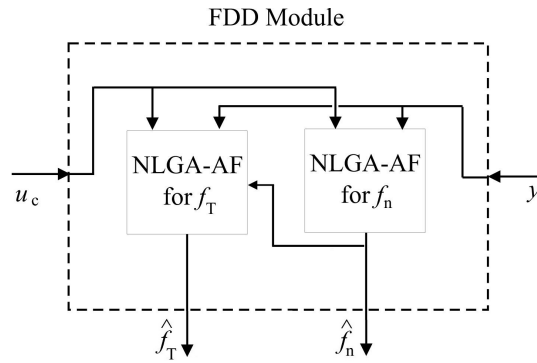
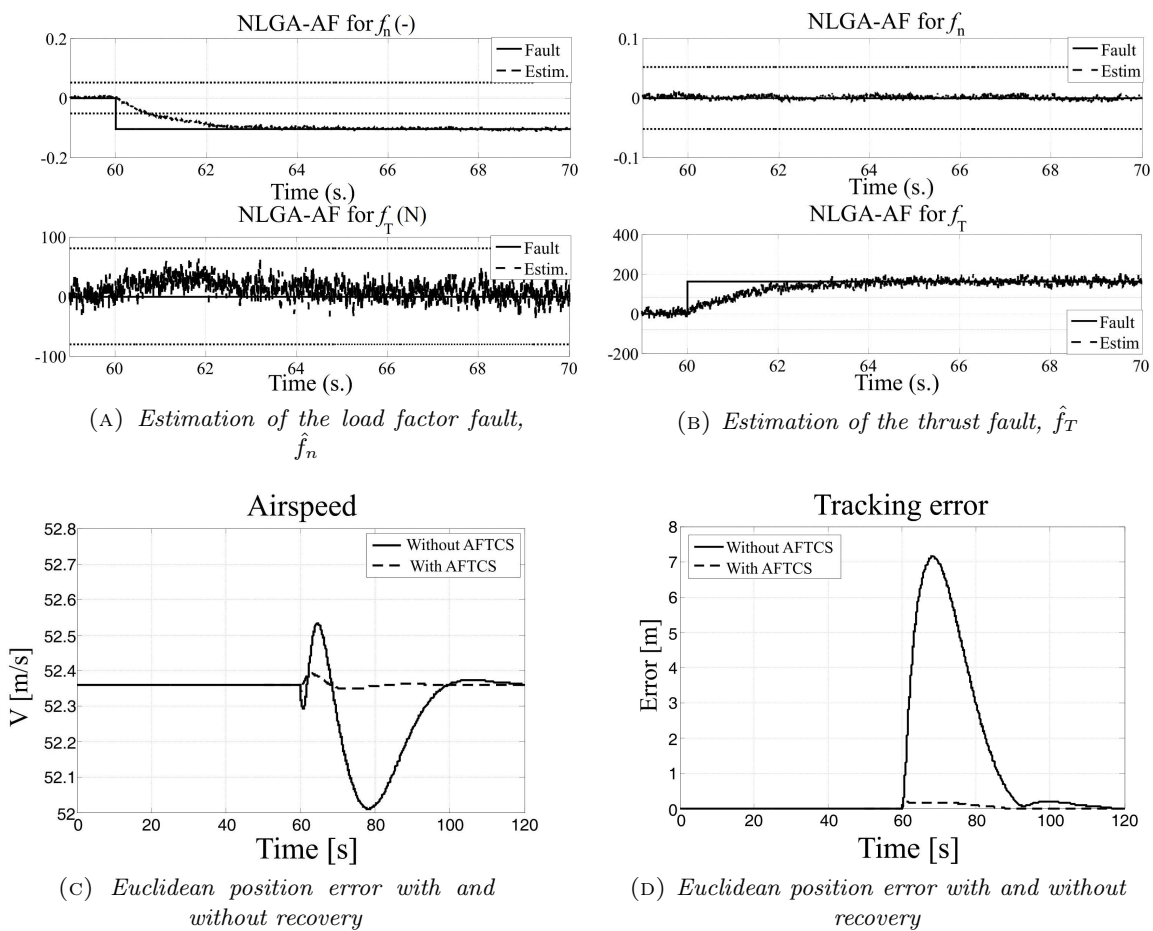FIGURE 3.21: Recursive Detection and Isolation Scheme based on Estimation

(A) *Estimation of the load factor fault, $\hat{f}_n$*

(B) *Estimation of the thrust fault, $\hat{f}_T$*

(C) *Euclidean position error with and without recovery*

(D) *Euclidean position error with and without recovery*

FIGURE 3.22: FW-UAV: Estimation and tracking performance

prompt fault reconstruction. Figure 3.22(A) shows the estimate of the signal $\hat{f}_T$ (dashed line) and compares it to the actual simulated fault f_T (continuous line). In particular, Figure 3.22(C) shows the airspeed signal V when the AFTCS recovers the fault (dashed line) and without fault accommodation (continuous line). Figure 3.22(D) shows the tracking error, one of the most meaningful aircraft variables that should assess the performances of the and AFTCS strategy, with (dashed line) and without (continuous line) fault recovery.

3.3 Satellite

In this thesis only the attitude dynamics of satellites is investigated. The model is represented by:

$$\begin{aligned}
\dot{\mathbf{R}}_{B\to I} &= \mathbf{S}\left(\mathbf{\Omega}_B\right)\mathbf{R}_{B\to I} \\
\mathbf{I}\dot{\mathbf{\Omega}}_B &= -\mathbf{\Omega}_B \times \mathbf{I}\mathbf{\Omega}_B + \sum \mathbf{M}_B
\end{aligned}$$

(3.37)

where the external momentums are the sum of three main contributions:

$$\sum \mathbf{M}_B = \mathbf{M}_{B,g} + \mathbf{M}_{B,a} + \mathbf{M}_{B,m} + \mathbf{M}_{B,e}$$

(3.38)

- $\mathbf{M}_{B,g}$ is the torque due to the gravitational field:

$$\mathbf{M}_{B,g} = \frac{3\mu}{R^3} \begin{bmatrix} \left(I_z - I_y\right)c_2 c_3 \\ \left(I_x - I_z\right)c_1 c_3 \\ \left(I_y - I_x\right)c_1 c_2 \end{bmatrix}$$

(3.39)

where μ is the gravitational constant, R is the orbital height, I_x, I_y and I_z are the principal inertia components and c_1, c_2 and c_3 represent the components of the director cosine describing the attitude with $[c_1, c_2, c_3]^T = \mathbf{R}_{I\to B}\mathbf{e}_1$;

- $\mathbf{M}_{B,a}$ represents the torque due to the aerodynamic disturbance (if the satellite flies in a non empty space):

$$\mathbf{M}_{B,a} = -\mathbf{r}_{CP} \times \mathbf{e}_2 \frac{1}{2}\rho V_a^2 S C_D$$

(3.40)

where $\mathbf{r}_{CP}$ represents the level arm from the center of pressure to the center of mass of the satellite, ρ is the air density (where present), V_a is the orbital speed, S is spacecraft cross section and C_D indicates the drag coefficient ($C_D \approx 2.2$);

- $\mathbf{M}_{B,m}$ is the torque due to the magnetic field (when present):

$$\mathbf{M}_{B,m} = \mathbf{m} \times \mathbf{B}$$

(3.41)

where $\mathbf{m}$ is the residual magnetic induction due to the currents circulating on board and $\mathbf{B}$ is the planet magnetic field;

- $\mathbf{M}_{B,e}$ indicates the manipulable inputs such are three reaction wheels aligned with the body axes:

$$\mathbf{M}_{B,e} = \mathbf{I}_{3\times 3} \begin{bmatrix} M_1 \\ M_2 \\ M_3 \end{bmatrix}$$
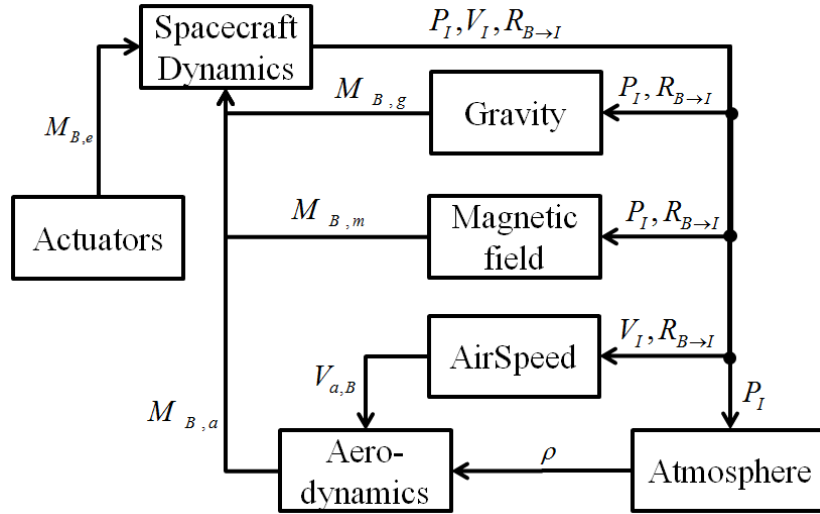
(3.42)

FIGURE 3.23: Satellite simulator scheme

Synthesis model

The synthesis model, for the following Active Fault Tolerant Control design, exactly matches the simulation model but neglects the magnetic torques because they are, when compared to the rest of phenomenons, negligible.

3.3.1 Active Fault Tolerant Control

If the torque due to the gravitational field can be considered known by data collected in past missions, the aerodynamic torque is quite unpredictable and constitutes a real disturbance. On the other hand the scenario considers the presence of non concurrent faults on the reaction wheels, $\mathbf{f}_{M_{B,e}} = [f_1, f_2, f_3]^T$ affecting $\mathbf{M}_{B,e} = [M_1, M_2, M_3]^T$. Then, the scenario of disturbance and fault is represented by $\mathbf{f} = \left[\mathbf{f}_{M_{B,e}}, \mathbf{M}_{B,a}\right]^T$, whereas the $\mathbf{f}_s$ and $\mathbf{d}_s$ are defined as follows:

- for the estimation of fault on the first and the second reaction wheel

$$\mathbf{f}_s = [f_1, f_2]^T \qquad \mathbf{d}_s = [f_3, \mathbf{M}_{B,a}]^T$$

- for the estimation of fault on the first and the third reaction wheel

$$\mathbf{f}_s = [f_1, f_3]^T \qquad \mathbf{d}_s = [f_2, \mathbf{M}_{B,a}]^T$$

- for the estimation of fault on the second and the third reaction wheel

$$\mathbf{f}_s = [f_2, f_3]^T \qquad \mathbf{d}_s = [f_1, \mathbf{M}_{B,a}]^T$$

(A) *Estimation of a step fault on the first reaction wheel*

(B) *Compensation of a step fault on the first reaction wheel: roll angle dynamics*
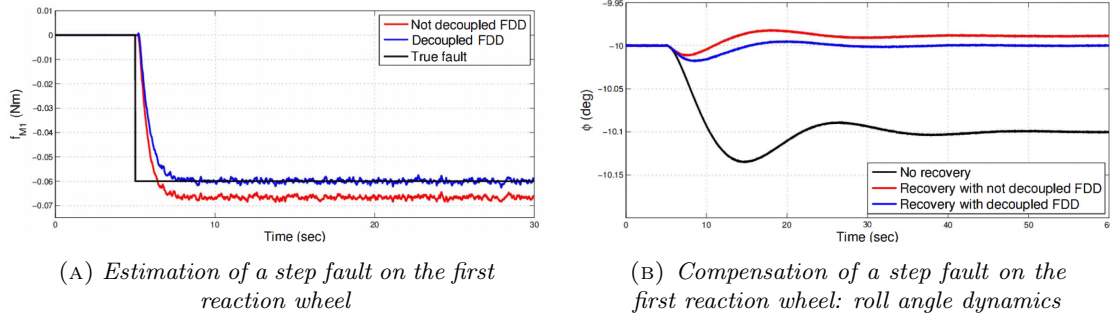
FIGURE 3.24: Satellite: Estimation and tracking performance - case of step faults

The residuals arising from these Identification architecture are called "generalized" and represent a solution to Problem 3.

Three kind of faults have been simulated such as step, ramp and sinusoidal functions, then, the selected estimation algorithm is a Radial Basis Function Neural Network. The controller has the backstepping structure: all the details have been published in [61].

Simulation results

Three types of additive faults are considered, affecting the actuated torque signal M_1 and commencing at $t = 5s$:

1. A step fault $f_1 = a_f$ with size $a_f = -0.06Nm$;

2. A ramp fault $f_1 = a_r t$ with slope $a_r = -0.004Nm/s$;

3. A sinusoidal $f_1 = a_s sin(2\pi t/T_f)$ with amplitude $a_s = 0.05Nm$ and period $T_f = 20s$.

Figure 3.24(A) shows the fault estimate obtained once the FDD module is activated. The black signal represents the true occurred fault, whereas the blue signal represents the fault estimation obtained by means of the designed aerodynamic decoupled NLGA RBF NN adaptive filters. As shown, the decoupled estimation results to be unbiased. Moreover, the estimation result is compared with the one obtained by means of not decoupled adaptive filters (red line). The not decoupled estimate presents a bias of about the 10% of the true fault size due to the estimation error of the adaptive filters not decoupled from the aerodynamic disturbance. These not decoupled filters are obtained by exploiting an approach similar to the one proposed in [60] and [101]. In this case, the adaptive filters are designed by completely neglecting the aerodynamic disturbance model in the satellite dynamic model (see [62] for further details). Hence, the use of the NLGA and RBF NN for the design of aerodynamic decoupled adaptive fiters allows a more accurate fault estimation with respect to a classical not disturbance decoupled
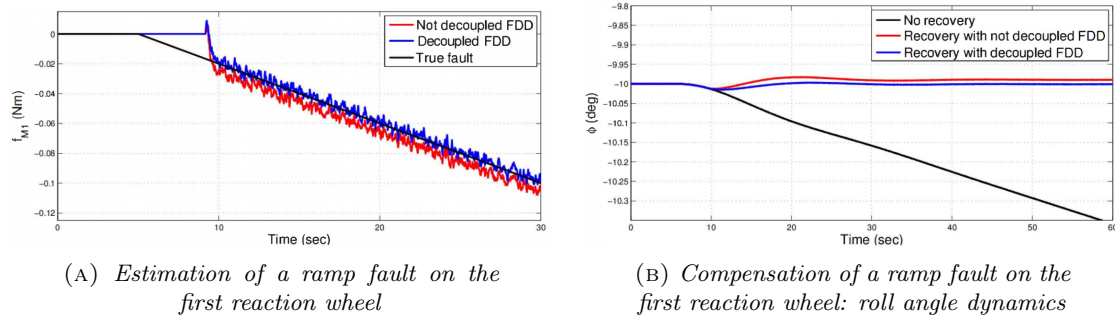
(A) *Estimation of a ramp fault on the first reaction wheel*

(B) *Compensation of a ramp fault on the first reaction wheel: roll angle dynamics*

FIGURE 3.25: Satellite: Estimation and tracking performance - case of ramp faults

(A) *Estimation of a sinusoidal fault on the first reaction wheel*

(B) *Compensation of a sinusoidal fault on the first reaction wheel: roll angle dynamics*
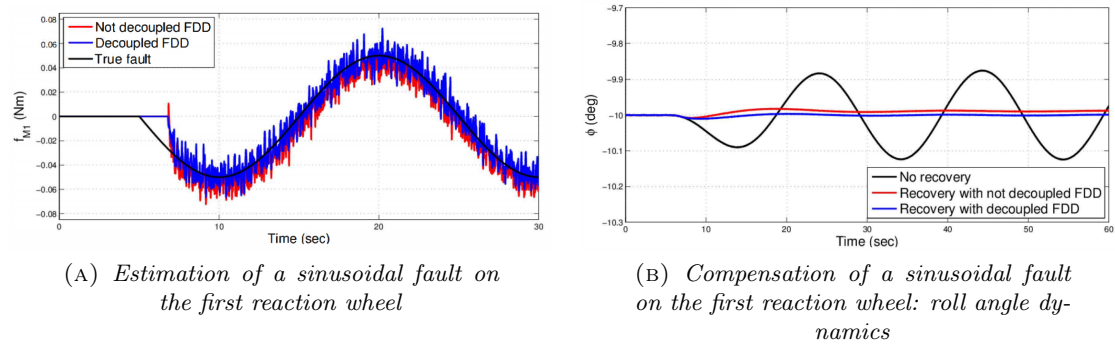
FIGURE 3.26: Satellite: Estimation and tracking performance - case of sinusoidal faults

estimation approach. Figure 3.24(B) shows the behavior of the roll angle ϕ. The behaviors of the pitch angle e and yaw angle are similar and not reported here. Figure 3.24(B) shows the obtained results by exploiting three different attitude control strategies. The black line represents the roll angle dynamics without the fault recovery (i.e. a large deviation from the reference value), whereas the blue and red lines represent the fault accommodation exploiting the aerodynamic decoupled and not decoupled FDD estimations respectively. The decoupled FDD estimation allows to return to the reference attitude condition with great accuracy, whereas the feedback of the not decoupled FDD estimation causes a deviation from the reference value. This comparison highlights the better attitude control performances obtained by the AFTCS relying on an aerodynamic decoupled FDD module. Considering the ramp fault, Figure 3.25(A) and Figure 3.25(B) show the fault estimate and the roll angle behavior respectively. As before, the not decoupled FDD estimations show a bias with respect to the true fault value. In this case, due to the ramp fault type, the FDI detection time is longer. Hence, also the activation of the FDD module takes more time. Considering the sinusoidal fault, Figure 3.26(A) and Figure 3.26(B) show the fault estimate and the roll angle behavior respectively. Also in this case, a bias is present in the not decoupled estimate together with a longer detection time with respect to the step fault case. The fault accommodation obtained by exploiting the decoupled fault estimate is still good.

3.4 Quad Rotor

The simulation model for quad-copters share some commonalities with the simulation model (3.1)-(3.2). In particular, the rotational dynamics it's the same whereas the translational dynamics is expressed in the inertial frame. The model is reported hereafter:

$$
\begin{aligned}
m\ddot{\mathbf{P}}_I &= \mathbf{R}_{B\to I}\left(\mathbf{F}_{prop} + \mathbf{F}_{body}\right) + mg\mathbf{e}_3 \\
\dot{\mathbf{R}}_{B\to I} &= \mathbf{S}\left(\mathbf{\Omega}_B\right)\mathbf{R}_{B\to I} \\
\mathbf{I}\dot{\mathbf{\Omega}}_B &= -\mathbf{\Omega}_B \times \mathbf{I}\mathbf{\Omega}_B + \mathbf{M}_{prop} + \mathbf{M}_{load} + \mathbf{M}_{body}
\end{aligned}
\tag{3.43}
$$

The forces acting on the quadrotor are induced by the propellers $\mathbf{F}_{prop}$ and by the drag due to the central body $\mathbf{F}_{body}$. The propellers forces are expressed in body frame as follows:

$$
\mathbf{F}_{prop} = \begin{bmatrix} N_x \\ N_y \\ T \end{bmatrix}
\tag{3.44}
$$

where the terms N_x and N_y are the side forces whereas the T indicates the thrust. The following expressions are common model for the propeller induced side forces:

$$
\begin{bmatrix} N_x \\ N_y \end{bmatrix} = -2\rho\left(\frac{2\pi}{60}\right)D^3\sum_{i=1}^{4}n_i C_Q\left(\frac{\mathbf{e}_3^T\mathbf{R}_{I\to B}\mathbf{V}_{a_I} + \mathbf{\Omega}_B\times\mathbf{l}_i}{n_i D}\right)\begin{bmatrix} 1 & 0 & 0 \\ 0 & 1 & 0 \end{bmatrix}\mathbf{R}_{I\to B}\mathbf{V}_{a_I}
\tag{3.45}
$$

The term D indicates the propeller diameter, $\mathbf{l}_i$ is the i-th engine arm, n_i represents the revolution per minutes of the i-th propeller, ρ is the air density, and C_Q is the propeller torque coefficient. The overall thrust is modeled as the sum of four single thrusts:

$$
T = -\rho\left(\frac{2\pi}{60}\right)^2 D^4\sum_{i=1}^{4}n_i^2 C_T\left(\frac{\mathbf{e}_3^T\mathbf{R}_{I\to B}\mathbf{V}_{a_I} + \mathbf{\Omega}_B\times\mathbf{l}_i}{n_i D}\right)
\tag{3.46}
$$

where C_T is the propeller thrust coefficient.

The airspeed expressed in inertial frame is defined as $\mathbf{V}_{a_I} = \mathbf{V}_I - \mathbf{W}_I$. The quadrotor central body induces an aerodynamic drag that can be modeled as:

$$
\mathbf{F}_{body} = \frac{1}{2}\rho\left|\mathbf{V}_{a_I}\right|^2 S\begin{bmatrix} C_x\left(\mathbf{R}_{I\to B}\mathbf{V}_{a_I}\right) \\ C_y\left(\mathbf{R}_{I\to B}\mathbf{V}_{a_I}\right) \\ C_z\left(\mathbf{R}_{I\to B}\mathbf{V}_{a_I}\right) \end{bmatrix}
\tag{3.47}
$$

with C_x, C_y and C_z are the central body aerodynamic drag coefficient and S represents the central body plan surface. The momentum induced by the aerodynamic drag is represented by:

$$
\mathbf{M}_{body} = \mathbf{l}_{body} \times \mathbf{F}_{body}
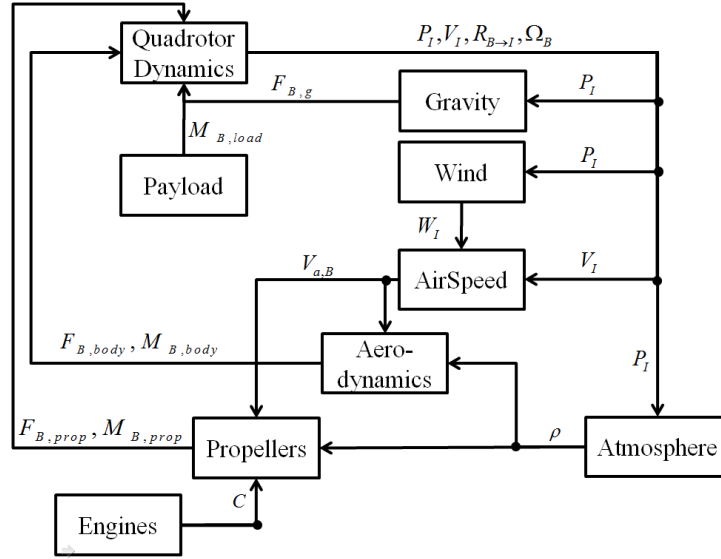\tag{3.48}
$$

FIGURE 3.27: Quadrotor simulator scheme

The propellers induce torques are the sum of two contributes, *i.e.* the aerodynamic and the gyroscopic momentums respectively indicated by $\mathbf{M}_{aero}$, by $\mathbf{M}_{gyr}$ and by $\mathbf{M}_{damp}$:

$$\mathbf{M}_{prop} = \mathbf{M}_{aero} + \mathbf{M}_{gyr} + \mathbf{M}_{damp} \tag{3.49}$$

$$\mathbf{M}_{aero} = \sum_{i=1}^{4} \left(\mathbf{l}_i \times \mathbf{F}_{prop} + \mathbf{e}_3 Q_i \right) \tag{3.50}$$

where the yaw torques Q_i are:

$$Q_i = k_i \rho \left(\frac{2\pi}{60} \right)^2 n_i^2 D^5 C_Q \left(\frac{\mathbf{e}_3^T \mathbf{R}_{I \to B} \mathbf{V}_{a_I} + \mathbf{\Omega}_B \times \mathbf{l}_i}{n_i D} \right) \tag{3.51}$$

with $k_i \in \{-1, 1\}$ and

$$\mathbf{M}_{gyr} \quad = \quad -\sum_{i=1}^{4} \mathbf{\Omega}_B \times I_{prop} \mathbf{n}_i \tag{3.52}$$

$$\mathbf{M}_{damp} \quad = \quad (2\pi) \pi \sigma \frac{\rho}{2} \left(\frac{2\pi}{60} \right)^2 \left(\frac{D}{2} \right)^5 \sum_{i=1}^{4} n_i^2 \begin{bmatrix} arctan\left(\frac{p}{\left(\frac{2\pi}{60} \right) n_i} \right) \\ arctan\left(\frac{q}{\left(\frac{2\pi}{60} \right) n_i} \right) \\ 0 \end{bmatrix} \tag{3.53}$$

The momentum $\mathbf{M}_{load}$ is due to the payload mass position relative to the center of gravity and due to the payload movements. Finally, also the actuators model have been implemented into the simulator:

$$I_{prop} \left(\frac{2\pi}{60} \right) \dot{n}_i = C_i - k_i \rho \left(\frac{2\pi}{60} \right)^2 n_i^2 D^5 C_Q \left(\frac{\mathbf{e}_3^T \mathbf{R}_{I \to B} \mathbf{V}_{a_I} + \mathbf{\Omega}_B \times \mathbf{l}_i}{n_i D} \right) \tag{3.54}$$
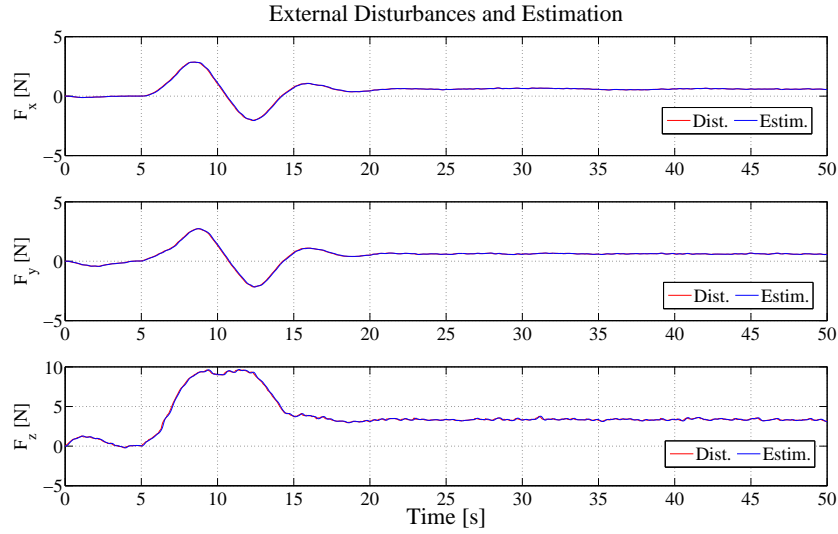
External Disturbances and Estimation

FIGURE 3.28: Exogenous disturbance and its estimation.

where C_i is the commanded torque on the i-th engine shaft and I_{prop} represents the propeller's inertia.

Synthesis model

The simulator model is too complex to be used for controller design purposes. So the following assumptions reduce the model to the so called "synthesis" model. The propeller thrusts are assumed as in static working conditions:

$$\bar{T} = -\rho \left(\frac{2\pi}{60}\right)^2 D^4 \sum_{i=1}^{4} n_i^2 C_T (0) \tag{3.55}$$

whereas the side forces are considered as negligible, *i.e.* N_x, $N_y \approx 0$. The simplified forces model is completed by neglecting also the $\mathbf{F}_{body}$ components.

On the other hand also the torques are approximated, and in particular:

$$\bar{\mathbf{M}}_{aero} = -\rho \left(\frac{2\pi}{60}\right)^2 D^4 \sum_{i=1}^{4} \left(\mathbf{l}_i \times \mathbf{e}_3 \bar{T} + \mathbf{e}_3 k_i \rho \left(\frac{2\pi}{60}\right)^2 n_i^2 D^5 C_Q (0)\right) \tag{3.56}$$

whereas the momentums induced the gyroscopic effects and the external payload are neglected. The dynamics of the propellers have been neglected because of the presence of RPM control systems which assure that the desired value of n_i is reached for each i-th engine. Thanks to this assumption the terms n_i are considered as system manipulable inputs.
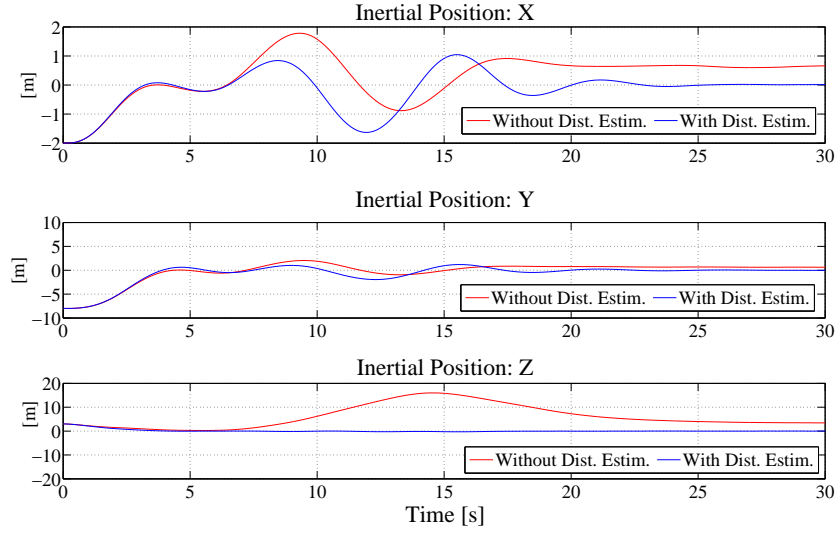
FIGURE 3.29: Inertial position in the case of the controller with and without disturbances compensation.

Finally, the synthesis model is:

$$
\begin{aligned}
m\ddot{\mathbf{P}}_I &= -\mathbf{R}_{B\to I}\mathbf{e}_3\bar{T} + mg\mathbf{e}_3 + \mathbf{F}_{I,a} \\
\dot{\mathbf{R}}_{B\to I} &= \mathbf{S}\left(\mathbf{\Omega}_B\right)\mathbf{R}_{B\to I} \\
\mathbf{I}\dot{\mathbf{\Omega}}_B &= -\mathbf{\Omega}_B \times \mathbf{I}\mathbf{\Omega}_B + \bar{\mathbf{M}}_{aero} + \mathbf{M}_{I,a}
\end{aligned}
\tag{3.57}
$$

where $\mathbf{F}_{I,a} = [F_{I,a_x}, F_{I,a_z}, F_{I,a_z}]^T$ and $\mathbf{M}_{I,a} = [M_{I,a_x}, M_{I,a_z}, M_{I,a_z}]^T$ represent equivalent forces and momentums, induced by model mismatching and real external disturbances such as wind, not included in the synthesis model.

3.4.1 Active Disturbance Rejection Control

Assuming that the disturbance components are generic functions, always concurrent, the NLGA procedure has been applied to create three new $\bar{\mathbf{x}}_1$-subsystems for the estimation of the elements of $\mathbf{F}_{I,a}$. The controller structure is that of a backstepping but the implemented control law also contains improving robustness features. Due to the generality of the signals to be identified the Radial Basis Function Neural Network has been chosen as estimation algorithm.

The NLGA procedure is applied three times, for the creation of a dedicated estimators set, with the following definitions:

- for the estimation of the first component of $\mathbf{F}_{I,a}$: $\mathbf{f}_s = F_{I,a_x}$ and $\mathbf{d}_s = [F_{I,a_z}, F_{I,a_z}]^T$;

- for the estimation of the second component of $\mathbf{F}_{I,a}$: $\mathbf{f}_s = F_{I,a_y}$ and $\mathbf{d}_s = [F_{I,a_x}, F_{I,a_z}]^T$;

- for the estimation of the third component of $\mathbf{F}_{I,a}$: $\mathbf{f}_s = F_{I,a_z}$ and $\mathbf{d}_s = \left[F_{I,a_x}, F_{I,a_y}\right]^T$;
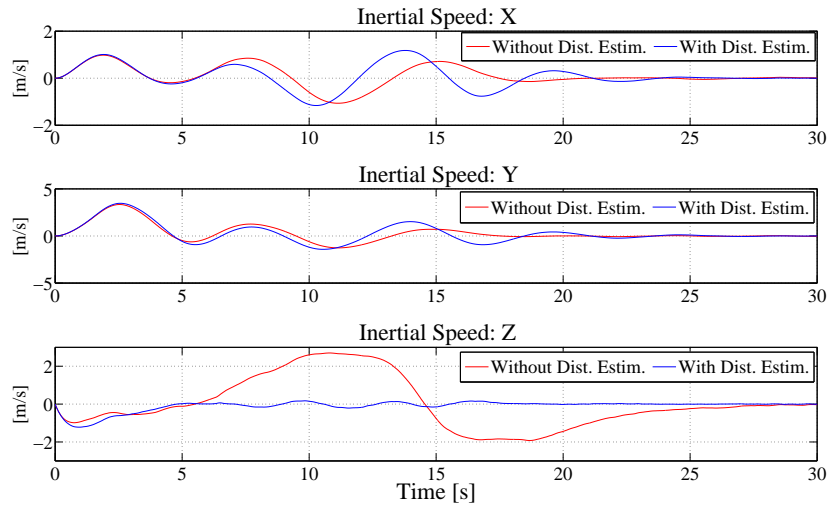
FIGURE 3.30: Inertial speed in the case of the controller with and without disturbances compensation.

The paper [65] contains all the details relative to this application.

Simulation results

Simulation results highlight the controller performance both with and without the exogenous disturbance estimation feedback.

The simulator implements the disturbance described in this section and an accurate wind field model. It is constituted by the following concurrent contributions: a Dryden turbulence (with zero mean), a wind shear model (to model mountain environments) and a discrete wind gust $(1 - \cos$ shape) (to take into account for asymptotically constant wind).

In the following simulation, the control objective is, starting from an erroneous initial position, a hovering at coordinates $\mathbf{P}_I = [0, 0, 0]'$. During the simulated maneuver (in presence of wind) the quad–rotor is subject to external unmodeled disturbances that can affect the control accuracy both during the transient and asymptotically.

Figure 3.28 shows the estimation filters performance in terms of both accuracy and readiness.

The benefits arising from the feedback of the estimated exogenous disturbances are highlighted in Figures 3.29 and 3.30. During the transient flight without the estimation feedback, the z–inertial axes position time-history in Figure 3.29 shows an error of about 15 meters (red line) that can be reduced at about 0.50 meter (blue line). Same observations can be done by observing the figure 3.30.

The compensation of external disturbances can be also useful to compensate constant wind induced position error. As can be seen in Figure 3.29, the implemented nominal controller (without estimation feedback, red line) is not able to compensate constant external disturbances. The feedback of exogenous signal estimations allows to reach without error the target position.

Chapter 4

Conclusions

A new control scheme has been presented in this thesis. Based on the NonLinear Geometric Approach, the proposed Active Control System represents a new way to see the reconfigurable controllers for aerospace applications. The presence of the Diagnosis module, mean feature of the depicted Active Control System, is a characteristic shared by three well known control systems: the Active Fault Tolerant Controls, the Indirect Adaptive Controls and the Active Disturbance Rejection Controls.

The standard NonLinear Geometric Approach has been accurately investigated and than improved to extend its applicability to more complex models. The standard NLGA procedure has been modified to take account of feasible and estimable sets of unknown signals. Furthermore the application of the Singular Perturbations approximation has led to the solution of detection and isolation problems in scenarios too complex to be solved by the standard NLGA.

Also the estimation process has been improved, where multiple redundant measuremtent are available, by the introduction of a new algorithm, here called "Least Squares - Sliding Mode". It guarantees optimality, in the sense of the least squares, and finite estimation time, in the sense of the sliding mode.

The Active Control System concept has been formalized in two controller: a nonlinear backstepping controller and a nonlinear composite controller. Particularly interesting is the integration, in the controller design, of the estimations coming from the Diagnosis module. Stability proofs are provided for both the control schemes.

Finally, different applications in aerospace have been provided to show the applicability and the effectiveness of the proposed NLGA-based Active Control System.

Future works? ... the research will never ends and further developments are foreseen, probably to remove the "input-affinity" constraint of the present NLGA.

Bibliography

[1] A. Zolghadri, D. Henry, J. Cieslak, D. Efimov, and P. Goupil. *Fault Diagnosis and Fault-Tolerant Control and Guidance for Aerospace Vehicles: From Theory to Application.* Springer, 2014.

[2] M. Mahmoud, J. Jiang, and Y. Zhang. *Active Fault Tolerant Control Systems: Stochastic Analysis ans Synthesis.* Springer, 2003.

[3] J. Chen and R. J. Patton. *Robust model-based fault diagnosis for dynamic systems.* Kluwer Academic Publisher, 1999.

[4] J. A. Aseltine, A. R. Mancini, and C. W. Sartune. A survey of adaptive control systems. *IRE Transactions on Automatic Control*, 3(6):102–108, 1958.

[5] P. A. Ioannou. *Robust Adaptive Control.* Prentice Hall, 1996.

[6] J. Han. Nonlinear design methods for control systems. *Proceedings of the 14th IFAC World Congress*, 1999.

[7] Z. Gao, Y. Huang, and J. Han. An alternative paradigm for control system design. *Proceeding of 40th IEEE Conference on Decision and Control*, 2001.

[8] Z. Gao. Active disturbance rejection control: A paradigm shift in feedback control system design. *Proceedings of 2006 American Control Conference*, 2006.

[9] R. Isermann. Supervision, fault detection and fault diagnoses methods - an introduction. *Control Engineering Practice*, 5(5):639–652, 1997.

[10] A. Emani-Neini, M. M. Ather, and S. M. Rock. Effect of model uncertainty on failure detection: The threshold selection. *IEEE Transactions of automatic Control*, 33(12):1106–1115, 1988.

[11] P. M. Frank. Analytical and qualitative model-based fault diagnosis - a survey and some new results. *European Journal of Control*, 2(1):6–28, 1996.

[12] R. J. Patton and J. Chen. Robust fault detection using eigenstructure assignment: A tutorial consideration and some new results. *Proceedings of the 30th IEEE Conference on Decision and Control*, pages 2242–2247, 1991.

[13] S. Yoon and J. F. MacGregor. Statistical and causal model-based approaches to fault detection and isolation. *AIChE Journal*, (46):1813–1824, 2000.

[14] P. M. Frank. Fault diagnosis in dynamic systems using analytical and knowledge-based redundancy - a survey and some new results. *Automatica*, 26(3):459–474, 1990.

[15] M. Baseville and I. V. Nikiforov. *Detection of abrupt changes: Theory and applications.* Prentice Hall, 1993.

[16] H. P. B. Dassanayake, C. Roberts, and C. J. Goodman. An architecture for system-wide fault detection and isolation. *Proceedings of the Institution of Mechanical Engineers, Part I: Journal of System Control Engineering*, 215:37–43, 2001.

[17] R. K. Douglas and J. L. Speyer. Robust fault detection filter design. *Journal of Guidance Control and Dynamics*, 19(1):214–218, 1996.

[18] P. M. Frank and X. Ding. Frequency domain approach to optimally robust residual generation. *Automatica*, 30(5):789–804, 1994.

[19] E. A. Garcia and P. M. Frank. Deterministic nonlinear observer-based approaches to fault diagnosis. *Control Engineering Practice*, 5(5):663–760, 1991.

[20] E. Y. Chow and A. S. Willsky. Analytical redundancy and the design of robust failure detection systems. *IEEE Transaction on Automatic Control*, 29(7):603–614, 1984.

[21] J. Gertler. Fault detection and isolation using parity relations. *Control Engineering Practice*, 5(5):653–661, 1997.

[22] R. Isermann. Process fault-detection based based on modelling and estimation methods: A survey. *Automatica*, 20(4):387–404, 1984.

[23] F. J. Hermans and M. B. Zarrop. Parameter estimation using sliding mode principles. *Proceedings of the IFAC Symphosium SAFEPROCESS'97*, pages 282–287, 1997.

[24] Z. Han and P. Frank. Physical parameter estimation based fdi with neural networks. *Proceedings of the IFAC Symphosium SAFEPROCESS'97*, pages 294–299, 1997.

[25] S. Tzafestas and K. Watanabe. Modern approaches to system/sensor fault detection and diagnosis. *Journal A*, 31(4):42–57, 1990.

[26] M. A. Massoumnia. A geometric approach to the synthesis of failure detection filters. *IEEE Transaction on Automatic Control*, 31(9):839–846, 1986.

[27] M. A. Massoumnia, G. C. Verghese, and A. S. Willsky. Failure detection and identification. *IEEE Transaction on Automatic Control*, 34(3):316–321, 1989.

[28] W. M. Wonham. *Linear Multivariable Control. A Geometric Approach. Third Edition.* Springer Verlag, 1992.

[29] C. Commault. On the disturbed fault detection and isolation problem. *Systems & Control Letters*, (38):73–78, 1999.

[30] S. Longhi and A. Monteriù. A geometric approach to fault detection and isolation problem for linear periodic systems. *Proceedings of the 49th IEEE Conference on Decision and Control*, pages 7724–7729, 2010.

[31] N. Meskin and K. Khorasani. A geometric approach to robust fault detection and isolation of markovian jump systems. *Proceedings of the 2008 American Control Conference*, pages 2822–2827, 2008.

[32] N. Meskin and K. Khorasani. A geometric approach to fault detection and isolation of continuous-time markovian jump systems. *IEEE Transactions on Automatic Control*, 55 (6):1343–1357, 2010.

[33] N. Meskin and K. Khorasani. Robust fault detection and isolation of time-delay systems using a geometric approach. *Automatica*, 45(6):1567–1573, 2009.

[34] N. Meskin and K. Khorasani. Fault detection and isolation of retarded time-delay systems using a geometric approach. *Proceeding of the 2008 IFAC World Congress*, pages 7326–7331, 2008.

[35] N. Meskin and K. Khorasani. A geometric approach to fault detection and isolation of neutral time-delay systems. *Proceedings of the 2008 American Control Conference*, pages 3293–3298, 2008.

[36] A. Baniamerian, N. Meskin, and K. Khorasani. Fault detection and isolation of fornasini-marchesini 2d systems: A geometric approach. *Proceedings of the 2014 American Control Conference*, pages 5527 – 5533, 2014.

[37] J. C. Martinez-Garcia, B. Del-Muro-Cuellar, and M. Malabre. Partial fault detection and isolation: A geometric approach. *Proceedings of the 16th International Symposium on Mathematical Theory of Networks and Systems*, 2004.

[38] A. Edelmayer, F. Szigeti, J. Bokor, and L. Keviczky. Robust detection filter design in the presence of time-varying system perturbations. *Automatica*, 33(3):471–475, 1997.

[39] A. Edelmayer, F. Szigeti, J. Bokor, and L. Keviczky. A geometrical view of observer-based methods for detection and isolation of faults in time varying and bilinear systems. *Proceedings of the IFAC Symposium SAFEPROCESS'97*, page 140–146, 1997.

[40] C. De Persis and A. Isidori. A geometric approach to non–linear fault detection and isolation. *IEEE Transactions on Automatic Control*, 45(6):853–865, 2001.

[41] R. Mattone and A. De Luca. Conditions for detecting and isolating sets of faults in nonlinear systems. *Proceedings of the 44th IEEE Conference on Decision an Control and European Control Conference*, pages 1005–1010, 2005.

[42] R. Mattone and A. De Luca. Relaxed fault detection and isolation: An application to a nonlinear case study,. *Automatica*, 42(1):109–116, 2006.

[43] H. C. B. Jensen. *Geometric Approach to Analysis and Nonlinear Fault Detection and Isolation.* Aalborg Universitetsforlag, Department of Electronic Systems Automation & Control, Ph.D. thesis, 2004.

[44] J. Bokor and Z. Szabo. Fault detection and isolation in nonlinear systems. *Annual Reviews in Control*, 33:113–123, 2003.

[45] E. Sobhani-Tehrani and K. Khorasani. *Fault Diagnosis of Nonlinear Systems Using a Hybrid Approach.* Springer, 2009.

[46] A. Baniamerian, N. Meskin, and K. Khorasani. Fault detection and isolation of riesz spectral systems: A geometric approach. *Proceedings of the 2014 European Control Conference*, pages 2145 – 2152, 2014.

[47] A. Baniamerian and K. Khorasani. Fault detection and isolation of dissipative parabolic pdes: Finite-dimensional geometric approach. *Proceedings of 2012 American Control Conference*, pages 5894–5899, 2012.

[48] A. De Luca and R. Mattone. An adapt-and-detect actuator fdi scheme for robot manipulators. *Proceedings of the 2004 IEEE International Conference on Robotics & Automation*, pages 4975–4980, 2004.

[49] R. Mattone and A. De Luca. Nonlinear fault detection and isolation in a three-tank heating system. *IEEE Transactions on Control Systems Technology*, 14(6):1158–1166, 2006.

[50] M. Bonfé, P. Castaldi, N. Mimmo, and S. Simani. Active fault tolerant control of nonlinear systems: The cart-pole example. *International Journal of Applied Mathematics and Computer Science*, 21(3):441–445, 2011.

[51] C. De Persis, R. De Sanctis, and A. Isidori. Nonlinear actuator fault detection and isolation for a VTOL aircraft. *Proceedings of the 2001 American Control Conference*, pages 4449–4454, 2001.

[52] N. Meskin and K. Khorasani. *Fault Detection and Isolation. Multi-Vehicle Unmanned Systems.* Springer, 2011.

[53] M. Benini, P. Castaldi, and S. Simani. *Fault Diagnosis for Aircraft System Models: An introduction from fault detection to fault tolerance.* VDM Verlag Dr. Muller, 2009.

[54] P. Castaldi, W. Geri, M. Bonfè, S. Simani, and M. Benini. Design of residual generators and adaptive filters for the fdi of aircraft model sensors. *Control Engineering Practice*, 18: 449–459, 2010.

[55] M. Bonfè, P. Castaldi, W. Geri, and S. Simani. Fault detection and isolation for on–board sensors of a general aviation aircraft. *International Journal of Adaptive Control and Signal Processing*, 8(20):381–408, 2006.

[56] P. Castaldi and N. Mimmo. Aircraft nonlinear aftc based on geometric approach and singular perturbations in case of actuator and sensor faults. *Proceedings of 19th IFAC Symposium on Automatic Control in Aerospace*, pages 90–95, 2013.

[57] P. Castaldi, N. Mimmo, and S. Simani. Fault tolerant control schemes for nonlinear models of aircraft and spacecraft systems. *Proceedings of the 18th IFAC world congress*, 18(13): 705–710, 2011.

[58] P. Castaldi, N. Mimmo, and S. Simani. Differential geometry based active fault tolerant control for aircraft. *Control Engineering Practice*, 32:227–235, 2014.

[59] P. Castaldi, N. Mimmo, and S. Simani. Nonlinear fault tolerant flight control for generic actuators fault models. *Proceedings of the 2014 American Control Conference*, pages 1267–1272, 2014.

[60] K. Meskin and N. Khorasani. Fault detection and isolation in a redundant reaction wheels configuration of a satellite. *Proedings of the IEEE International Conference on Systems, Man and Cybernetics*, pages 3153–3158, 2007.

[61] P. Baldi, P. Castaldi, N. Mimmo, and S. Simani. Satellite attitude active ftc based on geometric approach and rbf neural network - fault tolerant control for aerospace applications. *Proceedings of the 2nd International Conference on Control and Fault-Tolerant Systems*, pages 667 – 673, 2013.

[62] P. Baldi, P. Castaldi, N. Mimmo, and S. Simani. A new aerodynamic decoupled frequential fdir methodology for satellite actuator faults. *International Journal of Adaptive Control and Signal Processing*, (DOl: 1O.1002/acs.2379), 2013.

[63] P. Baldi, P. Castaldi, N. Mimmo, A. Torre, and S. Simani. A new longitudinal flight path control with adaptive wind shear estimation and compensation. *Proceeding of 50th IEEE Conference on Decision and Control and European Control Conference*, pages 6852–6857, 2011.

[64] P. Baldi, P. Castaldi, N. Mimmo, and S. Simani. Generic wind estimation and compensation based on nlga and rbf-nn. *Proceedings of the 2014 European Control Conference*, pages 1729 – 1734, 2014.

[65] P. Castaldi, N. Mimmo, R. Naldi, and L. Marconi. Robust trajectory tracking for underactuated vtol aerial vehicles: Extended for adaptive disturbance compensation. *Proceedings of 2014 IFAC World Congress*, pages 3184–3189, 2014.

[66] H.K. Khalil. *Nonlinear Systems – 3rd edition*. Prentice Hall, 2002.

[67] A. J. Krener and W. Respondek. Nonlinear observers with linearizable error dynamics. *SIAM, Journal of Control and Optimization*, 23(2):197–216, 1985.

[68] D. Bestle and M. Zeitz. Canonical form observer design for non-linear time-variable systems. *International Journal of Control*, 2(38):419–431, 1983.

[69] J. Birk and M. Zeitz. Extended luenberger observer for non-linear multivariable systems. *International Journal of Control*, 47(6):1823–1836, 1988.

[70] F. E. Thau. Observing the state of non-linear dynamic systems. *International Journal of Control*, (18):471–479, 1973.

[71] S. Raghavan and J. K. Hedrick. Observer design for a class of nonlinear systems. *International Journal of Control*, 2(59):515–528, 1994.

[72] S. X. Ding, P. Zhang, P. M. Frank, and E. L. Ding. Threshold calculation using lmi-techinque and its integration in the design of fault detection systems. *Proceeding of the 42th Conference on Decision and Control*, pages 469–474, 2003.

[73] T. Poggio and F. Girosi. Regularization algorithms for learning that are equivalent to multilayer networks. *Science*, 247:978–982, 1990.

[74] T. Chen and H. Chen. Approximation capability to functions of several variables, nonlinear functionals, and operators by radial basis function neural networks. *IEEE Transactions On Neural Networks*, 6(4), 1995.

[75] P. A. Ioannou and A. Datta. Robust adaptive control: a unified approach. *Proc. IEEE*, 79:1736–1768, 1991.

[76] P. A. Ioannou and P. V. Kokotovic. *Adaptive Systems with Reduced Models*. New York: Springer-Verlag, 1983.

[77] K. S. Narendra and A. M. Annaswamy. *Stable Adaptive Systems*. New York: Prentice-Hall, 1989.

[78] W. Zhenhua, S. Yi, and Xiaolei Z. Actuator fault detection and estimation for a class of nonlinear systems. *Transaction of the IEEE Seventh International Conference on Natural Computation*, pages 535–539, 2011.

[79] L. Fridman, Y. Shtessel, C. Edwards, and X. G. Yan. Higher-order sliding-mode observer for state estimation and input reconstruction in nonlinear systems. *Int. J. Robust Nonlinear Control*, 18(4-5):381–585, 2008.

[80] A. Levant. Higher-order sliding modes, differentiation and output-feedback control. *International Journal of Control*, 76(9/10):924–941, 2003.

[81] E. M. Mikhail and F. E. Ackermann. *Observations and least squares*. University Press of America, 1982.

[82] C. L. Lawson and R. J. Hanson. *Solving least squares problems*. Philadelphia:SIAM, 1995.

[83] A. Isidori. *Nonlinear Control Systems II*. Springer–Verlag, 1999.

[84] C. Edwards, T. Lombaerts, and H. Smaili. *Fault Tolerant Flight Control: A Benchmark Challenge*. Springer. Lecture Notes in Control and Information Sciences, 1st edn, 2010.

[85] P. Kokotovic, H. K. Khalil, and J. O'Reilly. *Singular Perturbation Methods in Control – Analysis and Design*. SIAM Classics in Applied Mathematics, 1999.

[86] A. Isidori. *Nonlinear Control Systems – Third edition*. Springer–Verlag, 1995.

[87] J. L. Boiffier. *The Dynamics of Flight: The Equations*. John Wiley & Sons, 1998.

[88] B. L. Stevens and F. L. Lewis. *Aircraft Control and Simulation*. John Wiley & Sons, 1992.

[89] *U.S. Standard Atmosphere*. U.S. Government Printing Office, Washington, D.C., 1976.

[90] *World Geodetic System 1984, Its Definition and Relationship with Local Geodetic Systems*. Department of Defense, NIMA TR8350.2., 1984.

[91] S. H. Pourtakdoust, M. Kiani, and A. Hassanpour. Optimal trajectory planning for flight through microburst wind shears. *Aerospace Science and Technology*, 15:567–576, 2011.

[92] *Flying qualities of piloted airplanes*. U.S. Military Handbook, MIL-HDBK-1797, 1997.

[93] *Flying qualities of piloted airplanes*. U.S. Military Specification, MIL-F-8785C, 1980.

[94] *Aerospace Blockset 3: User's Guide. Revised for Version 3.5*. MathWorks Inc., 2010.

[95] M. P. Fink and D. C. Freeman. *Full-scale wind-tunnel investigation of static longitudinal and lateral characteristics of a light twin-engine airplane*. Number TN D-4983. NASA Technical Note, 1969.

[96] J. Koziol. *Simulation Model For The Piper PA-30 Light Maneuverable Aircraft In The Final Approach.* Number DOT-TSC-FAA-71-11. NASA Technical Memorandum, 1971.

[97] H. Gray. *Wind Tunnel Test of Single and Dual rating tractor propellers at low blade angles of two and three blade tractor propellers at blade angles up to* 60°. Number L-316. NACA, 1943.

[98] *Lycoming O-320 Operator's Manual*, 2nd edition, 1973.

[99] R. M. Bray. *A wind tunnel study of the Pioneer remotely piloted vehicle.* Naval Postgraduate School, 1991.

[100] J. Roskam. *Airplane Flight Dynamics and Automatic Flight Controls, vol. I.* DARcorporation, 2001.

[101] T. Jiang, K. Khorasani, and S. Tafazoli. Parameter estimation based fault detection, isolation and recovery for nonlinear satellite models. *IEEE Transactions on Control Systems Technology*, 16(4):799–808, 2008.